Journal of the
OPTICAL SOCIETY *of* AMERICA

VOLUME 40, NUMBER 3 MARCH, 1950

Dean George R. Harrison

Frederic Ives Medalist for 1949

THE Optical Society of America, at its Buffalo meeting in October, 1949, awarded the Frederic Ives Medal for Distinguished Work in Optics to Dean George Russell Harrison. Dr. Harrison, the editor of the Journal of the Optical Society and a past president of the Society, is Dean of the School of Science of the Massachusetts Institute of Technology, where he has served most of his academic career.

The medal was presented to Dean Harrison on the occasion of the Society's annual banquet and was followed by an address by Dr. Harrison.

The Frederic Ives Medal Committee which had been appointed by President Kingslake consisted of Dr. George S. Monk, Chairman, Dr. Wallace R. Brode, Dr. Gerhard H. Dieke, Dr. Kasson S. Gibson, and Dr. Loyd A. Jones. President Kingslake opened the presentation ceremonies with the statement: "It is the crowning duty and privilege of the president of this Society to present the Frederic Ives medal for Distinguished Work in Optics, as his last official act before handing over the reins of office to his successor. This medal is awarded every two years by the Board of Directors from a fund presented to the Society in 1928 by Dr. Herbert E. Ives in memory of his father. This year, the medal is to be presented to Dr. George Russell Harrison, and I shall now call upon Dr. George Monk, Chairman of the Award Committee, to deliver the citation." The citation by the Award Committee was made by Dr. Monk as follows:

"In naming a scientist to join the illustrious group of previous recipients of the Frederic Ives Medal, the present Committee had what seemed at first to be a difficult task. Optics includes or impinges on the subjects of Geometrical Optics, Physical Optics, Photometry, Color, Physiological Optics, Spectroscopy, Photography, Astrophysics, and Astronomy, to say nothing of its services to the biological sciences and industry. Although the committee was obliged to consider the accomplishments of gifted and industrious workers in many fields, it very soon became evident that the name of only one man could be the unanimous choice—Dean George R. Harrison of Massachusetts Institute of Technology.

"Dr. Harrison is a comparatively young man. A native son of California, he graduated with an A.B. degree from Stanford University in 1919, A.M. in 1920, and Ph.D. in 1922 from the same institution. Beginning in 1922 and continuing to the present he has published steadily. I have counted 45 scientific papers in the journals. However, the number is not significant, but rather their importance. A survey of the titles discloses that while Dr. Harrison's first and primary interest has quite evidently been in problems of the structure of matter through the medium of spectroscopy, he has always had a compelling urge to make the observational data better, more complete, and with greater speed. So his fertile and energetic mind has, in the consideration of physical problems, inevitably turned to ways of improving observational techniques and data. An instance may be given from his earlier papers. The first, in 1922, was on 'Absorption of Light by Sodium and Potassium Vapors, A Preliminary Report.' Following this he published: 'A Simple Densitometer for Accurate Work,' in 1923; 'Series Limit of Absorption in Sodium Vapor,' in 1924; and in 1925 six papers: 'Spectral Energy Characteristics of the Mercury Vapor Lamp' (with G. S. Forbes), 'Precision Densitometer for Photographic Photometry,' 'Experimental Determination of Relative Transition Probabilities in the Sodium Atom,' 'Photographic Sensitometry with Fluorescent Oils,' 'Line Breadths and Absorption Probabilities in Sodium Vapor' (with J. C. Slater), 'Spectral Energy Characteristics of the Constricted Mercury Vapor Lamp' (with G. S. Forbes), 'Character of Photographic Materials in the Ultraviolet.'

"This list, quite obviously relating to the purpose of completely exhausting all phases of work with Sodium

and Potassium Vapor and their spectra, betrays a most compelling urge to explore every part of a given problem, and especially to improve the means for collecting and evaluating data. In following years this tendency toward completeness and thoroughness in investigation grew in power. Beginning in 1928 he began publication of a most important series of three papers on the spectrum of titanium: 'I. Intensity Relations in the Spectrum of Titanium'; 'II. Relative Intensities of the Stronger Multiplets of Titanium I'; 'III. Supermultiplet Intensities in the Titanium Spectrum.' This last paper, published in 1929, contains what I believe is the first extension to a supermultiplet of the sum-rule for spectral line intensities. It was the prelude to a veritable deluge of precise and extensive work by Dr. Harrison or under his direction in the measurement of wave-lengths and intensities in complex spectra, culminating finally in his epoch-making development of mechanical robots for spectrum work. A few titles will illustrate: 1935, 'Automatic Measurement of Spectra'; 1938, 'Interval Recorder for the Analysis of Spectra' (this work was preceded, however, by his paper on the 'Spectrum Interval Sorter' in 1933) and many others, followed by a still more stupendous publication of data on the Zeeman Effect in Spectra of Cerium, Ruthenium, Tungsten, Praesodymium, and other elements.

"Parenthetically I can testify to the devastating effect of these machines on current work in spectroscopy, for each one automatically swept out of existence a number of promising master's theses which others of us hoped to have worked out by older laborious methods. Following the building of Harrison's robots, one simply had to send the plates to Cambridge to be run through the appropriate machine.

"In 1948, Dr. Harrison announced his greatest spectrum-measuring device in a paper on 'The Direct Determination of Wave-lengths from Fabry-Perot Patterns,' a machine involving a half-a-dozen mechanical innovations. Nor can we omit reference to the *M.I.T. Wavelength Tables*, a product of Dr. Harrison's directive genius, during depression years. These Tables, precise and complete beyond compare, have, for most scientific and industrial work, relegated to the archives all other tables of wave-length data.

"Science and industry are able to work better and faster because of Dr. Harrison's compelling urge to do his chosen work most thoroughly. But this is not the sum of his accomplishments. He has served at length as dean, administrator, and founder and director for several years of the M. I. T. Spectroscopic Conferences; he served as president of the Optical Society from 1945 to 1947; he has set a standard of excellence in his editorship of the Journal of this Society, and, I am sure, has made our meetings more enjoyable with his presence.

"I express the sentiments of the Committee for the Ives Medal Award for 1949 in saying we are proud to have nominated Professor Harrison."

The Frederic Ives Medal was then presented to Dean Harrison by President Kingslake with an expression of appreciation on behalf of the Society for Dean Harrison's many outstanding contributions to the field of Optics.

On presentation of the medal, Dean Harrison expressed his gratitude in the following statement:

"Mr. President, I have witnessed the bestowal of the Frederic Ives Medal on at least seven recipients, and have noticed in each case that the medalist was reduced, at least temporarily, to speechlessness. In seeking reasons as to why I should have been chosen to receive this most handsome medal, I can only conclude that the Committee of Award wished to carry out an experiment to see whether I too could be made speechless; as you will note the test has failed, for I continue to emit sounds, and become not speechless but merely incoherent.

"When I received notice that the Frederic Ives Medal Committee had selected me to receive this award, my first reaction was one of disbelief, my second was one of great pleasure, and my third reaction was one of shock. This last occurred when I realized that I would be called upon by the President of the Society, as I have no doubt I shall be in a few moments, to give a sort of *apologia pro vita mia* before this assembly, and that I should have to prepare for public display in the journal a list of my writings, so that all the world might see whether or not the medal had been awarded justifiably.

"It is good to have an occasional opportunity for taking stock, and in preparing for this evening a bird's-eye view of my investigations over the past twenty-five years, I have found that there actually is a definite connective order between one project and the next. I was somewhat chagrined, however, to note that the main line of progress appears to have been backward. In 1921 I started out to study the characteristics of atoms as revealed in the intensities of spectrum lines emitted by them, but soon found that interpretation of the results was necessarily incomplete because of our lack of knowledge of perturbations in complex atoms. Investigating methods of getting the desired information, I found that more work was badly needed on the classification of spectra in such atoms, and on the determination of the energy levels from which the spectrum lines originate. I therefore attacked the classification of spectra in atoms of the rare earths, but found that my patience and industry were inferior to what was needed for success in this field, so I developed two gadgets, the interval sorter and the interval recorder, to lighten this type of work. Though these two devices were unexpectedly successful, they soon revealed that progress in analyzing very complex spectra by application of the Ritz Combination Principle could be expected to be slow and uncertain until better wave-length determinations were available. I therefore turned my attention to the procurement of improved wave-length data with large diffraction grat-

ings, and designed an automatic comparator to facilitate such measurements. This in turn was moderately successful, but was of limited use because of the paucity of precise secondary standards of wave-length. It soon became apparent that if better standards were to become available in great numbers some improvement would have to be made in our methods of reducing Fabry-Perot spectrograms, and a machine was devised to aid such a program. This machine, the Winmac, was constructed, and now awaits more intensive use, but in the meantime it has become evident that much wave-length precision could also be gained by improvements in large diffraction gratings, and I have turned my attention to the development of a large interferometrically controlled ruling engine; this work has now resulted in the design of a new type of spectrograph that should greatly simplify all the steps outlined above.

"Thus I can point only to a series of some seven frustrations, each marked by the introduction of a new gadget that has set me back one step farther from my original intention. I can, however, hope that the award of the Frederic Ives Medal will reverse this trend; that we may soon have good echelle spectrographs which will provide precise wave-lengths in profusion for the classification of complex spectra, so that perturbations in atoms can be related to their structures, and thus their line-intensities can be explained.

"In gratefully accepting this medal, Mr. President, I think of the man who was honored by its initiation, and of the son who so honored the memory of his father, and made possible this biennial encouragement by the Society of workers in Optics. I thank you, the Directors of the Society, the members of the Frederic Ives Medal Committee, and the members of the Society, and hope that I—but now, I really am speechless!"

LIST OF SCIENTIFIC PUBLICATIONS OF GEORGE R. HARRISON

(1) "The absorption of light by sodium and potassium vapors," Proc. Nat. Acad. Sci. **8**, 260 (1922).
(2) "A simple densitometer for accurate work," J. Opt. Soc. Am. **7**, 999 (1923).
(3) "Photographic photometry in the ultraviolet" (with Cedric E. Hesthal), J. Opt. Soc. Am. **8**, 471 (1924).
(4) "Series limit absorption in sodium vapor," Phys. Rev. **24**, 466 (1924).
(5) "Spectral energy characteristics of the mercury vapor lamp" (with George Shannon Forbes), J. Opt. Soc. Am. **10**, 1 (1925).
(6) "Precision densitometers for photographic photometry," J. Opt. Soc. Am. **10**, 157 (1925).
(7) "Experimental determination of relative transition probabilities in the sodium atom," Phys. Rev. **25**, 768 (1925).
(8) "Spectral energy characteristics of the constricted mercury vapor lamp—an extremely concentrated source of ultraviolet illumination" (with George Shannon Forbes), J. Opt. Soc. Am. **11**, 99 (1925).
(9) "Line breadths and absorption probabilities in sodium vapor" (with J. C. Slater), Phys. Rev. **26**, 176 (1925).
(10) "Photographic sensitometry with fluorescent oils," J. Opt. Soc. Am. **11**, 113 (1925).
(11) "Characteristics of photographic materials in the ultraviolet," J. Opt. Soc. Am. **11**, 341 (1925).
(12) "The constricted mercury arc as a source of light for photochemical work" (with George S. Forbes), J. Am. Chem. Soc. **47**, 2449 (1925).
(13) "A comparator-microphotometer," J. Opt. Soc. Am. **16**, 63 (1928).
(14) "Intensity relations in the spectra of titanium. I. Line intensities in the stronger multiplets of Ti I and Ti II," J. Opt. Soc. Am. **17**, 389 (1928).
(15) "Intensity relations in the spectra of titanium. II. Relative intensities of the stronger multiplets of Ti I" (with Harry Engwicht), J. Opt. Soc. Am. **18**, 287 (1929).
(16) "On the elimination of errors when wire screens are used as neutral filters for photographic photometry," J. Opt. Soc. Am. **18**, 492 (1929).
(17) "Intensity relations in the spectra of titanium. III. Intensities in super-multiplets of Ti I," J. Opt. Soc. Am. **19**, 109 (1929).
(18) "Instruments and methods used for measuring spectral light intensities by photography," J. Opt. Soc. Am. **19**, 267 (1929).
(19) "Homochromatic spectrophotometry in the extreme ultraviolet" (with Philip A. Leighton), J. Opt. Soc. Am. **20**, 313 (1930).
(20) "Fluorescent dry plates for photographic photometry" (with Philip A. Leighton), Phys. Rev. **36**, 779 (1930).
(21) "Intensity summation rules and perturbation effects in complex spectra" (with M. H. Johnson, Jr.), Phys. Rev. **38**, 757 (1931).
(22) "Spectral fluorescence efficiencies of certain substances with applications to heterochromatic photographic photometry" (with Philip A. Leighton), Phys. Rev. **38**, 899 (1931).
(23) "A 21-foot vacuum spectrograph for the extreme ultraviolet," Rev. Sci. Inst. **2**, 600 (1931).
(24) "Dichromatic projection microphotometer," Rev. Sci. Inst. **3**, 572 (1932).
(25) "Mechanical aid to the analysis of complex spectra," Rev. Sci. Inst. **3**, 753 (1932).
(26) "Improved design of the mechanical interval sorter and its application to the analysis of complex spectra," Rev. Sci. Inst. **4**, 581 (1933).
(27) "Spectroscopy at the Massachusetts Institute of Technology," Am. Phys. Teacher **1**, 109 (1933).
(28) "Improvements in 21-foot normal incidence vacuum spectrograph," Rev. Sci. Inst. **4**, 651 (1933).
(29) "Current advances in photographic photometry," J. Opt. Soc. Am. **24**, 59 (1934).
(30) "Simply constructed ultraviolet monochromators for large area illumination," Rev. Sci. Inst. **5**, 149 (1934).
(31) "Automatic measurement, reduction and recording of wavelengths from spectrograms," J. Opt. Soc. Am. **25**, 169 (1935).
(32) "The ultraviolet spectrum of ammonia" (with A. B. F. Duncan), Phys. Rev. **49**, 211 (1936).
(33) "The application of physics to agriculture," Rev. Sci. Inst. **7**, 295 (1936).
(34) "Practical possibilities in spectrographic analysis," Metals and Alloys **7**, 290 (1936).
(35) "The applied physicist," J. App. Phys. **8**, 569 (1937).
(36) "More precious than rubies," Harper's **175**, 635 (1937).
(37) "When physics goes farming," Atlantic Monthly **160**, 69 (1937).
(38) "Tomorrow's telephones," Tech. Rev. **40**, 22 (1937).
(39) *Measurement of Radiant Energy*, Chapter on Densitometer and Microphotometer, W. E. Forsythe, Editor (McGraw-Hill Book Company, New York, 1937).
(40) "The Frederic Ives Medal for 1937," J. Opt. Soc. Am. **27**, 425 (1937).
(41) "Preliminary analysis of the first spark spectrum of cerium-Ce II (with W. E. Albertson), Phys. Rev. **52**, 1209 (1937).

(42) "Rapid calibration and correction of comparator screws and the photographic production of scales," Rev. Sci. Inst. **9**, 15 (1938).
(43) "Spectroscopy in food research," Food Research **3**, 121 (1938).
(44) "Spectroscopy in industry," J. Franklin Inst. **226**, 1 (1938).
(45) "An interval recorder for analysis of spectra," J. Opt. Soc. Am. **28**, 290 (1938).
(46) "A high speed method of absorption spectrophotometry for the range 10,000 to 2000A," *Proc. Sixth Spectroscopy Conf.* (Technology Press, Cambridge, Massachusetts, 1938).
(47) Editor and twenty-seven co-authors, *Spectroscopy in Science and Industry* (Technology Press, Cambridge, Massachusetts, 1938).
(48) "Apprenticed sunlight," Tech. Rev. **40**, 315 (1938).
(49) "From shellac to symphony," Tech. Rev. **41**, 17 (1938).
(50) "Compilations of spectroscopic data," J. App. Phys. **10**, 760 (1939).
(51) *Atoms in Action* (William Morrow & Company, New York, 1939), 365 pp.; Armed Services edition, 1945; British edition, Swedish edition, Portuguese edition, 1940; Spanish edition, 1941; Danish edition, 1942; Dutch edition, 1945; German edition, 1947.
(52) *M. I. T. Wavelength Tables*, Editor (John Wiley & Sons, Inc., and Technology Press, New York, 1939).
(53) "Spectroscopic photography," Chapter in *Handbook of Photography* (McGraw-Hill Book Company, New York, 1939), p. 804.
(54) "High speed device for absorption spectrophotometry," abstract from paper presented to Optical Society of America, October 7, 1938, J. Opt. Soc. Am. **29**, 143 (1939).
(55) "Eyes that see through atoms," Sci. Am., **161**, 132, 212 (1939); Reader's Digest, 117 (November, 1939).
(56) "Spectroscopy and its applications at the Massachusetts Institute of Technology," Sci. Monthly **49**, 387 (1939).
(57) *Proc. Sixth Spectroscopy Conf.*, Editor (Technology Press, Cambridge, Massachusetts, 1939).
(58) "New tables of spectral lines," *Proc. Sixth Spectroscopy Conf.* (Technology Press, Cambridge, Massachusetts, 1939), p. 118.
(59) "The doctor consults the physicist," Atlantic Monthly **163**, 649 (1939).
(60) "Zeeman effects in complex spectra at fields up to 100,000 gauss" (with F. Bitter), Phys. Rev. **57**, 15 (1940).
(61) "The testing and use of concave diffraction gratings," *Proc. Seventh Spectroscopy Conf.* (Technology Press, Cambridge, Massachusetts, 1940), p. 59.
(62) "New methods in spectroscopy," Science **91**, 225 (1940).
(63) "An improved high speed recording spectrophotometer" (with E. P. Bentley), J. Opt. Soc. Am. **30**, 290 (1940).
(64) "Photoelectric measurement of scale marks and spectrum lines" (with Julius P. Molnar), J. Opt. Soc. Am. **30**, 343 (1940).
(65) "Zeeman effects in the arc spectrum of ruthenium" (with J. Rand McNally, Jr.), Phys. Rev. **58**, 703 (1940).
(66) "Interactions in the tungsten atom, W I., in a magnetic field" (with J. H. Roberson and J. E. Mack), Phys. Rev. **58**, 895 (1940).
(67) *Proc. Seventh Spectroscopy Conf.*, Editor (Technology Press, Cambridge, Massachusetts, 1940).
(68) "What's the matter with popular science?" Saturday Review of Literature **21**, 3 (1940).
(69) "Spectroscopy in industry," Annual Report of the Smithsonian Institution, 1939 (August, 1940), p. 203.
(70) "Zeeman effect data and further classification of the first spark spectrum of cerium-Ce II" (with Walter E. Albertson and Norman F. Hosford), J. Opt. Soc. Am. **31**, 439 (1941).
(71) "Zeeman effect data and preliminary classification of the spark spectrum of praseodymium-Pr II" (with Nathan Rosen and J. Rand McNally, Jr.), Phys. Rev. **60**, 722 (1941).
(72) "The M.I.T. wave-length project," The Physical Society, Reports on Progress in Physics (Taylor and Francis, Ltd., London, 1941), Vol. 8, p. 212.
(73) Chapter in *New Worlds in Science* (Robert McBride, New York, 1941).
(74) *How Things Work* (William Morrow & Company, New York, 1941, 1945), 300 pp.; Swedish edition, 1942; British edition, 1943; Italian edition, 1948; Japanese edition, 1948.
(75) "First spark spectrum of neodymium—preliminary classification and Zeeman effect data" (with W. E. Albertson and J. R. McNally, Jr.), Phys. Rev. **61**, 167 (1942).
(76) "First spark spectrum of thorium—classification and Zeeman effect data of Th. II." (with J. Rand McNally, Jr. and Helen B. Park), J. Opt. Soc. Am. **32**, 334 (1942).
(77) "The summer conference on spectroscopy and its applications," Sci. Monthly **55**, 386 (1942).
(78) "Scientist extraordinary," Tech. Rev. **45**, 73 (1942).
(79) "Science at M.I.T.," Technique, 1944 (June, 1943).
(80) "Zeeman effects in the arc, first spark, and second spark spectra of yttrium" (with J. Rand McNally, Jr.), J. Opt. Soc. Am. **35**, 584 (1945).
(81) "Serving through science, 'the spectroscope: a master key to new materials,'" a radio talk; one of a series delivered by American Scientists on the New York Philharmonic-Symphony Program, U. S. Rubber Company (1945).
(82) "Zeeman effect data for the spectra of lanthanum-La I and La II (with Nathan Rosen and J. Rand McNally, Jr.), J. Opt. Soc. Am. **35**, 658 (1945).
(83) "The importance of scientific research in the postwar era," Science **103**, 125 (1946).
(84) "Direct determination of wave-lengths from Fabry-Perot interferometer patterns," J. Opt. Soc. Am. **36**, 644 (1946).
(85) "A hollow cathode source applicable to spectrographic analysis for the halogens and gases" (with J. Rand McNally, Jr. and Eugene Rowe), J. Opt. Soc. Am. **37**, 93 (1947).
(86) "The story of engineering," *World Book Encyclopedia* (The Quarrie Corporation, Chicago, 1947).
(87) "Industry and the atom," Am. Gas Ass. Monthly **29**, 159 (1947).
(88) "New advances in science," Food Tech. **2**, 45 (1948).
(89) "The sinking of the well," Accent on Living, Atlantic Monthly **182**, 87 (1948).
(90) *Practical Spectroscopy* (with Richard C. Lord and John R. Loofbourow) (Prentice-Hall, Inc., New York, 1948).
(91) Optics—a history of Divisions 16 and 17, N.D.R.C., by G. H. Kirk Stephenson and Edgar L. Jones. (A section in Applied Physics: Electronics, Optics, and Metallurgy, edited by C. G. Suits, G. R. Harrison, and Louis Jordan, Little Brown & Company (Atlantic Monthly Press), Boston, 1948).
(92) "Spectroscopy," *Encyclopedia Americana* (Americana Corporation, New York and Chicago, 1949).
(93) "The production of diffraction gratings. I. The development of the ruling art," J. Opt. Soc. Am. **39**, 413 (1949).
(94) "The production of diffraction gratings. II. The design of echelle gratings and spectrographs," J. Opt. Soc. Am. **39**, 522 (1949).
(95) "Ultrafrequency excitation of Hg 198 lamps for interferometer illumination" (with Edward Jacobsen), abstract from paper presented to Optical Society of America, October, 1949, J. Opt. Soc. Am. **39**, 1054 (1949).

Retrogression in Spectroscopy*

GEORGE R. HARRISON
Massachusetts Institute of Technology, Cambridge, Massachusetts
(Received January 5, 1950)

I WAS led into spectroscopy as a field of investigation in 1920 by the suggestion of my major professor, Dr. David L. Webster of Stanford University, that I select as a thesis topic the series limit absorption of sodium vapor previously reported by R. W. Wood. After working on this and related topics for several years, both at Stanford and as a postdoctorate fellow with Professor Theodore Lyman at Harvard, I found myself on my return to Stanford in 1925 interested in elucidating line intensities in multiplets and in complex atomic spectra in general. Apart from several side excursions into vacuum spectroscopy, absorption spectrophotometry, and other fields of optical spectroscopy, I find a definite continuity in the later line of my chief interest, even though this appears to have led me away from a study of atomic perturbations to preoccupation with a series of mechanical devices culminating in the re-constitution of an engine for ruling diffraction gratings. I shall try in these few minutes to demonstrate that this retrogression has not been without purpose, and to express the hope that the delay in a direct attack on the original problem will eventually make possible its more complete solution.

My initial study of complex atomic spectra, which led to the promulgation of the "extended Sum Rule" [21],† convinced me that the analysis of few complex spectra was sufficiently complete to make possible a detailed explanation of their perturbations, so I turned to the classification of spectrum lines in terms of their parent energy levels to obtain the needed data.

The problem of locating the energy levels of an atom appealed to me as a glorified puzzle in which scientific value was added to entertainment. However, a few hours spent subtracting all of the seven-figure wave numbers in a column containing some thousands of entries from all others within a given wave number range, while endeavoring to find frequently occurring differences which might represent true intervals between pairs of wave numbers in the atom, convinced me that my talents lay elsewhere. Also there loomed ahead as most important the spectra of the rare earths, the solution of which the greatest analyst of them all had confided might well require the lifetimes of several men younger than either of us. A small section of a typical quadratic array obtained in a rare earth analysis is shown in Fig. 1.

In considering this problem, which obviously depended mainly on the routine rapid subtraction of large numbers, I thought of mechanical, then photoelectric, then photographic methods of subtraction. The latter appealed to me as most convenient, and during the summer of 1932, while acting as a visiting professor at Stanford University, I designed and built the "interval sorter" [25, 26], shown in Fig. 2. A thousand-foot roll of 35-mm opaque paper (Fig. 3), punched to be driven by sprocket wheels like motion picture film, was placed in the punching device shown in the foreground of Fig. 2. A suitable scale, such as 4 mm per wave number, having been chosen, a dial was arranged so that wave numbers could be read directly as the tape was reeled past the punch. A round hole was then punched at known wave number intervals to give a fiducial pattern, and a rectangular hole at the proper position for each spectral line, the two rows of holes being displaced slightly as in Fig. 3. After the wave numbers of all the lines had been recorded on the tape, this was threaded into the interval sorter, through which it could be run at high speed. A long mercury arc was hung over the tape; this, after moving horizontally for one meter, passed over a roller and back under itself for one meter to the take-up reel. Beneath the two layers of tape a sheet of photographic paper one meter wide passed at right angles, at any desired speed less than that of the wave number tape. Whenever a hole in the upper tape section passed over a hole in the lower tape section a small spot on the paper received a latent image whose position represented the wave number difference of two spectrum lines. A tiny section of a typical record is shown in Fig. 4. By passing a vertical straight-edge across this chart it was possible to determine readily those wave number differences which occurred most frequently.

Later it was found that the problem of identifying the pairs of lines which combined to give meaningful differences was unnecessarily tedious, and the "interval recorder" shown in Figs. 5 and 6 was built [45]. The tape used in the interval sorter was sent through a pick-up beam as shown in Fig. 5, the two sprockets S and S' being adjusted by means of a differential to turn with one of the constant wave number differences shown by the interval-sorter chart to be of importance. When holes in the upper and lower tape sections passed simultaneously through the beam the photo-cell fired a stroboscope lamp, which caused the instantaneous readings of the two wave number dials corresponding to the upper and lower holes to be photographed, as in Fig. 7. Thus the wave numbers of all pairs of lines in the list having the desired interval could be recorded in a few minutes, the process being then repeated for

* Based on an address given at the presentation of the Frederic Ives Medal at the Thirty-Fourth Annual Meeting of the Optical Society of America, Buffalo, New York, October 28, 1949.

† Numbered references enclosed in brackets are to the Bibliography of publications immediately preceding this article.

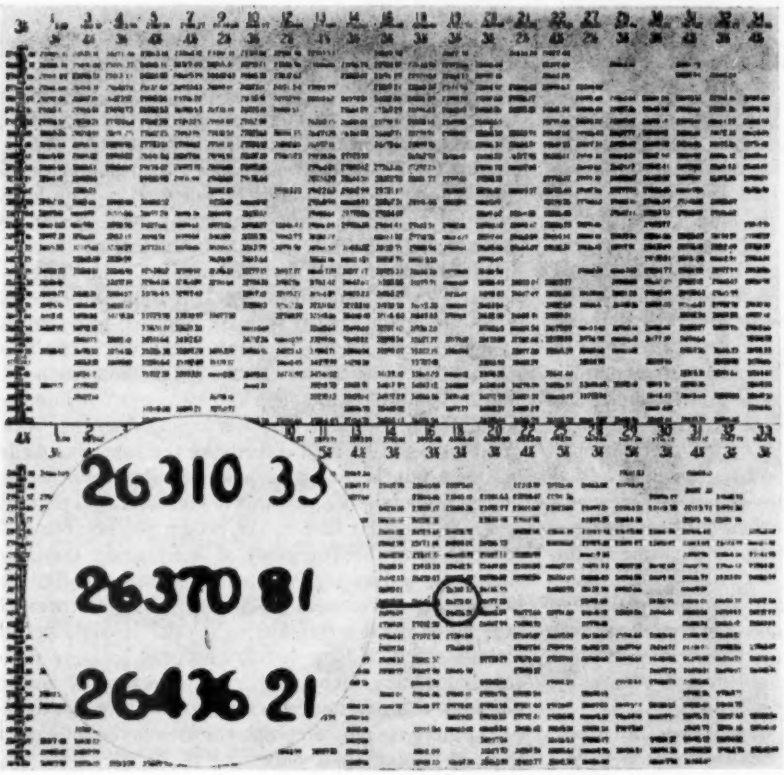

FIG. 1. A portion of a typical quadratic array for a rare-earth atom, with columns representing upper energy levels and rows representing lower levels. Obtaining such an array for as many lines as possible represents a first step in an analysis of the spectrum.

the other differences shown by the interval sorter to be important for study.

These two devices were applied to the analysis of the spectra of Ce II [41, 70], and several other complex atoms; however, it soon became evident that more precise wave-length values were required if the Ritz Combination Principle was to be used for the analysis of such complex spectra. Accordingly, we proceeded on a program of wave-length measurements.

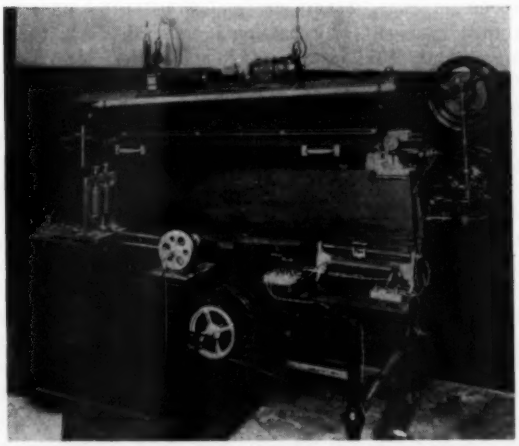

FIG. 2. The spectrum interval sorter (background) with the magnetic punch for producing wave number tapes (foreground). Any desired length of loop can be accommodated between the upper and lower tape sections, to provide for recording intervals in any desired wave number range.

In the Spectroscopy Laboratory at the Massachusetts Institute of Technology a 10-meter concave grating ruled by Wood at Johns Hopkins was set up in a Paschen-Runge mount [27, 56, 61]. A portion of this is shown in Fig. 8. With this spectrograph hundreds of exposures were made to the spectra of atoms not yet classified; a short section of a typical spectrum is shown in Fig. 9. The problem of measurement was to determine the center of density of each line, to a precision of one-sixtieth of the width of the narrowest, and to reduce this to wave-lengths in angstroms according to a slowly varying non-linear relationship between position and wave-length, which relationship could be determined by measuring on the same plate the positions of standard lines of known wave-length.

Use of the ordinary spectrum comparator, with its poorly legible dial, to measure these plates was found to be tedious and slow, and it was obvious that many years would be required to make the measurements needed to analyze the remaining complex spectra.

Experiment showed that measurements could be greatly speeded up by using a projection system of setting on lines; then a system was devised whereby the dials of the engine could be made to read wave-lengths directly in angstroms rather than in millimeters along the plate. After this had been in use for a few months a photoelectric method of locating the density maxima of the lines to within one-sixtieth of their breadth was devised, and this was made to fire a strobolamp which photographed the rotating wave-length dials whenever a density maximum passed. In this way, through several intermediate models, the automatic comparator [31, 42, 64] shown in Fig. 10 was developed. With it as many as 2000 seven-figure wave-length measurements could be recorded from a 20-inch plate in 120 seconds. A short section of a typical record is shown in Fig. 11.

During the four years following the first successful operation of the automatic comparator some 20 million wave-length determinations were made with it. Two models were kept busy for several years providing films, principally for spectra of complex metallic atoms, which were reduced and averaged by WPA workers, and ultimately resulted in a long catalog of wave-lengths, many of which were published in the *M.I.T. Wavelength Tables* [50, 52, 58, 72]. An analysis of the results obtained with it indicated that the automatic comparator, besides vastly increasing the speed of measurement, also increased precision by a factor of from two to ten. This precision was ultimately found to be limited by the paucity and unsuitability of the iron lines which serve as international secondary standards of wave-length.

In the meantime availability of the new wave-lengths had made possible considerable progress in the analysis of rare earth spectra, and sufficient experience was obtained to make obvious the desirability of supplementing the Combination Principle with other criteria contributing to energy level classification. At this stage I was most fortunate in that my colleague, Professor Francis Bitter, became interested in producing intense magnetic fields, and designed for the Spectroscopy Laboratory a solenoid especially designed to give fields up to 100,000 oersteds for Zeeman effect work [60]. This magnet was immediately successful, and many hundreds of spectrograms have been taken with it of rare earth and other complex metallic spectra. The intense field was produced without iron by applying 170 volts to send 10,000 amperes through a 200-turn copper spiral cooled by 100 gallons of water per minute.

FIG. 3. Short section of 35-mm paper strip punched with round holes for fiducial marks and rectangular holes for the wave numbers of spectrum lines. Light passing through superposed holes as the tape sections pass through the sorter records wave number intervals on photographic paper.

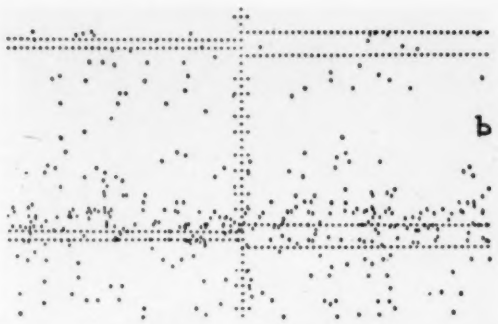

FIG. 4. Small section of a typical record from the interval sorter, in which wave number differences appear plotted horizontally against wave numbers vertically.

This magnet is shown in Fig. 12, with a water-cooled arc in place. An enlarged section of a typical Zeeman spectrogram is shown in Fig. 13, and Fig. 14 shows sections of traces of typical patterns as recorded by the automatic comparator.

The new Zeeman effect data quickly proved their value, and made it possible to break into a number of rare earth and other complex spectra not previously analyzed [65, 66, 70, 71, 75, 76, 80, 82]. A limitation, only now being removed, was the increase in arc excitation produced by the magnetic field, so that only lines from ionized atoms were observed. Its unique indication of the quantum numbers of the two parent levels of a given line makes Zeeman pattern study a tool of unexcelled power, and when taken in conjunction with the Combination Principle and improved wave-length data makes possible the immediate classification of almost any unknown spectrum.

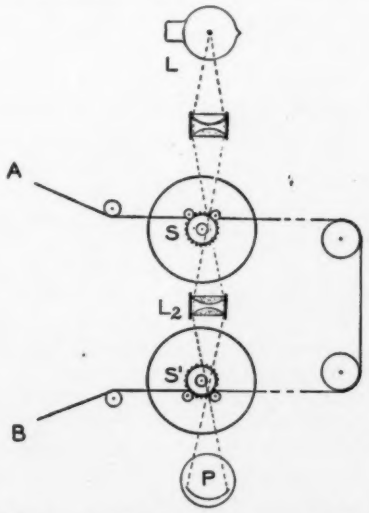

FIG. 5. Optical principle of the interval recorder, in which light passes through pairs of holes having the pre-set wave number interval, to fire a strobolamp and record the corresponding wave numbers.

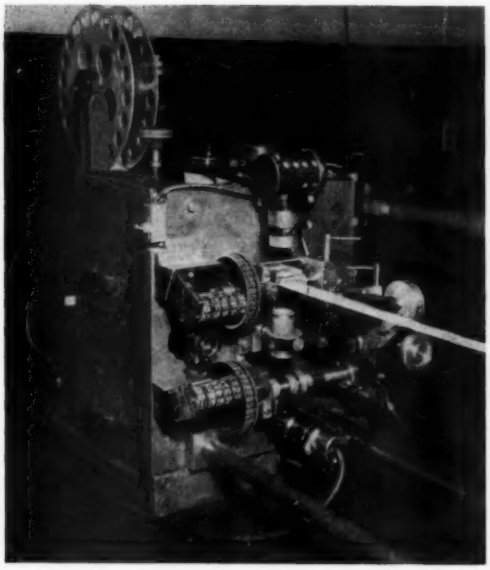

FIG. 6. The interval recorder.

Operation of the magnet was interrupted for some seven years by the war, and it was only put into operation again in 1948. Owing to internal corrosion its maximum field has fallen some 10 percent, but excellent

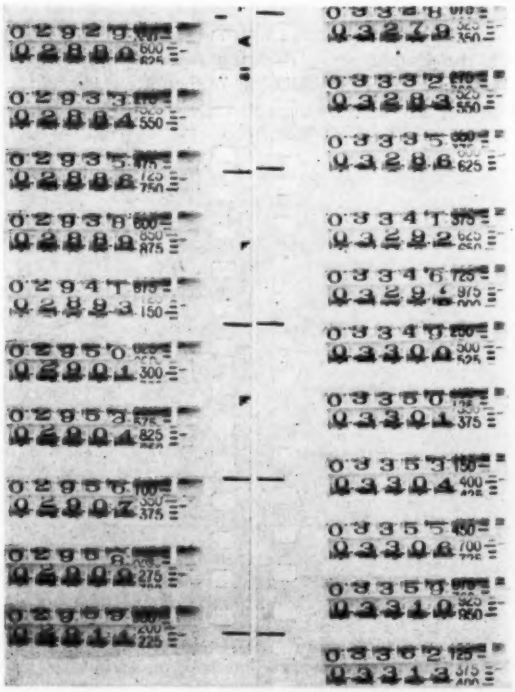

FIG. 7. Short section of a film record from the interval recorder.

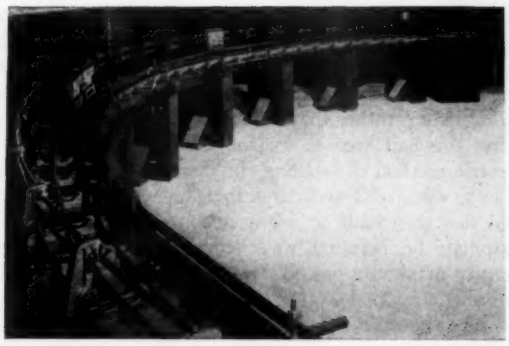

FIG. 8. A section of the plate-track of the 10-meter grating of the M.I.T. Spectroscopy Laboratory.

spectrograms are again being obtained with it. When used in conjunction with the 10-meter grating it has made possible an almost tenfold increase in precision of determining the Landé splitting factor g of an energy level.

Turning again to the improvement of wave-lengths, dependent as this appeared to be on having better sec-

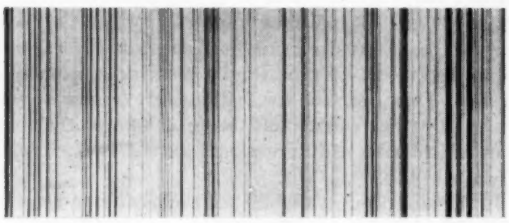

FIG. 9. Small section of a spectrogram from the 10-meter grating.

ondary standards, I studied the technique of taking spectrograms by crossing a Fabry-Perot interferometer with a stigmatic grating. It was soon apparent that the principal limitation of this method was the extreme complexity of the calculations needed to determine

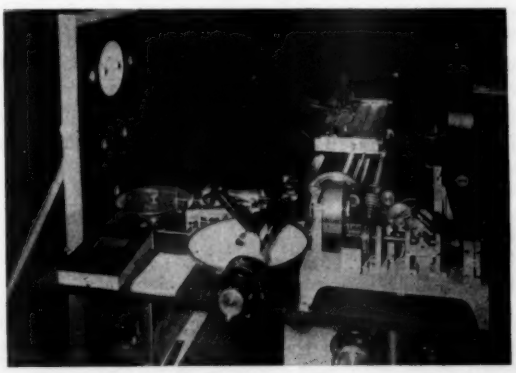

FIG. 10. The automatic comparator, from the operator's seat.

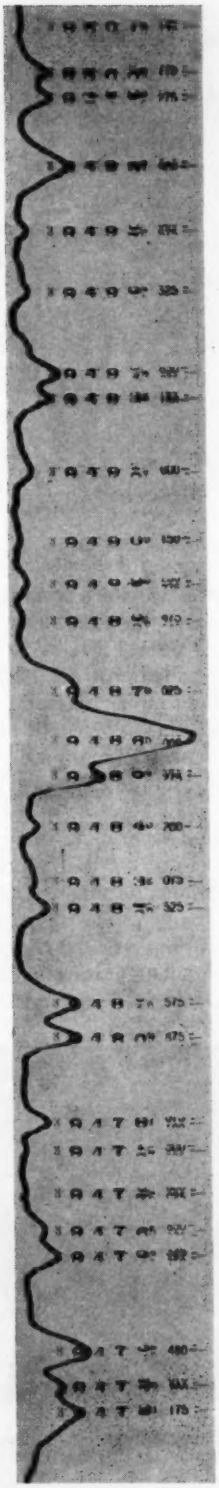

FIG. 11. Short section of a record from the automatic comparator, with wave-lengths automatically recorded on a density trace of the spectrogram.

FIG. 12. The Bitter 1700-kw electromagnet giving 100,000-oersted magnetic fields, with water-cooled arc in place.

wave-lengths from fringe diameters in the pattern. The mathematics of this reduction was then analyzed and was found to be simply susceptible to calculations made by means of gears, differentials, and integrators like those used in the automatic comparator, together with a few new principles such as the use of variable optical magnification for automatic three-figure multiplication. One of the automatic comparators was accordingly

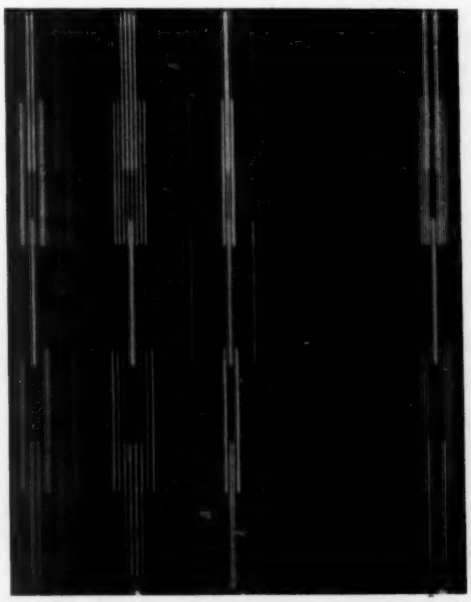

FIG. 13. Sections of a Zeeman spectrogram for rhodium.

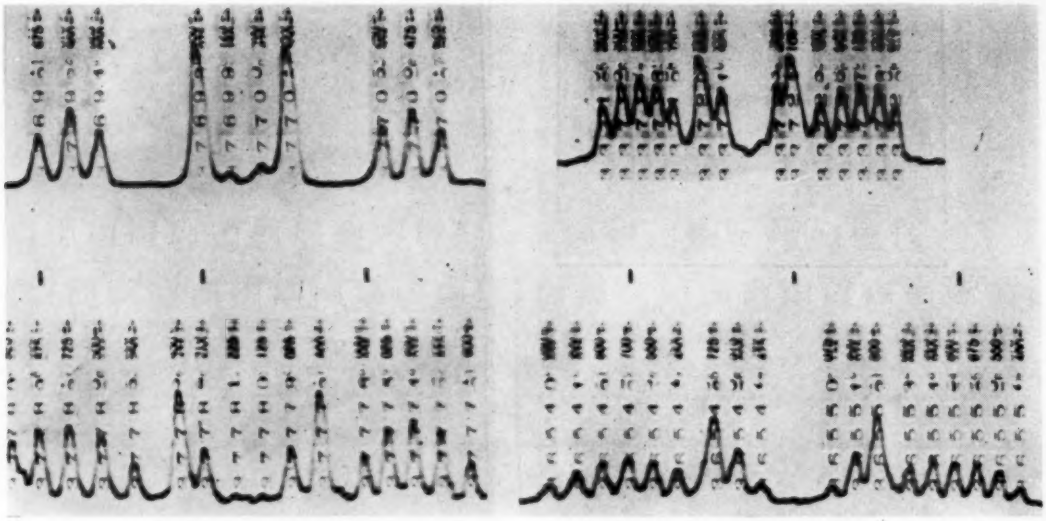

FIG. 14. Sections of typical records of Zeeman patterns made with the automatic comparator.

modified and extended to become the Winmac (wave-length interferometric measurement and computation) shown in Fig. 15 [84]. In tests against orthodox methods it was found that with this device hundreds of patterns on a single plate could be reduced in the time previously taken for one, with some accompanying increase in precision, provided three lines whose wave-lengths were known were photographed on each plate. Sufficiently precise wave-lengths are now available from mercury 198, neon, and krypton to furnish such intermediate standards.

Recently the Winmac has been provided with an electronic scanning arrangement which records the peak position of each fringe, thus increasing the precision further and making possible determinations to about 0.003 order. The Winmac is now being readied for what it is hoped will be an extensive series of wave-length determinations of intermediate wave-length standards in cerium, thorium, and other elements.

At the time when it seemed possible to make a post-war return to an integrated program, higher resolution appeared desirable both in our magnetic spectrograms and in those designed for wave-length measurements. Many Zeeman patterns of importance remained unresolved, and it seemed unlikely that stronger magnetic fields would soon be available. Also it was theoretically possible to make wave-length measurements with a 10-meter grating precise to 0.001A, yet seldom was a single pair of measurements consistent to closer than 0.005A, because of changing line shape with density induced by the optical imperfections of the grating.

The problem of obtaining gratings of better groove form and having resolving power greater than the

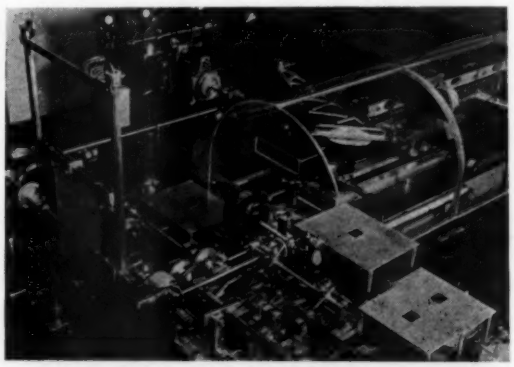

FIG. 15. The Winmac, arranged for the automatic reduction of Fabry-Perot spectrograms with electronic fringe location.

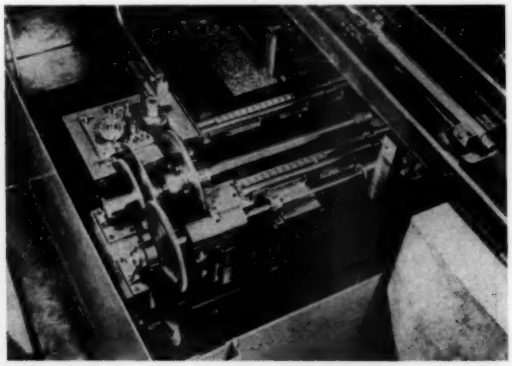

FIG. 16. A portion of the Michelson ruling engine at M.I.T. The scale is indicated by the fact that the screw is 3.5 inches in diameter.

FIG. 17. Diagram showing the mode of illumination of an echelle.

200,000 we had available over the range 2000 to 10,000A seemed too great for direct attack, but late in 1947 we were presented by the University of Chicago with a large partially completed ruling engine [93], begun by Michelson in 1900 and several times rebuilt. It contained an excellent screw having 20 inches of thread, and if it could be put into operation might possibly rule gratings up to 13 inches in width. A section of the partially reassembled engine is shown in Fig. 16.

Prior to completing this engine it seemed desirable to undertake an extensive study of previous attempts at grating ruling, and this was done [93]. At the same time, further consideration was given to the realization that a most useful type of interferometer would be one in which the orders used were higher than the first to fifth, as in the case of diffraction gratings, and lower than the 30,000 or higher used with the Fabry-Perot etalon and the reflection echelon. Orders between the 500th and 2000th seemed especially useful, and consideration of methods to make them available resulted in the design of the "echelle" [94].

In setting up the Michelson ruling engine I was determined not to spend the remainder of my life bumping against the same difficulties that had defeated other workers who had spent so much time in attempting to rule gratings of resolving power greater than 400,000. Our problems, while as great, could at least be new ones. Accordingly it was decided to attempt the application of interferometric control to the ruling engine. A double attack was decided on; first, to develop improved methods of calibrating the screw by means of interference fringes; second, to use fringes directly for groove-spacing control. It was decided to build the engine so that it could be used both for the ruling of ordinary gratings, and for the production of echelles.

The main requirement of the echelle, whose mode of illumination is shown in Fig. 17, is that one face of each step-groove be smooth and accurately positioned to within one-twentieth of the wave-length of the light being analyzed by it. Only from 100 to 500 grooves need be produced per inch. Theoretically, then, an entire echelle can be ruled within a few hours, which greatly improves the feasibility of interferometric control.

After the theory of the echelle had been worked out, based on that of the reflection echelon, numerous new advantages became apparent. Designed to be crossed with an ordinary small stigmatic spectrograph, the echelle should give resolution approaching one million, dispersion equivalent to that of the most finely ruled grating, the speed and compactness of a small spectrograph, and freedom from the curse of light-wasting astigmatism.

The properties of the echelle were discussed before various local optical groups late in 1948. The Bausch and Lomb Optical Company immediately put a small group to work to attempt the production of echelles, and just a year later were able to hand me a six-inch echelle having resolving power, dispersion, and other properties superior to those of any diffraction grating previously available to me. With a ruling engine designed by David Mann of Lincoln, Massachusetts, David Richardson and Gilbert Sheldon of Bausch and Lomb during the past year have produced a series of echelles, each better than the last. Figure 18 shows the degree of concentration of light of Hg 5461A in the 400th order of echelle No. 11, which contains one-third of the total input intensity; the two neighboring orders together contain

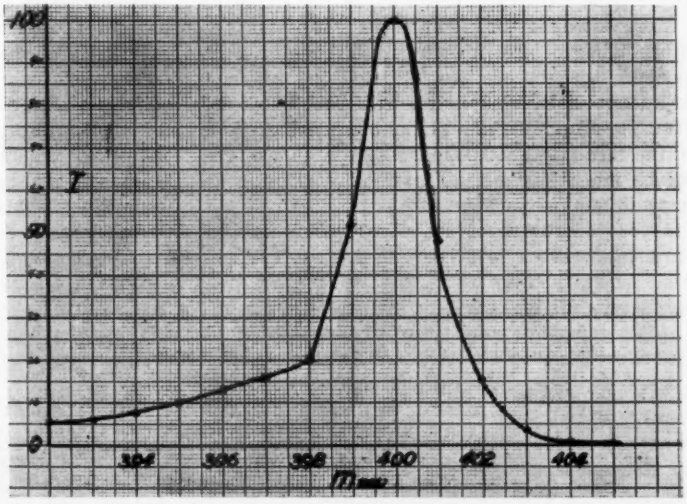

FIG. 18. Measured intensity distribution of Hg 5461 in various orders of an echelle between 393 and 404.

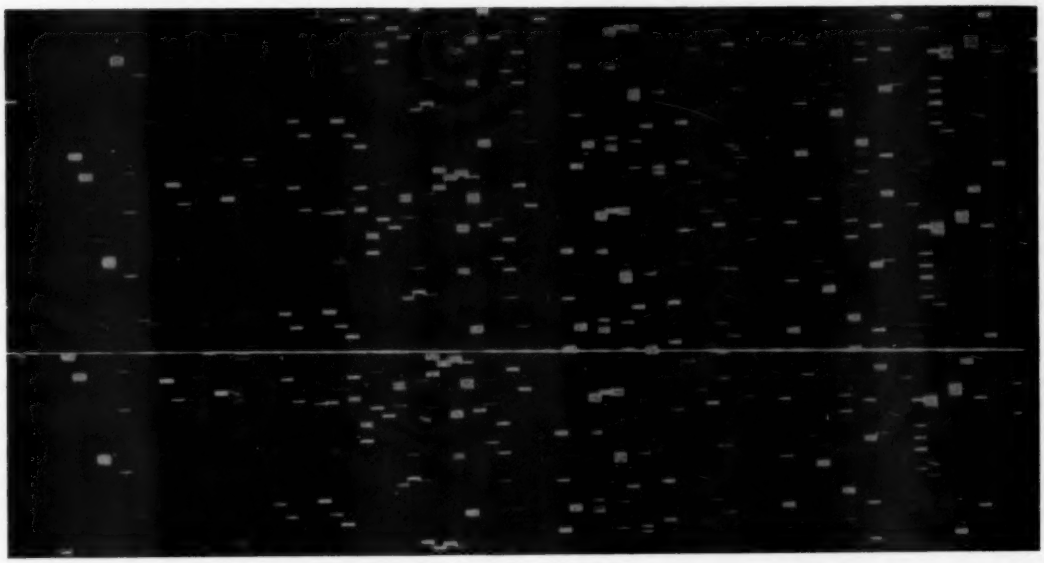

FIG. 19. A portion of the iron spectrum between 3600 and 4400A as obtained by crossing a Bausch and Lomb echelle with a quartz Littrow spectrograph. Several vertical echelle cycles are shown, and the orders used vary from the 570th at one end of the plate to the 695th at the other. The horizontal streak arises from light directly reflected from the back of the prism, which serves as a fiducial mark.

another third; the remaining light is distributed among the remaining 401 orders. Still more light will be concentrated in the desired orders when the step-face can be kept flatter. It should be emphasized that the concentration of light is in direction rather than in order, so that light of half the wave-length will be found concentrated in the 800th order, etc.

A portion of the iron spectrum photographed with echelle No. 13 placed behind the quartz prism of a Bausch and Lomb large Littrow spectrograph from which the reflecting coating had been removed is shown in Fig. 19. Only some two inches of the aperture of the six-inch echelle was used, instead of the full 2.7 inches that was available at 63° illumination. The hyperfine structure of Hg 5461 was clearly resolved into seven components with echelle No. 12, and the resolving power measured by this means appeared to exceed 300,000. The cause of the lowering of resolving power below the theoretical 500,000 at 5000A is known, and should be much less difficult to remove than in an ordinary diffraction grating.

It is my present hope to obtain a 10- or 12-inch echelle, which I plan to cross simultaneously with three prism spectrographs covering the ranges 2000–3200A, 3000–5200A, and 5000–10,000A, respectively. This will be used with the Bitter magnet to resolve Zeeman patterns which at present resist separation, and to determine wave-lengths at double the dispersion and resolving power previously available. It is expected that line shape will be greatly improved over that obtained with present gratings, and that the Winmac can be modified to permit rapid automatic scanning of the cycles of an echelle spectrogram to give wave-lengths precise to 0.001A or better for all but the broadest lines.

With the improved wave-lengths and atomic splitting factors then to be available it is hoped that the spectra of the remaining complex atoms can be analyzed and the relevant atomic perturbations determined, so that the attack on intensity relationships begun so many years ago can be more intelligently and effectively resumed.

Variation of Visual Acuity with Various Test-Object Orientations and Viewing Conditions*

G. C. Higgins and K. Stultz
Kodak Research Laboratories, Eastman Kodak Company, Rochester, New York
(Received December 12, 1949)

Visual acuity was measured in terms of the reciprocal of the angle in minutes subtended by the individual lines in a parallel-line test object at the limit of perception of the lines when the observer was allowed to see the target for less than one millisecond. Visual acuity, measured with the lines passing either vertically or horizontally through the visual field, was found to be approximately 20 percent higher than when measured with the lines passing diagonally through the visual field at angles of 45 and 135 degrees with the horizontal. These results indicate that the variation in the visibility of a parallel-line test object as a function of its orientation is not produced by preferential directions for eye movements. The variation of visual acuity with test-object orientation was also measured as a function of pupil diameter and fixation point, but these data do not give any conclusive evidence as to the factors producing the variations.

INTRODUCTION

A HIGHER visual acuity is obtained from measurements with a parallel-line test object when the lines are vertical or horizontal than when they pass diagonally through the visual field.[1] It has been suggested[2] that this variation in the visibility of parallel lines as a function of their orientation may be explained by assuming that the eye acts as a sphere held in orientation by two pairs of elastic muscles, and that the eye movements produced by these muscles are damped by viscous friction. With this dynamic system, an involuntary "jump" of the eye would be followed by damped oscillations which would lead to preferential vibrations in the horizontal and vertical planes. On assuming a dynamic theory of visual acuity,[3] these preferred directions of motion would lead to preferred directions for maximum visual acuity. If this explanation for the variation in visual acuity with the orientation of a parallel-line test object is correct, the effect should disappear when observation times are made sufficiently short. Consequently, to check this hypothesis, visual acuity was measured with various orientations of a parallel-line test object with less than one-millisecond viewing time.

EXPERIMENTAL PROCEDURE AND RESULTS

A print of a parallel-line test object was made on photographic paper. The individual black-and-white lines on the print were 0.4 mm wide and the entire circular test object was 5.5 cm across. This print was mounted in the center of a gray octagon, the parallel sides of which were 35 cm apart. The mounted print was placed in the center of the 280-cm-square front wall of an observation room. The area surrounding the print consisted of diffusing screens which were illuminated from behind by banks of lamps. The ceiling, the floor, and the two side walls of the observation room were white, and the back of the room was closed by means of a black drape. The observer was located at different distances from the test object, and, at the maximum viewing distance, the diffusing screens subtended a visual angle of approximately 70 degrees.

The diffusing screens, which surrounded the test object and filled the remaining area of the front wall of the observation room, were adjusted to a luminance of 2 ft.-L. With no additional room light, the observer was unable to detect the position of the lines in the test object. By means of a control switch, the observer could illuminate the test object by flashing a Kodatron Speedlamp. The total duration of the flash was less than one millisecond and 80 percent of the energy in the flash was delivered in less than one half of a millisecond. The average illuminance on the sample was 50,000 ft-c.

During the experiment, the experimenter oriented the parallel lines in the test object at one of four positions: vertical, horizontal, at an angle of 135 degrees with the horizontal, and at an angle of 45 degrees with the horizontal. The various orientations were presented in a random order, and, after flashing the lamp, the observer was required to designate the orientation of the test object as it appeared to him. While he was encouraged to give an answer if possible, he was allowed to state that no lines were visible if such a result were obtained. The observer was first stationed at such a distance from the test object that, during the flash, he was able to see all orientations of the pattern. The observation distance was then increased and a new set of readings were taken. This procedure was repeated, with the observation distance being increased by steps, until that distance was reached at which the observer was unable to determine the orientation of the lines in any position.

Each observer made 80 observations at those viewing distances for which the answers were not all correct. From these data the psychometric curves shown in Fig. 1 were obtained by plotting the frequency of perception of the individual parallel lines at each view-

* Communication No. 1305 from the Kodak Research Laboratories.
[1] G. C. Higgins and K. Stultz, J. Opt. Soc. Am. 38, 756 (1948).
[2] W. R. J. Brown, J. Opt. Soc. Am. 39, A1057 (1949).
[3] L. A. Jones and G. C. Higgins, J. Opt. Soc. Am. 38, 398 (1948).

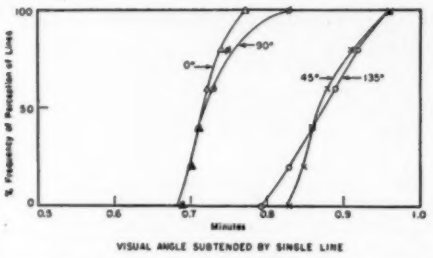

FIG. 1. Influence of the orientation of parallel-line test object upon the perception of the individual lines with a viewing time of less than 1 millisecond. Inclination of the lines with respect to the horizontal is shown on the curves.

ing distance against the corresponding angle in minutes subtended by a single line in the test chart. The data plotted in Fig. 1 represent the composite results for four observers. Additional readings were made by nine other observers, and, although insufficient data were taken to permit inclusion of these results with the quantitative data shown in Fig. 1, sufficient data were taken to show that, without exception, the observations for each individual observer were in qualitative agreement with those shown in this figure. The value of visual acuity, as measured with each orientation of the test object, was taken as $1/\alpha$, where α was the angle in minutes subtended by a single line in the test object, when the lines were just perceptible 50 percent of the time.

The values of visual acuity, as measured at the various orientations of the parallel-line test object for a viewing time of less than 1 millisecond, are shown in the first line of Table I. The values of α in minutes are shown in the second line of Table I, and the maximum percentage variation between the values of visual acuity is shown in the last column of the table. It is clear from Fig. 1 and Table I that the individual lines in the parallel-line test object are appreciably more visible when they are oriented either vertically or horizontally than they are when they pass diagonally through the visual field at an angle of either 135 degrees or 45 degrees with the horizontal. These results obtained with a short viewing time are in agreement with those reported previously[1] for observations made when the observer was allowed an unlimited time to state whether or not he could definitely perceive the individual lines in the test object. During the course of these investigations, more than 25 different individuals were employed as observers, and, without a single exception, each observer reported that the lines in the test object were more easily perceived when they passed through the visual field either vertically or horizontally than when they passed through the visual field diagonally.

The data given in Table I, as well as the data given in the previous report, are for binocular vision. However, as in the case of unlimited time of observation, these data for the 1-millisecond observation time were also found to represent quite well the results obtained by monocular observations.

Since even with the observation time of less than 1 millisecond, the vertical or horizontal lines are still more clearly visible than those passing diagonally through the visual field at an angle of either 135 degrees or 45 degrees with the horizontal, it appears that this phenomenon cannot be explained in terms of preferential directions for eye movements. In an attempt to find some other explanation for this phenomenon, the variation in visual acuity with test-object orientation was measured as a function of the pupil diameter of the observer. The conditions of observation and the method of taking data were the same as those described in our previous paper.[1] A parallel-line transparency was placed in a projector and an enlarged image of the test object was viewed on a rear-projection screen. The rear-projection screen, which has a diameter of 7.5 cm, was located in the center of the front wall of the observation room described earlier.[1] The luminance of the test field with no sample in place was maintained at 50 ft-L and the variation of the field surrounding the test object to a level of 16 ft-L, 2 ft-L, and, with the field surrounding the test object illuminated to a level of 2 ft-L, in the four corners only. The area illuminated in each of the four corners was a square approximately 55 cm on a side.

By means of a shutter, the observer was allowed to examine the image of the parallel-line test object for 1/25 second and was then requested to report the orientation of the lines. The observer was stationed at a constant distance of 200 cm from the front wall of the observation room, and the magnification of the image was varied in discrete steps from that value at which all orientations could be detected to that value for which no orientations could be determined. At each magnification, the sample was presented to the observer in a random order of orientations and from these data

TABLE I. Variation of visual acuity as measured with various orientations of a parallel-line test object. Measurements were made with a variable viewing distance and less than 1-millisecond viewing time.

	Inclination of parallel lines with respect to horizontal				Maximum variation, %
	0°	90°	45°	135°	
$1/\alpha$	1.37	1.39	1.15	1.14	
α	0.73	0.72	0.87	0.88	21

TABLE II. Variation of visual acuity as measured with various orientations of a parallel-line test object. Measurements were made with a constant viewing distance and 1/25-second viewing time.

Pupil diameter, mm	Visual acuity $1/\alpha$ Inclination of parallel lines with respect to horizontal				Maximum variation %
	0°	90°	45°	135°	
3.0	1.75	1.72	1.59	1.49	12.7
4.0	1.36	1.41	1.34	1.30	4.9
5.5	1.32	1.36	1.30	1.30	3.2

psychometric curves similar to those shown in Fig. 1 were obtained. The average results for two observers are shown in Table II. It is clear from these data that, for these two observers at least, the smaller the pupil diameter, the greater was the observed maximum variation in visual acuity between the values measured with the parallel lines passing through the field horizontally or vertically, as compared with these lines passing through the field diagonally at an angle of 135 degrees or 45 degrees with the horizontal.

It is reported by Zoethout[4] and Duke-Elder[5] that the optical axis of the eye is located approximately 5 degrees temporally and 3½ degrees downward from the visual axis. Since images formed off the optic axis are subject to many aberrations, a fixation point was placed in the visual field at such a position that the image of the parallel-line test object would fall upon the optic axis rather than upon the visual axis. Using the variable magnification method as described, measurements were made of visual acuity with various orientations of the parallel-line test object. The time of observation was 1/25 second, in order to assist the observer in holding fixation. All observations were made by monocular vision employing the right eye, and with a fixation point 5 degrees to the left and 3½ degrees upward with respect to the test object as seen by the observer. It was found that, for each of four observers, the visual acuity measured with the lines passing through the visual field either vertically or horizontally was higher than that measured with the lines passing through the visual field at an angle of either 135 degrees or 45 degrees with the horizontal. However, the increased visibility of the lines passing diagonally through the visual field at an angle of 135 degrees with the horizontal, compared with the visibility of the lines passing diagonally through the field at an angle of 45 degrees with the horizontal, was very pronounced. This difference in visibility between the two sets of diagonal lines was so pronounced that the fixation point was moved around the center of the test pattern at intervals of 45 degrees, the fixation point in all cases being about 5 degrees removed from the center of the test field. It was found that, irrespective of the position of the fixation point, those lines in the test field, which were parallel to the line joining the center of the test object and the fixation point, were clearly more visible than those lines which were perpendicular to the line joining the center of the test object and the fixation point.

[4] W. D. Zoethout, *Physiological Optics* (Professional Press, Inc., Chicago, 1947), p. 103.

[5] Duke-Elder, *Textbook of Ophthalmology* (Mosby, St. Louis, 1946), Vol. 1, p. 769.

CONCLUSIONS

Visual acuity measured with a parallel-line test object is appreciably lower when the lines pass through the visual field at an angle of either 135 or 45 degrees with the horizontal than when they pass through the visual field either vertically or horizontally. This effect persists essentially undiminished, even when the time of observation is less than one millisecond, and consequently it appears that it cannot be explained by preferential directions of eye movements.

The data on the variation of visual acuity with the orientation of the parallel-line test object as a function of pupil diameter and fixation point do not appear to give any conclusive evidence as to the factors producing these variations.

ACKNOWLEDGMENT

The authors would like to acknowledge the assistance of Mr. Walter R. J. Brown and Dr. David L. MacAdam, in obtaining these data.

Method of Colorimetric Integration Using Punched-Card Accounting Machines*

DAVID L. MACADAM
Kodak Research Laboratories, Eastman Kodak Company, Rochester, New York
(Received January 3, 1950)

When colorimetric specifications of a large number of samples need be computed from spectrophotometric data, an important saving of time can be realized by use of standard IBM punched-card computing equipment. The method employs weighted ordinates, and results for two light sources can be obtained with very little more expenditure of time than for one. The method is described, with detailed instructions for the machine operators.

THE use of punched-card accounting machines for colorimetric integration was mentioned first by Knudsen in 1942,[1] who referred to the determination by Nickerson of tristimulus values for 425 Munsell colors for each of four sources.[2] Further work has been done by Nickerson,[3] using the method suggested by Knudsen. This method is so useful when many examples are to be computed, especially when results are desired for more than one source, that the following description and details of procedure may be of value. In principle, this procedure is the same as that used by Knudsen, Nickerson, and their associates, who have encouraged this publication of an account of the method. Some details differ from their procedure and the following can be modified in accordance with equipment and ideas available elsewhere.

The procedure employs the weighted-ordinate method of colorimetric computations. Briefly, this involves the determination of the sums,

$$X=\sum T_\lambda \bar{x}_\lambda P_\lambda$$
$$Y=\sum T_\lambda \bar{y}_\lambda P_\lambda$$
$$Z=\sum T_\lambda \bar{z}_\lambda P_\lambda,$$

where the values of T_λ at equal intervals of wave-length are characteristic of each sample, and where the products, $\bar{x}_\lambda P_\lambda$, $\bar{y}_\lambda P_\lambda$, $\bar{z}_\lambda P_\lambda$, are tabulated at 10-m$\mu$ intervals in standard works on colorimetry.[4,5] The desired chromaticity coordinates are the ratios,

$$x=X/(X+Y+Z), \quad y=Y/(X+Y+Z).$$

Since Z, alone, is not used, fewer operations are involved if the sum $(X+Y+Z)$, which will be abbreviated S, is determined directly. Therefore, the procedure to be described evaluates the sums,

$$X=\sum T_\lambda \bar{x}_\lambda P_\lambda$$
$$Y=\sum T_\lambda \bar{y}_\lambda P_\lambda$$
$$S=\sum T(\bar{x}_\lambda P_\lambda+\bar{y}_\lambda P_\lambda+\bar{z}_\lambda P_\lambda),$$

and the ratios,

$$x=X/S, \quad y=Y/S.$$

The sums of the products of spectral transmittance (or reflectance) and the tristimulus values of the spectra of two sources can be formed simultaneously by a method of multiplication by addition. In the present work, thirty-one values of spectral transmittance (at 10-mμ intervals from 400 to 700 mμ) were used for every sample. The data for each sample were all rounded off to the same number of decimal places, such that the maximum value of transmittance was given to three significant figures. Each value of spectral transmittance was punched in a separate card, together with codes identifying the sample and wave-length.

Tristimulus values, $\bar{x}_\lambda P_\lambda$, $\bar{y}_\lambda P_\lambda$, and the sum of the tristimulus values, $\bar{x}_\lambda P_\lambda+\bar{y}_\lambda P_\lambda+\bar{z}_\lambda P_\lambda$, for the spectra of

TABLE I. Data cards.

λ	$1000T$	$\bar{x}P_s$	$\bar{y}P_s$	$(\bar{x}+\bar{y}+\bar{z})P_s$
400	605	108	2	623
410	665	329	9	1908
420	725	1238	37	7224
430	753	2997	122	17747
440	762	3975	262	24175
450	759	3915	443	24996
460	748	3362	694	23355
470	734	2272	1058	18302
480	716	1112	1618	12191
490	695	363	2358	7995
500	667	52	3401	6317
510	639	89	4833	6442
520	608	576	6462	7750
530	570	1523	7934	9845
540	526	2785	9149	12129
550	480	4282	9832	14200
560	428	5880	9841	15760
570	370	7322	9147	16489
580	306	8417	7992	16425
590	255	8984	6627	15621
600	209	8949	5316	14272
610	168	8325	4176	12503
620	129	7070	3153	10225
630	100	5309	2190	7499
640	78	3693	1443	5136
650	67	2349	886	3235
660	64	1361	504	1865
670	59	708	259	967
680	54	369	134	503
690	49	171	62	233
700	50	156	56	212
Check totals		98041	100000	316144

* Communication No. 1308 from the Kodak Research Laboratories.

[1] L. F. Knudsen, J. Am. Statistical Assn. 37, 496 (1942).

[2] Kelly, Gibson, and Nickerson, J. Opt. Soc. Am. 33, 355 (1943).

[3] Granville, Nickerson, and Foss, J. Opt. Soc. Am. 33, 376 (1943).

[4] D. B. Judd, J. Opt. Soc. Am. 23, 359 (1933).

[5] Committee on Colorimetry, J. Opt. Soc. Am. 34, 633 (1944).

the sources (adjusted so that the total of the values of $\bar{y}_\lambda P_\lambda$ is 100,000 as listed in references 4 and 5) previously punched in a set of 31 master cards, were automatically transcribed to all of the transmittance cards for the corresponding wave-lengths. The values of wave-length, transmittance and tristimulus values for I.C.I. source *C* punched in the transmittance cards for one of the samples are shown in Table I. Tristimulus values for as many as five sources can be punched in a single set of cards. The values for only two sources can be integrated at one time, however, so only the treatment of I.C.I. sources *A* and *C* will be mentioned in this paper. Only source *C* is illustrated in the example given in Tables I and II. Any other pair of sources might be chosen from the five punched in the cards. The tristimulus values given in references 4 and 5 for 380 mμ and 390 mμ were added to the values at 400 mμ and the total was punched in the master and transmittance cards for 400 mμ. Similarly, the values from 700 to 770 mμ were totaled and punched in the cards for 700 mμ. In effect, this assumes that the spectral transmittances of all samples are constant for all wavelengths short of 400 mμ and greater than 700 mμ. In the case of I.C.I. source *C*, this assumption results in an error less than 0.0001 in the tristimulus value for each (10-mμ interval) spectral transmittance that differs from the value at 400 mμ (or 700 mμ) by less than the amounts shown in Fig. 1.

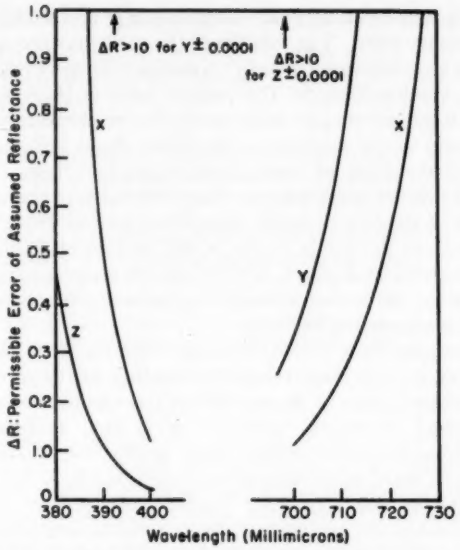

FIG. 1. Permissible errors of reflectances assumed for weighted-ordinate integrations using 10-mμ intervals, of such magnitude that each contributes an error of only 0.0001 to the designated tristimulus value (on the basis of $Y=1.0$ for perfect white). The assumption of constant reflectances equal to the values at 400 mμ and 700 mμ beyond those limits is shown to be adequate.

TABLE II. Progressive digiting method of colorimetric integration.

1000*T*, multiplier digits Hundreds	Tens	Units	Progressive totals $\Sigma\bar{x}P_e$	$\Sigma\bar{y}P_e$	$\Sigma(\bar{x}+\bar{y}+\bar{z})P_e$
		9	20902	14066	57135
		8	42738	36682	121639
		7	45139	40969	131191
		6	57453	59728	171936
		5	68475	68761	205307
		4	71116	69953	224112
		3	74113	70075	241859
		2	79449	70841	267899
		1†	79449	70841	267899
		0‡	*98041*	*100000*	*316144*
	9		3630	23580	79950
	8		46450	121900	221950
	7		171830	307140	536650
	6		335740	399520	1036680
	5		507030	475930	1637140
	4		542360	483490	1873020
	3		565970	542400	2120460
	2		735700	764200	2573840
	1		746820	780380	2695750
	0‡		*980410*	*1000000*	*3161440*
7			1887100	423400	12799000
6			2038800	2129900	15902500
5			2469600	3838200	18099900
4			3485800	5805500	21095900
3			5059700	7519400	24387300
2			6853000	8713700	27376600
1			8923400	9665600	30399300
0‡			*9804100*	*10000000*	*31614400*
Totals of progressive totals			34911764	42496156	164524917

† Since none of the values of transmittance in the present example ended with the numeral 1, no progressive-total card was obtained for that digit. The progressive digiting method depends upon having a complete sequence of progressive-total cards for all digits, from the maximum that occurs (7, in the final—(hundreds)—case), down to and including 1. Therefore, the totals for the preceding digit (2) are duplicated on a card representing each missing digit (1, in the example).

‡ The final totals for each sample, in each of the progressive digiting runs should be appropriate powers of ten times the totals at the bottom of Table II. However, the totals on zero-digit cards (shown here in italics) should be excluded from the final totals of the progressive totals.

The transmittance cards for each sample were sorted according to the last significant figure of the transmittance. The cards punched "9" were picked up first and placed ahead of those punched "8," and so on, in the reverse of the usual order of arranging sorted cards. An electric accounting machine was then used to print a table like the top nine lines of Table II, for each sample, and to punch new (summary) cards with those progressive totals of the tristimulus values and their sums, for the two selected sources. These progressive totals were taken, separately for each sample, at the end of each group having the same final significant figure in the value of transmittance, as shown in Table II. The effect of this procedure is to include the tristimulus values which should be multiplied by 9 in the totals punched in nine summary cards (discarding the final 0-card). The tristimulus values to be multiplied by 8 were likewise included in the totals punched in eight summary cards, and so forth. Occasionally, one or more values of the final significant figure did not occur among the transmittances for a certain filter (such as 1, in the example). Since no summary cards were punched for those figures, duplicates of the summary for the next higher multiplier value had to be prepared and inserted in the file of summary cards to fill in the sequence from the highest number that occurs down to and including 1. This was done by inserting blank

cards wherever numbers were missing in the file of summary cards. The total from the card that preceded each was then automatically transcribed (gang-punched) into the blank cards. The printed table of progressive totals indicated most conveniently where numbers were missing in the sequence of multiplier digits and facilitated the filing of blank cards to replace them. The final printed totals (usually for the 0 value of the controlling significant figure, shown in italics in Table II) should be the totals shown at the bottom of Table I. This provides a check against lost or incorrect transmittance cards and also against incorrect functioning of the accounting machine.

Keeping those for each sample together, the transmittance cards were resorted according to the second significant figure of the multipliers (transmittance) and arranged in reverse order, 9, 8, 7, etc., as before. Progressive totals, within each group, for a single sample, taken at the end of those punched 9, 8, 7, etc., in the second significant figure, were printed and punched in new summary cards, at locations one column to the left of the progressive totals previously obtained. In effect, this displacement multiplies all of the progressive totals by 10, in accordance with the position-value of the second significant figure. The numerical value of that figure governed the number of progressive totals (excluding that for 0) in which each tristimulus value was included. Duplicate cards were again supplied for missing numbers in each sequence of multiplier digits. Finally, keeping the cards for each sample together, they were rearranged in reverse order of the first significant figure. Progressive totals were printed and summary-punched, one column farther to the left, corresponding to the position-value of the first significant figure of the multiplier, 100 times the last figure and 10 times the second figure. Duplicate summary cards were prepared as before wherever numbers were missing in the sequence of multiplier digits.

The three sets of summary cards for each sample were then placed together, omitting all zero cards, and the grand totals of the progressive totals were printed as in Table II, and punched in a final set of summary cards. These were the desired sums of the products, $\sum T_\lambda \bar{x}_\lambda P_\lambda$, $\sum T_\lambda \bar{y}_\lambda P_\lambda$, $\sum T_\lambda (\bar{x}_\lambda + \bar{y}_\lambda + \bar{z}_\lambda) P_\lambda$, that is, the values, X, Y, and S, for the two sources. The chromaticity coordinates, x, y, were then easily found by dividing X by S and Y by S. These coordinates were punched in the final summary cards, and all of the values of X, Y, S, x, and y were then printed by the accounting machine.

The following detailed instructions can be followed by any operator of IBM accounting machines. If the requisite data for the samples, observer, and two sources are supplied, the results for 500 samples can be completed in about 40 hours.

APPENDIX I

Procedure for Colorimetric Integrations

1. Key-punch 31 master cards, X-34, wave-length in columns 5–7, $\bar{x}_\lambda P_a$ in 11–15, $\bar{y}_\lambda P_a$ in 16–19, $(\bar{x}_\lambda + \bar{y}_\lambda + \bar{z}_\lambda) P_a$ in 20–24, similarly for P_c in 25–38, similarly for three other sources, as desired, in 39–80.

2. Key-punch transmittance values (as many as 26 samples per set of 31 cards, with first two significant figures of wave-length in columns 1, 2).

3. Reproduce to make transmittance cards (31 per sample), identification in 1–4, wave-length in 5–7, T (or R) in 8–10.

4. Sort master cards ahead of transmittance cards on columns 7, 6, 5.

5. Gang-punch columns 11–80 from master cards to transmittance cards, control on X-34.

6. Sort transmittance cards on column 10, remove from sorter in reverse order (9's first, then 8's, etc.).

7. Sort on columns 4, 3, 2, 1. (File masters.)

8. Tabulate and summary-punch progressive totals of columns 11–15 and other fields as specified for P_a and P_c. Control on column 10. Print progressive card count. Clear all counters when 1–4 changes. Punch progressive totals with final figures in columns 19, 28, 37, 46, 55, and 64. Repunch columns 1–4, 10 in summary cards. Do not list separate transmittance cards.

9. Sort summary cards on column 10 to remove 0's. Keep others in original order. Sight-check 0-cards or check on collator or reproducer for equal punching in columns 11–64.

10. Sort transmittance cards on column 9. Remove from sorter in reverse order. Do this sorting by groups having same punching in columns 1–4.

11. Tabulate and summary-punch as in Step 8 but control on column 9. Punch progressive totals one column to left of positions used in Step 8. Repunch columns 1–4, 9 (not column 10).

12. Same as Step 9, but sort on column 9.

13. Same as Step 10, but sort on column 8.

14. Tabulate and summary-punch as in Step 8 but control on column 8. Punch progressive totals two columns to left of positions used in Step 8. Repunch columns 1–4, 8 (not columns 9 or 10).

15. Same as Step 9, but sort on column 8.

16. Insert blank cards having X-69 to fill in sequences in columns 10, 9, 8 as shown by the tabulations from Steps 8, 11, and 14.

17. Gang-punch everything from no-X masters to X-69 blank cards.

18. Hand-sort, or collate, three decks of summaries and new duplicates together on columns 1–4. Keep in order on columns 8–10.

19. List everything. Total and summary-punch fields 11–19, 20–28, 29–37, 38–46, 47–55, 56–64. Control on columns 1–4. Punch totals into same fields. Repunch columns 1–4.

20. Divide 11–19 by 29–37, punch first 4 decimal places in 65–68. Divide 20–28 by 29–37, punch first 4 decimal places in 69–72. Divide 38–46 by 56–64, punch first 4 decimal places in 73–76. Divide 47–55 by 56–64, punch first 4 decimal places in 77–80.

21. List.

Channeled Infra-Red Spectra Produced by Birefringent Crystals

JOSEPH W. ELLIS AND LEONARD GLATT
Department of Physics, University of California, Los Angeles, California
(Received December 6, 1949)

An infra-red absorption spectrum produced by a section of a birefringent crystal often has superimposed upon it a channeled spectrum when the beam is plane polarized, or is partially polarized. This channeling is absent when the electric vector E_i of the incident polarized beam parallels one of the principal index axes of the crystal, and usually appears with greatest visibility when E_i makes a $\pm 45°$ angle with such an axis. However, even in the latter instance, it does not occur provided the index axes in the crystal surface are parallel and perpendicular, respectively, to the plane of incidence of the dispersing prisms, unless there is some uncompensated optical rotation in the spectrograph system. The maxima and minima of the channeled spectrum are caused by a combination of a wave plate interference action within the crystal section and an analyzer action involving reflection losses at the prism faces. Optical rotation in the system also usually causes the visibility contrast between maxima and minima to vary, with one or more zero visibility positions resulting.

WHILE using plane polarized radiation to study near infra-red pleochroism as a part of our investigation of absorption spectra of certain organic crystals, we obtained some interference maxima and minima in our automatically recorded tracings. These were at first thought to be an ordinary Haidinger interference phenomenon, but computation revealed that the spacings between maxima were some twenty times too great to be produced by that effect. Actually they arose from wave plate interference action within the birefringent crystal plate being investigated.

In a well-controlled experiment these interference features do not appear. An attempt is usually made to have the two principal index axes in the crystal surface aligned vertically and horizontally, and to have the electric vector E_i of the incident plane polarized beam parallel to one of these axes. E_i then retains its direction during passage through the crystal. If, however, this vector makes an angle α with a principal index axis, the linear E_i vibration develops into an ellipse of gradually changing form and inclination as the crystal is traversed. For certain wave-lengths this vibration resumes its original azimuth upon emergence from the crystal. For other intermediate wave-lengths it emerges as a plane polarized vibration rotated through an angle 2α. The crystal is acting as a multiple whole wave plate and as an (odd) multiple half-wave plate, respectively, for these two sets of waves. These two types of waves may be designated by E_λ and $E_{\lambda/2}$, respectively. Thus in Fig. 1 principal index axes x and z make angles α respectively with the horizontal h and vertical v. E_i and E_λ are parallel to v, whereas $E_{\lambda/2}$ makes an angle $(90° - 2\alpha)$ with the horizontal. Plane polarization was accomplished by using a Glan-Thompson prism.

If the principal index axes of the crystal were vertical and horizontal and E_i should not coincide with one of these, and if the spectroscope should not have uncompensated optical activity in its prisms (or lenses, if present), no interference maxima and minima would occur. But if, as was the case in our experiment, E_i is horizontal or vertical and the crystal plate is rotated so that α is not zero, then maxima and minima do appear, i.e., a channeled spectrum occurs. This would be true even if there were no uncompensated optical rotation in the optical system. The reason for the above effect is as follows. The prism faces act as an analyzer of polarized light, as explained by Fresnel's equations, which are applicable to such faces. Those waves, for example, whose E_i vector makes the smallest angle with the horizontal (plane of incidence) are transmitted with the greatest intensity and form the maxima in the channeled spectrum. The E_i vectors of the waves upon which the crystal acts in whole wave plate and half-wave plate fashions make angles zero and 2α (or their complements) with the plane of incidence. The envelopes of the maxima and minima are essentially the tracings that would be made by removing the crystal plate from the beam and using polarized light with E_i vibrating at angle zero or 2α (or their complements), respectively. For this statement to be completely true correction would have to be made for reflection and absorption losses in the crystal.

Faces of the prisms other than the initial one contribute to the analyzer action and enhance the contrast between maxima and minima, i.e., they increase the visibility V. If there is optical activity in the prisms, rotation of E planes occurs, and because of the analyzer action of succeeding faces envelope curves alter, crossing each other one or more times. This means that maxima and minima disappear, and V equals zero, at such intersections.

After weak channeled spectra, formed as outlined above, were observed, some with enhanced visibility were produced by making α equal to 45°. In A and B of Fig. 2, are shown such spectra produced with β-succinic acid $(CH_2COOD)_2$ in which the hydroxyl hydrogen has been replaced by deuterium. The thickness of the crystal was approximately 0.2 mm. Its faces contained the a and c crystal axes (not mutually perpendicular) and the x and z principal index axes, with z nearly parallel to c. The birefringence is large, with indices for sodium light equal to 1.450 and 1.610 along x and z

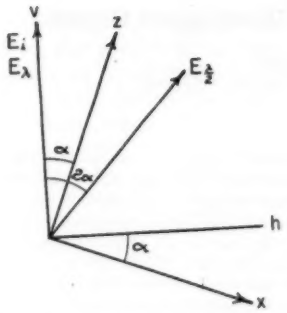

FIG. 1. Vibration direction diagram.

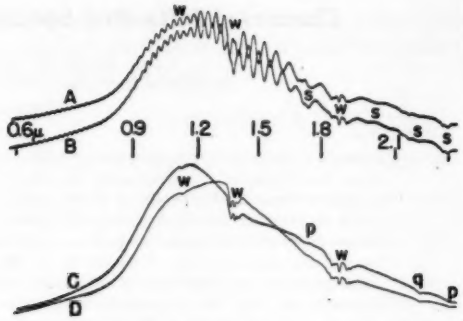

FIG. 2. A. Channeled spectrum produced by a 0.2-mm $b(010)$ section of $(CH_2COOD)_2$ crystal with $\alpha=45°$ (see Fig. 1) and E_i vertical. B. As in A but with E_i horizontal. C. Transmitted energy distribution with crystal section removed and E vertical. D. As in C but with E horizontal. s, p, q, w are absorption bands produced by crystal specimen, polarizing prism, quartz dispersing prisms and atmospheric water vapor, repsectively.

respectively. The envelopes of maxima and minima, when α equals 45°, are essentially the curves that would be produced without the crystal with E_i vibrating horizontally and vertically, respectively.

The recording spectrograph upon which the spectra were recorded has two prisms, one of right-handed and the other of left-handed, crystalline quartz. The light rays return through these prisms after reflection at a plane Wadsworth mirror. Since these rays do not traverse the prisms strictly at minimum deviation, there is a slight uncompensated optical rotation, which results in a $V=0$ position near 0.8μ. This wave-length position must represent an intersection of the two "true" corrected envelope curves, as explained above. However, the two curves shown in C and D of Fig. 2, taken without the crystal and with E_i vertical and horizontal, respectively, do not intersect at this wave-length position owing to accidental adjustment of intensity ordinates to unequal scales. Unsubstituted β-succinic acid $(CH_2COOH)_2$ was also studied but interference features were partly obscured by intense continuous absorption arising from hydrogen-bonded OH groups.[1]

Rotation of the Glan-Thompson prism, and hence of E_i, from the vertical to the horizontal causes an interchange of maxima and minima locations. This effect is clearly shown in A and B of Fig. 2.

The infra-red channeled spectra herein described are similar to some obtained in the visible by Sundararajan,[2] who used a different organic crystal, chrysene. In that instance the more widely spaced system of maxima and minima had superposed upon it another system of closely spaced Haidinger fringes arising from multiple internal reflections at the crystal faces. One system, in effect, modulated the other. In the records of A and B of Fig. 2, Haidinger fringes, had the crystal faces been regular enough to form them, would probably have been too closely spaced for the instrument to resolve, owing to the crystal thickness.

In Sundararajan's arrangement a polarizing prism analyzer was placed between the crystal and the spectrograph slit, with its vibration plane either parallel or perpendicular to that of the polarizer. Thus, the analyzer action did not arise naturally at the faces of the dispersing prisms, as it did in our experiment.

The results recall similar ones that sometimes occur when polarized visible and ultraviolet spectra are formed with a Hilger $E1$ quartz spectrograph.[3–5] In the Hilger instrument the relatively closely spaced maxima and minima arise as a consequence of the interference action of a 90° reflecting crystalline quartz prism in the optical system acting as a thick wave plate. The prism corresponds to the crystal specimen of the present experiment. The principal index axes of the prism were vertical and horizontal. Greatest visibility of fringes occurred when E_i made a 45° angle with the vertical. Optical rotation was necessary in the optical system; this resulted from the use of the thick crystalline quartz lens in the Littrow mounting. Zero visibility positions consequently also occurred.

Two practical applications exist of the type of channeled spectrum discussed in the present paper. The first is in the re-calibration of a spectrograph or in the transfer-calibration to another instrument. A crystal section, previously used to record such a spectrum with an already calibrated spectrograph, can be preserved and again used with the new, or newly-adjusted, instrument. A section of the inorganic crystal, sodium nitrate, should also serve well owing to its relatively large birefringence. The second application is in the alignment of a crystal section with respect to the polarizer. With proper alignment no fringes appear.

[1] L. Glatt and J. W. Ellis, J. Chem. Phys. 15, 880 (1947).
[2] K. S. Sundararajan, Indian J. Phys. 9, 141 (1934).
[3] J. W. Ellis and J. Kaplan, J. Opt. Soc. Am. 25, 357 (1935).
[4] G. Bolla, Nuovo cimento 12, 241 (1936).
[5] H. Yoshinaga, Japan. J. Phys. 12, 1 (1937).

The Spatial Photographic Recording of Fine Interference Phenomena*

ROBERT N. WOLFE AND FRED C. EISEN
Kodak Research Laboratories, Eastman Kodak Company, Rochester, New York
(Received December 8, 1949)

Interference bands as close together as 0.4μ were recorded with the Kodak Type 548 Spectroscopic Plates. The penetration of these bands into the emulsion layer was detected by microscopic examination of a vertical section of the photographic record. The photographic record of such bands, the spacing between which depends only upon the angular tilt of a Lloyd mirror and the wave-length of the radiant energy being used, should prove useful as a stage micrometer. Since these photographic records behave as diffraction gratings, the spacing between the band images was checked by measuring the diffraction angle, using radiant energy having a wave-length shorter than the spacing.

INTRODUCTION

IT was shown conclusively by Wiener,[1] in 1890, that standing waves of electromagnetic radiant energy can be produced. Shortly thereafter, Lippmann[2] developed a method of color photography based on the fact that these standing waves can be set up in a suitably transparent photographic emulsion in such a way that a series of laminar layers lying parallel to the emulsion surface are formed. Ives[3] obtained photomicrographs of cross sections of these laminae, which were separated by a distance of one-half the wave-length of the mercury green spectrum line, i.e., 0.26μ, by the expedient of swelling the sections with water after they were cut. In this way, the spacing is increased sufficiently so that the separate laminae can be recorded on a photo-micrograph.

These results indicate that photographic emulsions of the type used by Lippmann are capable of recording lines in which the spacing between them is as small as 0.26μ. Since "Lippmann" colors can be obtained on certain commercially available photographic materials, such as Kodak Type 548 Spectroscopic Plates, they likewise must be capable of recording lines as closely spaced as this. In practice, however, it is found that the spacing between the most closely spaced line-pattern which can be recorded by focusing an image of a subject onto this kind of photographic material with a large numerical-aperture microscope is approximately 1μ. Line-patterns much closer together than this cannot be recorded, because of the aberrations and diffraction effects occurring in this optical system and because the depth of focus is small compared to the emulsion thickness, the emulsion layers above and below the plane of best focus receiving out-of-focus images. If the lines of the pattern are separated by much less than 1μ, these aberrations, diffraction effects, and lack of depth of focus make it impossible to reproduce the lines photographically.

Since the standing waves or bands of radiant energy which form the closely spaced laminar layers just mentioned are an interference phenomenon, it should be possible to obtain laminar layers lying perpendicular to, rather than parallel to, the surface of the photographic emulsion by means of some type of interferometric technique. According to simple interferometric theory, the distance between such layers might vary from infinity to the distance between the layers formed by the standing waves, i.e., one-half the wavelength of the incident radiant energy. Thus, by an interferometric technique, it should be possible to obtain on the commercial photographic materials mentioned a photographic record which, when viewed normal to the emulsion surface, would appear as a pattern of equally spaced parallel lines, with a line spacing of considerably less than 1μ.

The Lloyd mirror is a convenient interferometer for obtaining such narrow bands of radiant energy. It is perhaps the simplest type of interferometer to set up and bring into adjustment. The distance between the bands of radiant energy which it produces is controlled by the angular tilt of a single mirror and the wavelength of the radiant energy being used. The irradiance distribution in a plane normal to these bands is accurately known.[4,5,†] This irradiance distribution is such that, at a small distance from the edge of the mirror, the ratio between the maximum irradiance of a band and the minimum irradiance in the space immediately adjacent to the band is nearly independent of the distance between bands. Thus, at a small distance from the edge of the mirror it is possible to irradiate two adjacent bands on the photographic film so that the ratio between the irradiance at the center of each of the bands to the irradiance midway between the bands is approximately the same value, whether the distance between the bands is a fraction of a micron or ten microns, for example. This is impossible with a microscope objective.

* Communication No. 1302 from the Kodak Research Laboratories.

[1] O. Wiener, Ann. d. Physik 40, 203 (1890).
[2] M. G. Lippmann, Comptes Rendus 112, 274 (1891).
[3] H. E. Ives, Astrophys. J. 27, 325 (1908).
[4] R. N. Wolfe and F. C. Eisen, J. Opt. Soc. Am. 38, 706 (1948).
[5] J. B. Green, J. Opt. Soc. Am. 7, 299 (1923).
† In the authors' paper (see reference 4) proper credit was not given to Green (see reference 5) for his analysis of the influence of slit width on the irradiance distribution in the Lloyd mirror interference pattern. His prior work is hereby acknowledged.

Interference patterns having various distances between bands were formed, by means of a Lloyd mirror, on Type 548 Spectroscopic Plates and on film coated with Type 548 emulsion, and the details of the resulting photographic records were examined and studied. It will be helpful to outline briefly the elementary theory of the Lloyd mirror before presenting the experimental procedure.

LLOYD MIRROR

Figure 1 illustrates the essential features of the Lloyd mirror. It consists of a plane front-surface mirror which forms a virtual image of the source of radiant energy, S_A, at S_B, S_A, and S_B, thus being coherent. Interference takes place between the radiant energy emitted by the source, S_A, and that apparently emitted by its image, S_B. The interference under consideration is that taking place at I in the plane p. The point, I, is at a distance, P, from the rear edge of the mirror. The distance between adjacent bands of the interference pattern is determined by the angle, θ, at which the mirror is

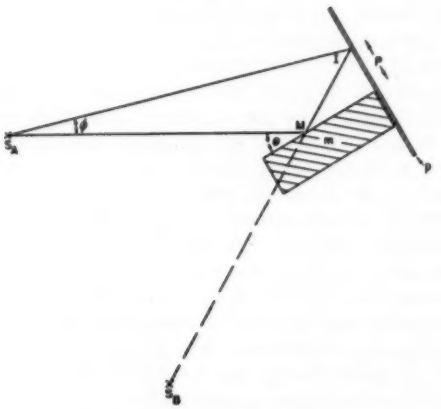

FIG. 1. Lloyd mirror.

tilted relative to a line joining the point of incidence, M, and S_A. Lines S_AI and S_AM diverge from S_A at an angle, θ, which, in practice, is small. Bands of radiant energy which are very nearly parallel with the surface of the mirror fall on plane, p, and are recorded in the manner to be described in the next section. Since the spectral band width and the slit width can be neglected in the present experiment, the distance between adjacent bands of radiant energy in the vicinity of I is given by the well-known expression:

$$S=\lambda/(2\sin\theta),$$

where S is the distance between the bands, λ is the wave-length of the radiant energy, and θ is the angular tilt of the mirror.

EXPERIMENTAL PROCEDURE

The Lloyd mirror used in this work was a front-surface aluminized mirror, approximately 50 mm in length and 20 mm in width. The mirror was oriented with the short dimension extending toward the source of radiant energy. This was a slit 12μ in width, irradiated with a high pressure, Type H-6, air-cooled mercury arc. The radiant energy was filtered to obtain a spectral band in the neighborhood of the 5461A mercury line. Spectrally homogeneous radiant energy could not be obtained because of the pressure broadening of the lines. The effect of elliptical polarization on the energy distribution in the interference pattern was reduced to a minimum by polarizing the radiant energy normal to the mirror surface with a sheet of Polaroid film placed between the mirror and the mercury arc. It was approximately 700 mm from the arc to the position near the rear edge of the mirror, where the interference patterns were obtained. The distance between the lines in the patterns was controlled by the tilt angle of the mirror.

Photographic records were obtained on Type 548GH Spectroscopic Plates for a number of different line-spacings. The minimum spacing which was recorded and observed by visual examination of the photographic record with a microscope was 0.4μ. Since this line-spacing was too small to be reproduced satisfactorily for illustration in this paper, a slightly wider line-spacing was selected (0.5μ). A photo-micrograph of this record is shown in Fig. 2(a).

This same record is shown in Fig. 2(b), but with the detail of the grain pattern along the length of the lines purposely made out of focus to show the line structure more clearly than is shown in Fig. 2(a). This was done by introducing a cylindrical lens into the optical system used for making the final enlargement from the photomicrographic negative. The cylindrical lens was oriented so that its axis was perpendicular to the line-pattern, thus making the grain structure along the length of the lines out of focus.

In order to see if these bands projected into the emulsion normal to its surface, a Type 548-O emulsion was coated on film base so that vertical cross sections could be readily obtained. This coating, originally made for another purpose, was especially thin (2.5μ) and was only blue-sensitive (Class O). These features, however, had no connection with the present experiment, except that 0.54μ mercury radiant energy could not be used for exposing because the emulsion was not green-sensitive. Instead, 0.36μ ultraviolet mercury radiant energy was used, and the mirror was set at the proper angle to give a line-pattern having a spacing of 0.5μ. A photo-micrograph of a vertical cross section of a photographic record having this line-spacing is shown in Fig. 3.

The photo-micrographs in Figs. 2 and 3 demonstrate that a three-dimensional record of interference phenomena can be obtained with the Type 548 Spectroscopic Plates, in which the interference bands are as close together as 0.5μ. It should be possible, by means of microscopic examination of cross sections of the more

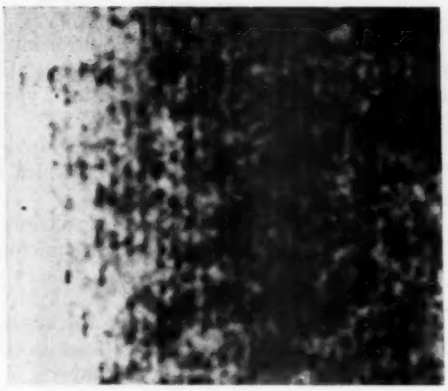

FIG. 2(a). Record of interference pattern on Type 548GH plate. Distance between lines is 0.5μ.

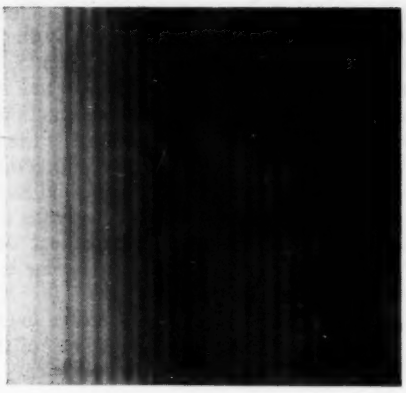

FIG. 2(b). Same record as shown in Fig. 2(a), but with a cylindrical lens introduced into the optical system used for making the final enlargement from the photo-micrographic negative. This lens is used to make the grain detail along the length of the lines out of focus.

closely spaced lines, to demonstrate that a three-dimensional record of interference bands separated by 0.4μ could be obtained, and even finer patterns could be observed and studied by other techniques, such as ultraviolet or electron microscopy.

USE OF A PHOTOGRAPHIC RECORD OF INTERFERENCE BANDS AS A STAGE MICROMETER

The stage micrometer is a scale, usually not over 2 mm in length, which has a short section divided into 10-μ intervals. The primary use of this device is for the calibration of the eyepiece scale of a microscope in order to make microscopic measurements in absolute units. The bands in the Lloyd mirror interference pattern, which are uniformly spaced, can be separated by any specified distance, ranging from distances of the order of tenths of a millimeter to fractions of a micron, depending upon the angular tilt of the mirror and the wave-length of the radiant energy which is used for obtaining the interference pattern. Thus, an interference pattern can be set up having spacings between the successive bands of, for example, 10μ, with an uncertainty in the spacings of not more than one percent, because it is determined by λ and θ, λ being known at least to one part in 10^5 and θ being known to within one percent. Thus, a photographic record of such an interference pattern has the essential attributes of a stage micrometer, namely, it consists of a series of very fine lines which are precisely and accurately separated by a known spacing.

Also, S can be conveniently checked by making use of the fact that such a record of interference lines will behave as a diffraction grating. It has been known for some time that a photographic record of interference lines would behave as a grating, and recently Hopkins and Clapper[6] made small gratings in this way. In accordance with the simple theory of the diffraction grat-

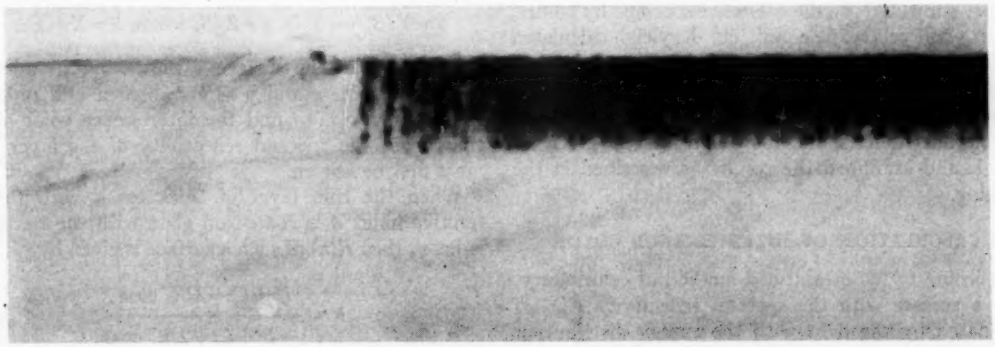

FIG. 3. Vertical section across interference pattern on Type 548-O film. Distance between lines is 0.5μ.

[6] R. E. Hopkins and F. R. Clapper, J. Opt. Soc. Am. 38, 661 (1948).

ing, if radiant energy of wave-length, λ, is incident on such a record, the energy will be diffracted by the line-structure at various angles depending upon S, provided that λ is less than S. Now, λ is known to a small fraction of one percent, and the angle of diffraction can be determined on a spectrometer table to less than 0.1 percent. Thus, by measuring the angle of diffraction of radiant energy from a known spectral line and making use of the well-known grating equations relating angle of diffraction to line-spacing, an independent determination of S can be made, in which the error is not more than 0.1 percent.

Such a photographic record of interference lines, in which S has been determined by one or both of these methods, should be useful as a stage micrometer.

SUMMARY

1. Photographic records of Lloyd mirror interference bands were obtained, in which the distance between adjacent bands was as small as 0.4μ using Type 548GH Spectroscopic Plates.

2. A vertical cross section of a photographic record of interference bands was obtained, in which the distance between adjacent bands was 0.5μ.

3. It is suggested that a photographic record of interference bands should be useful as a stage micrometer.

ACKNOWLEDGMENT

The authors wish to acknowledge the assistance of Mr. R. P. Loveland, of these Laboratories, in obtaining the photo-micrographs shown in this paper.

JOURNAL OF THE OPTICAL SOCIETY OF AMERICA VOLUME 40, NUMBER 3 MARCH, 1950

On the Interference Color of Thin Layers on Glass Surface

HIROSHI KUBOTA

Department of Applied Physics, 2nd Faculty of Engineering, Tokyo University, Tokyo, Japan

(Received November 17, 1949)

To effect the precise examination of the interference colors of thin layers, the author calculated them in cases of non-reflecting layers and Newton's rings, and plotted the results on the I. C. I. graph. The significance of several results indicated by the graphs is discussed.

I. INTRODUCTION

ALONG with the recent development of the study and industrialization of non-reflecting layers, the determination of the thickness of thin layers by observing their interference color has been more and more employed, as the most simple and sufficiently accurate method. Newton studied the interference color of a thin layer illuminated by white light in case of the Newton's ring[1] and there are some other records of experimental researches. But their descriptions, however, are very subjective, as the colors are specified by names, such as vivid yellow, pale pink, etc. Rayleigh calculated some interference colors, using Maxwell's result of measurements of colors.[2]

The author has calculated interference colors using the colorimetric data and coordinate system given by I. C. I. and examined the results as described in the following.

2. CALCULATION OF INTERFERENCE COLOR

According to the established method of colorimetry, when a surface with the spectral reflectivity $R(\lambda)$ is illuminated by the light with the energy distribution $E(\lambda)$, the color of the reflected light is given by the following tristimulus values,

$$X=\int E\cdot\bar{x}\cdot Rd\lambda,\ Y=\int E\cdot\bar{y}\cdot Rd\lambda,\ Z=\int E\cdot\bar{z}\cdot Rd\lambda. \quad (1)$$

In the above, the integration must cover the entire visible spectrum, and $\bar{x}$, $\bar{y}$, $\bar{z}$, are the three stimulus values of the spectrum. Normalizing them, we get the following chromaticity coordinates,

$$x=X/S,\ y=Y/S,\ z=Z/S,\ \text{where } S=X+Y+Z.$$

The color of the surface is shown by the point on the graph with x and y as its abscissa and ordinate, respectively. So, to find the interference color of the thin layer, the spectral reflectivity of the layer $R(\lambda)$ must first be known.

When the thin layer of thickness d with the refractive index n is coated on glass with the refractive index n_g then $R(\lambda)$ of such a surface is given by

$$R=\frac{B^2+C^2+2BC\cos\delta}{1+B^2+C^2+2BC\cos\delta}, \quad (2)$$

where B and C are the reflectivity of the upper and lower boundaries of the layer. In case of perpendicular in-

[1] I. Newton, *Optics* (G. Bell and Sons, London, 1931), p. 208.
[2] Lord Rayleigh, Scientific Papers (University Press, Cambridge, 1886) Vol. II, p. 498.

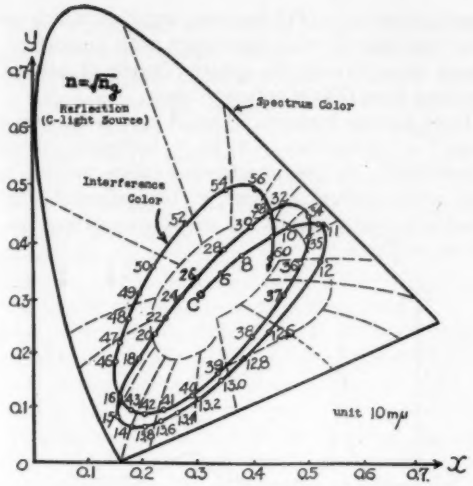

FIG. 1. Interference color in I. C. I. diagram.

cidence $B=(1-n)/(1+n)$, $C=(n-n_g)/(n+n_g)$, and $\delta=(4\pi/\lambda)nd$ is the phase difference of the light waves reflected by these two surfaces.

When the refractive index of the thin layer satisfies the amplitude condition of non-reflection, that is $n=(n_g)^{\frac{1}{2}}$, then $B=C$.

If the squares of B and C are small compared with 1, formula (2) will become $R=4B^2\cos^2(\delta/2)$.

For the light source, we used the C light-source of I. C. I. We have integrated Eq. (1) numerically, considering n and n_g as constant (that is, neglecting the dispersion). The results are correct to 3 figures, which are sufficiently exact for practical uses.

Figure 1 shows these results plotted on the graph taking nd as parameter (in units of 10 mμ).

3. THE COLOR OF NEWTON'S RING, ETC.

In case of the so-called Newton's ring, the interference is caused by a thin layer of air between the glass plates. Therefore

$$n=1, \quad C=-B \quad \text{and} \quad R=4B^2\sin^2(\delta/2).$$

The interference color is the complementary of that of the non-reflecting layer. This is shown in Fig. 2, where d is specified in 1 mμ units.

In case of non-reflecting layers for which $n\neq(n_g)^{\frac{1}{2}}$ the formula (2) becomes, assuming the denominator can be put to 1,

$$R=4BC[\epsilon+\cos^2(\delta/2)], \tag{3}$$

where

$$\epsilon=\frac{(B-C)^2}{4BC}=\frac{(n^2-n_g)^2}{(n^2-1)(n_g-n^2)}.$$

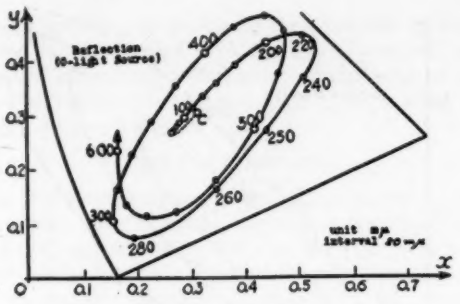

FIG. 2. Newton's ring.

Therefore, the tristimulus values (X', Y', Z') are

$$\begin{cases} X'=\epsilon\int E\cdot\bar{x}d\lambda+\int E\cdot\bar{x}\cdot\cos^2(\delta/2)d\lambda=a\epsilon+X \\ Y'=\epsilon\int E\cdot\bar{y}d\lambda+\int E\cdot\bar{y}\cdot\cos^2(\delta/2)d\lambda=b\epsilon+Y \\ Z'=\epsilon\int E\cdot\bar{z}d\lambda+\int E\cdot\bar{z}\cdot\cos^2(\delta/2)d\lambda=c\epsilon+Z, \end{cases} \tag{4}$$

where a, b, c are the tristimulus values of the light source and X, Y, Z are those of the reflected light when $n=(n_g)^{\frac{1}{2}}$.

From those equations, we get the chromaticity coordinates (x', y', z') as follows:

$$x'=\frac{a\epsilon+X}{k\epsilon+S}, \quad y'=\frac{b\epsilon+Y}{k\epsilon+S}, \quad z'=\frac{c\epsilon+Z}{k\epsilon+S},$$

where $k=a+b+c$. As the above equations represent a straight line on the I. C. I. graphs with parameter ϵ, the interference color for varying n will be given by

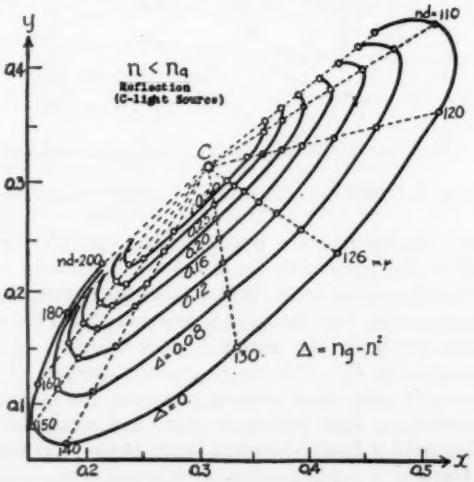

FIG. 3. Change of interference color with n.

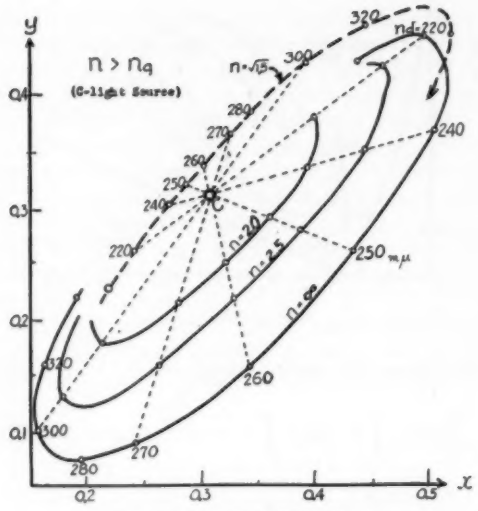

FIG. 4. Change of color with n.

the point on the straight line connecting the point showing the color of reflected light when $n=(n_0)^{\frac{1}{2}}$ (given by formula (4) by making $\epsilon=0$—call this point P) and the point showing the color of the light source (given by formula (4) by making $\epsilon=\infty$—call this point Q). Let the point given by (x', y') be R; then $\langle PQ\rangle/\langle RQ\rangle = 1+\epsilon(k/S)$.

From formula (3), it is evident that, when $n<n_0$ then $\epsilon>0$. Therefore $\langle PQ\rangle$ is always larger than $\langle RQ\rangle$,

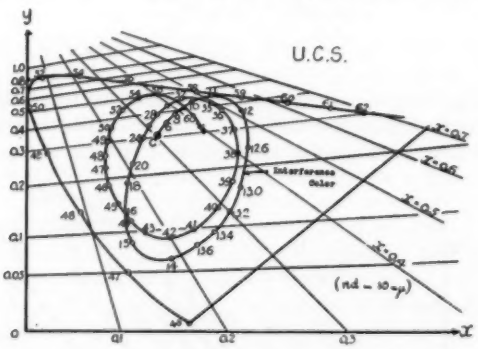

FIG. 5. Interference color in MacAdam's U. C. S. diagram.

which means that the point showing the interference color of the layer with $n=(n_0)^{\frac{1}{2}}(\epsilon=0)$ is remotest from Q. So the color is most vivid, having the largest degree of saturation. And the more it gets away from the condition $n=(n_0)^{\frac{1}{2}}$, the nearer it approaches Q on the straight line PQ. This means gradual decrease of the degree of saturation without changing the dominant wave-length, thus becoming more and more dull in color, until it finally becomes white at $n=n_0$ as shown in Fig. 3.

When n becomes larger than n_0, ϵ assumes a large negative value, so $\langle PQ\rangle$ becomes negative, which means that the color is complementary with respect to the above case, having the greater degree of saturation, receding from Q as n becomes larger.

If we assume formula (3) valid even when n is very large,* ϵ approaches -1 as n increases; therefore $R\sim\sin^2(\delta/2)$. So the interference colors become more and more similar to those of the reflected light of Newton's ring. Results of the above procedure are shown in Fig. 4.

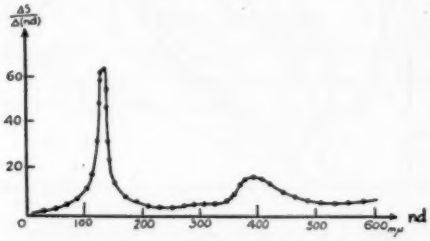

FIG. 6. Change of color sensitivity with nd.

4. ON THE SENSITIVE COLOR

The intensity of light through a thin plate of uniaxial crystal placed between parallel Nicol prisms is proportional to $\cos^2\delta$, where δ is the retardation between ordinary and extraordinary ray given during the passage through crystal. So when white light is passed through such a system, its color is also shown by Fig. 1. In this case, it is a well-known fact that, if adequate retarda-

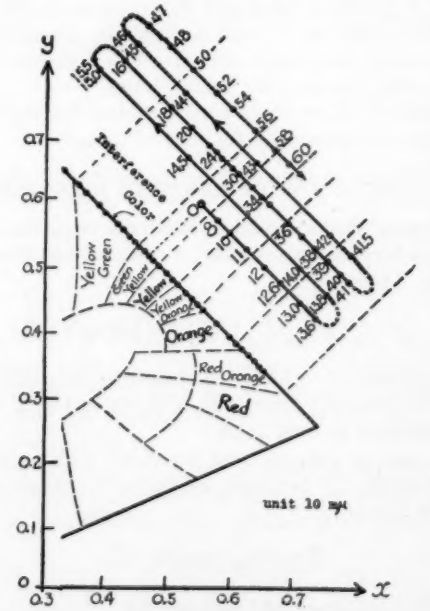

FIG. 7. Interference color with yellow light.

* Practically, when n becomes very large, B, C, etc., are not negligible compared with 1. So, this assumption is not admissible.

tion is given, there occurs a condition of most sensitive change of color with slight change of retardation. This is the phenomenon called "sensitive color," whose sensitivity can be given quantitatively by $\Delta S/\Delta(nd)$, where $\Delta(nd)$ is the change of retardation and ΔS is the corresponding change of color.

If we use the "uniform chromaticity scale" (U. C. S.), ΔS of the two colors will be proportional to the distance between the two points on the graph, showing the two colors respectively.

Therefore, to study the sensitive color, we have to get the loci of the interference color on some U. C. S. diagram. If we use MacAdam's U. C. S.,[3] for example, we are able to get those loci by projecting Fig. 1 on this scale, as shown in Fig. 5. (Note: d expressed in 10 mμ units as in Fig. 1.) From this graph, we can calculate $\Delta S/\Delta(nd)$ as shown in Fig. 6. From the above, we learn that the neighborhood of purple in the first- and second-order interference is the most sensitive part for the variation of thickness, which conforms with the phenomenon of "sensitive purple" in the case of double refraction by crystal.

In the case of the non-reflecting layer, this is also the thickness in which the luminance of the reflecting light (given by Y in formula (1)) is minimum and most effective thickness in reducing the reflection. But as shown above, at this thickness the color change is very sensitive and irregularity of color is apt to appear, which often gives rise to the troubles in the manufacturing process. We can avoid this unstable point of color by reducing or increasing the thickness of layer a little, but it will result in a negligible increase in reflectivity. Accordingly, the most practical color of the non-reflecting layer is not pure purple but it must be bluish purple or red pink.

[3] D. MacAdam, J. Opt. Soc. Am. **27**, 294 (1937).

5. THE USE OF FILTER

The interference color resulting from the use of any light source other than C-light sources may be found by the above method, if $E(\lambda)$ of the light source is known. In particular, the interference colors resulting from the use of a "sharp cutting" yellow filter over the C-light source may be directly obtained by eliminating the terms corresponding to the absorbed part from the original numerical integrations.

For example, in case of a yellow filter which absorbs below 550 mμ the stimulus value of $\bar{z}$ is zero, giving the tristimulus coordinates $(x,y,0)$. So, all the colors lie on a straight line in I. C. I. diagram, as shown in Fig. 7. By projecting Fig. 7 into U. C. S. and calculating $\Delta S/\Delta(nd)$ therefrom, we learn that the color also sensitively changes with thickness from orange to yellow at the neighborhood of $nd=140$ mμ. In this case, the sensitive color is not purple as before but yellow. From this, it is evident that the commonly known "sensitive purple" gets its purple color incidentally by a certain energy distribution of the light source and is not the inherent property of the purple color itself.

The author wishes to acknowledge the valuable assistance, in performing the numerical integrations, of the members of his laboratory in the University.

JOURNAL OF THE OPTICAL SOCIETY OF AMERICA VOLUME 40, NUMBER 3 MARCH, 1950

The Compensation for Seeing in Stellar Photoelectric Spectrophotometry*

W. A. HILTNER AND A. D. CODE
Yerkes Observatory, University of Chicago, Williams Bay, Wisconsin
(Received November 14, 1949)

A method for the compensation of a variable light source in photoelectric spectrophotometry is presented. The outputs of a scanning photo-cell and a monitoring cell are fed to two amplifiers. The outputs of these amplifiers are then fed to a self-balancing recording potentiometer. The equipment has laboratory as well as astrophysical applications. The limiting magnitude at which useful spectrophotometry with a resolution of 1A is approximately 4. Further development work is in progress.

INTRODUCTION

THE analysis of stellar spectra in which intensities of absorption and emission lines are considered has been based exclusively on intensities of these lines as measured by the photographic process. The intensities measured in this fashion are sufficiently accurate for many investigations; however, it has become increasingly important to obtain intensities of appreciably higher accuracy than is possible by the usual methods employed in spectrophotometry. The intensities must be accurate not only in a relative sense but also accurate absolutely. The photographic process does not hold much hope for increased accuracy and hence if one wishes to exceed the present accuracy new methods of analyzing the star light must be sought. It is felt that if one should scan the spectrum with a photo-cell all

* Supported in part by ONR contract No. N8onr-565.

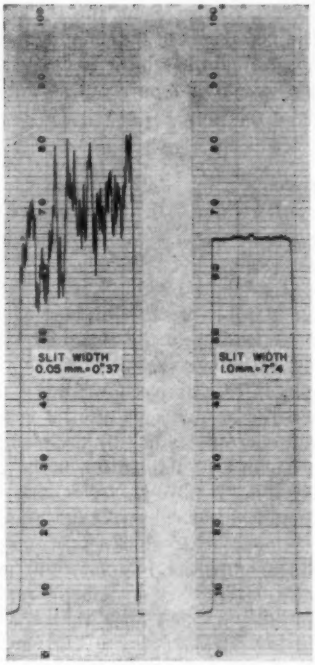

FIG. 1. Fluctuations in the transmission of a narrow slit caused by variations in the seeing disk. The tracing on the right shows the constancy of a stellar image when the entrance slit of the spectrograph is sufficiently wide to pass the entire stellar image. The tracing on the left shows the variation of the transmitted light when the slit is of such width that only 14 percent of the total light is transmitted. Cassegrain focus of 82-inch reflector of the McDonald Observatory.

systematic errors would be eliminated except those resulting from scattered light in the spectrograph and from the finite resolution of the spectrograph.

However, if one places a photo-cell behind a narrow entrance slit of a stellar spectrograph, the intensity recorded by the recording meter will vary by the order of 2 when the time constant of the recording system is 1 sec. These fluctuations are caused by variations in the seeing disk. Figure 1 illustrates the character of these fluctuations when the slit is 0".37 wide on a night of average seeing. On this particular night 14 percent of the incident light passed through the 0".37 slit. Obviously, before high resolution scanning of stellar spectra is feasible it is imperative that a device must be constructed capable of compensating for these fluctuations. The present paper presents a solution to the problem at hand. Furthermore, the identical problem exists in the laboratory when a variable light source is employed, and it will be shown that this problem has thus far been more satisfactorily solved than that of the variable seeing disk.

COMPENSATION FOR SEEING

If two photo-cells are placed at the focus of a stellar spectrograph and so arranged that one cell integrates over a narrow wave-length band (we shall call this the scanning or analyzing cell) and the second cell integrates over an appreciably wider wave-length band with the same mean wave-length (we shall call this the monitoring cell), we should expect to find that the fluctuations of the output of the two cells are identical. If it were possible for the output of the monitoring cell and its amplifier to control the amplification of the analyzing cell's amplifier in such a way that it would exactly compensate for any fluctuations in light intensity passing through the spectrograph slit, then the primary problem of scanning stellar spectra photoelectrically would be solved. The only remaining difficulty would be that of light level. In other words, if the signals from

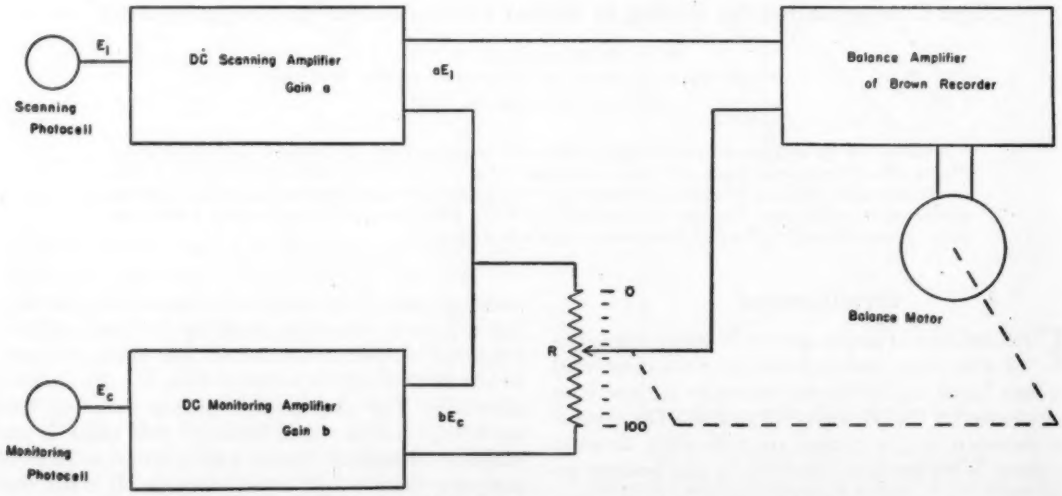

FIG. 2. Schematic diagram of the electrical circuit employed for the compensation of seeing.

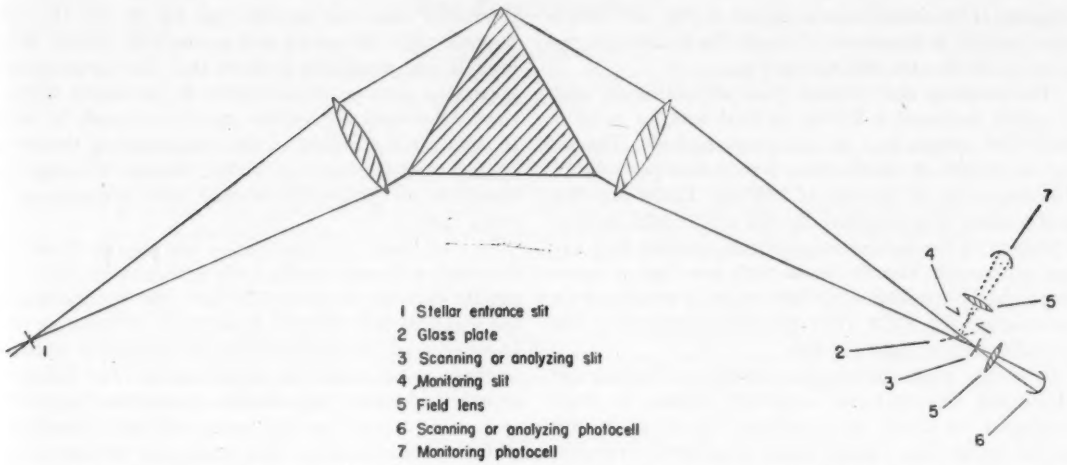

FIG. 3. Schematic diagram of the optical system employed for the photoelectric scanning of stellar spectra.

the scanning and monitoring cells were combined in a circuit for which the output signal was the ratio of these two signals then compensation for the seeing disk would be achieved.

A schematic diagram of a circuit to record the ratio of the scanning and monitoring cells is shown in Fig. 2. The recording instrument is a self-balancing potentiometer type such as the Brown Electronic Strip-Chart Recorder. The linear slide wire resistance, R, is tapped by a moving contact driven by the balance motor. The recording pen is attached to this sliding contact and hence records the ratio of the resistance tapped, r, to the total resistance, R, as a function of time. The reading of the instrument therefore equals r/R. Whenever the balance amplifier receives a signal from the scanning cell and amplifier, the balancing motor turns in a direction determined by the polarity of that signal until the readjustment of the slide wire tap removes the signal. If a and b are gains of the scanning and monitoring amplifiers, respectively, then the voltage across r is

$$e=ir=(bEc/R)r.$$

To achieve balance (zero input to the balance amplifier) we must have the condition

$$(bEc/R)r=aE_1.$$

Hence,

$$aE_1/bEc=r/R.$$

Since aE_1 and bEc are proportional to the radiation received by the scanning and monitoring cells respectively, it follows that

$$I_1/I_c=r/R.$$

This implies that the scanning and monitoring amplifiers must be linear (a and b constants) and properly zeroed. It is further required that the two amplifiers have the same time constant so that the fluctuations appear in aE_1 and bEc simultaneously. In practice these conditions are not difficult to satisfy.

EXPERIMENTAL TESTS OF THE COMPENSATING CIRCUIT

In order to make laboratory and observing tests of the compensating circuit, a scanning slit and cell and a monitoring cell were installed on the Coudé spectrograph[1] of the McDonald Observatory. A simplified

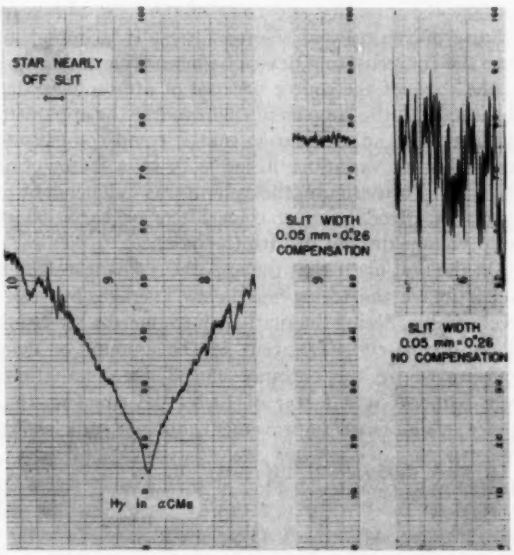

FIG. 4. The tracing to the right again shows seeing fluctuations while in the center figure are the same fluctuations when compensated for by the apparatus described in the text. The figure to the left is a tracing of $H\gamma$ in αCMa. Coudé focus of 82-inch reflector of the McDonald Observatory.

[1] G. Van Biesbroeck, McDonald Observatory Contribution No. 1, 103 (1936).

diagram of the installation is shown in Fig. 3. A simple spectrograph is illustrated although the Coudé spectrograph is of the autocollimating type.

The scanning unit consists of an adjustable slit back of which is placed a Fabry, or field lens, in order to focus the camera lens on the photo-cathode. The slit can be driven at speeds from $\frac{1}{4}$ to 4 mm per minute. The dispersion is 3A/mm at λ4400A. The monitoring unit consists of a plane parallel flat which reflects about 8 percent of the incident radiation to another field lens and photo-cell. The flat is of such size that a wavelength band approximately 40A wide is employed for monitoring. An RCA 1P21 photo-multiplier was employed for either light receiver.

In stellar photoelectric photometry at Yerkes and McDonald Observatories amplifiers similar to those developed by Kron[2] are employed. However, in this special application a single ended amplifier is desirable, and, after some experimentation, an amplifier similar to the one designed at the MIT Radiation Laboratories[3] was adopted. The output of the scanning amplifier is attached to the Brown Recorder in the normal fashion while the monitoring amplifier is connected directly to the 40-ohm slide wire of the recorder.

Laboratory tests of the equipment ran parallel with stellar observational tests. In order to place the optical and electrical equipment in operation an incandescent lamp was used as a light source. This lamp was connected to a variable transformer so that its intensity and color could be varied at will. Also it was possible to vary the intensity and color of the light source by the use of neutral and colored filters. It is important that the compensating device be insensitive to changes in the color of the source because of atmospheric dispersion. With the lamp as the light source the apparatus was placed in adjustment so that it could compensate accurately for variations in intensity by a factor of at least five. Furthermore, the system was independent of color; an introduction of color filters or variation of lamp voltage did not disturb the balance.

On the first night that the apparatus was tested on a stellar image the seeing was below average, but relatively stable. Seeing fluctuations introduced a variation of approximately 40 percent in the amount of light transmitted by the entrance slit. These fluctuations were reduced by a factor of 10 by the compensating device; a significant improvement, but not sufficient to profitably trace line profiles (see Fig. 4). On the subsequent night the seeing was appreciably better. However, it was surprising to learn that the compensating apparatus gave no improvement in the seeing fluctuations. Obviously a complete search was made in order to discover the failure of the compensating device to operate satisfactorily on stellar images although its operation on laboratory sources was satisfactory in every respect.

It was found on analysis of the signals from the scanning and monitoring cells individually that the signals were not in phase. In fact, the fluctuations at the scanning cell exceeded those at the monitoring cell. In other words, fluctuations were introduced in addition to those at the stellar spectrograph slit. The difficulty appeared obvious; imperfections in the analyzing slit, such as dust particles and non-parallelism, introduced additional fluctuations. This conclusion was borne out by additional observations. For example, satisfactory compensation was achieved with a wide analyzing slit; the imperfections of the slit were then insignificant. Laboratory tests were equally conclusive. When the seeing is good only a small portion of the scanning slit is used. The small motions of the stellar image cause the light to pass through different portions of the scanning slit, and if the scanning slit is not accurately parallel or contains irregularities, the intensity of the radiation observed by the scanning cell will vary in addition to the seeing fluctuations at the entrance slit. These additional variations cannot be compensated for since they do not occur at the monitoring cell. The solution to this difficulty may be found by employing an analyzing slit of greater precision and by introducing a cylindrical lens before the entrance slit. The latter permits the continuous use of a large portion of the analyzing slit.

In laboratory spectroscopy one often encounters variable light sources, particularly if an arc is employed. Consequently, the method described above for the compensation of variations in stellar images may have applications in the laboratory.[4] An attempt was made to analyze the iron arc which is normally used for the comparison spectrum. It was found that if the arc is focused on the entrance slit no significant compensation for its variation in intensity was achieved. However, when a diffuse light from the arc was focused on the slit, despite an intensity variation of the order of ten, the compensation was effective and no fluctuation appeared while the lines were traced in direct intensities.

[2] G. Kron, Electronics **21**, 103 (1948).
[3] MIT Radiation Lab. Series No. 18, Vacuum Tube Amplifiers, p. 480.
[4] Dieke and Crosswhite, J. Opt. Soc. Am. **35**, 480 (1945).

The Torus Grating

HEINZ HABER
USAF School of Aviation Medicine, Randolph Air Force Base, Texas
(Received October 26, 1949)

The torus grating is defined as a calotte of a circular torus bearing a grating ruling on its concave side. In contrast to the spherical grating, the torus grating is capable of eliminating astigmatism, in general, for two points in the spectrum. These two stigmatic points can be adjusted to any desired wave-length within a wide range of the spectrum by choosing suitable values for the angles of incidence and diffraction. In the rest of the spectrum produced by a torus grating, astigmatism is considerably smaller than that prevailing in spectra of spherical gratings. Moreover, astigmatism is negligible in the proximity of the two stigmatic points, giving rise to "quasi-stigmatic" ranges in the torus grating spectrum. The extension of these quasi-stigmatic ranges depends on the size of tolerable astigmatism. If based upon an astigmatism equal to the diffraction width of the spectral images, a quasi-stigmatic range can be wider than 1000A. With light sources of small size a considerable gain in spectral intensity results from the lack of astigmatism. The theory of the torus grating which has been attempted in this paper further demonstrates that coma, aberration, and curvature of spectral lines in the torus grating spectrum are generally smaller than the same image imperfections in the spectrum of the spherical grating.

I. INTRODUCTION

THE Fraunhofer diffraction grating, in the shape of Rowland's[1] concave grating, is the only spectral apparatus capable of producing and imaging a spectrum by a single katoptric process. Yet, this property is gained at a sacrifice: the spectral images produced by a concave grating are distorted by astigmatism to a considerable extent. Astigmatism makes a concave grating unserviceable for all examinations of individual sections of light sources, such as is required in spectro-helioscopy, interference spectroscopy and other allied fields. A further disadvantage of astigmatism is the loss in intensity which is most obstructive in dealing with light sources of small area, such as electric sparks, stellar images, and others. Furthermore, astigmatism makes it difficult to introduce a comparison spectrum.

All methods hitherto applied to eliminate astigmatism of concave gratings[2-4] destroy its outstanding advantage, namely, the advantage of having the spectrum produced and imaged by a single diffraction from the ruled spherical surface. Yet, it can be demonstrated that there is a surface which is better adapted to the twofold task of an auto-imaging grating, i.e., a grating which produces and images a spectrum simultaneously. This surface is the right circular torus, a surface of revolution generated by revolving a circle about any straight line, lying in the plane of the circle, as an axis.

In the present paper an attempt has been made to develop the theory of the torus grating. H. G. Beutler[5] recently published a general theory of the spherical grating, fully covering the image formation and its imperfections, as resulting from such a grating. Because of Beutler's exhaustive study, we need describe only the special properties of the torus grating and its image formation in comparison to that of the spherical grating.

II. THE EQUATION FOR THE SPECTRUM OF THE TORUS GRATING

The torus used may be generated by revolving a circle of radius ρ lying in the $x'z'$ plane about the z' axis (Fig. 1). The center of the circle lies on the x' axis at a distance $R-\rho$ from the axis of revolution which is a secant of the circle. In case $\rho=R$, a sphere is generated as a special case of the torus. Hence, the torus grating also comprises the Rowland concave grating as a special case, if $\rho=R$.

The equation for the torus as expressed in Cartesian coordinates x', y', z' is:

$$[(x'^2+y'^2)^{\frac{1}{2}}-(R-\rho)]^2+z'^2=\rho^2. \quad (1)$$

When applying the coordinate transformation formulas:

$$x'=x-R; \quad y'=y; \quad z'=z, \quad (2)$$

Eq. (1) will become the vertex equation for the torus:

$$x^2+y^2+z^2=2Rx-2R(R-\rho)+2(R-\rho)[(R-x)^2+y^2]^{\frac{1}{2}}. \quad (3)$$

In this position of the torus, the grooves of the grating are intersections of the torus surface with a family of planes parallel to the x,z plane, the distances D between the planes being equal (D=grating constant). In the following it is assumed that a light ray leaves the point A (x_a, y_a, z_a), hits the ruled torus surface at the point P (x, y, z), is then reflected and finally reaches the point B (x_b, y_b, z_b) (see Fig. 2).

By variation of the point P over the entire area of the ruled surface of the torus grating, the various lengths of the light paths AP and PB can be determined, and formation and imperfections of the image can be examined. The actual grating involves only a small area of the torus surface around the immediate proximity of the origin O of the coordinate system; hence, it can

[1] H. A. Rowland, Phil. Mag. [5], 13, 469 (1882).
[2] F. L. O. Wadsworth, Astrophys. J. 3, 54 (1896).
[3] Runge and Paschen, Ann. d. Physik 61, 641 (1897).
[4] Runge and Mannkopff, Zeits. f. Physik 45, 13 (1927).
[5] H. G. Beutler, J. Opt. Soc. Am. 35, 311 (1945).

be concluded that y and z are of the second order as compared to ρ and R, whereas x is of the fourth order as compared to ρ and R, i.e., x is of the second order as compared to y and z. According to these considerations, (3) can be developed as follows:

$$x^2+y^2+z^2=2Rx-2R(R-\rho)$$
$$+2(R-\rho)(R-x)\left[1+\frac{y^2}{(R-x)^2}\right]^{\frac{1}{2}}=2Rx-2R(R-\rho)$$
$$+2(R-\rho)(R-x)\left[1+\frac{1}{2}\frac{y^2}{(R-x)^2}-\frac{1}{8}\frac{y^4}{(R-x)^4}\right]\cdots$$
$$+\text{sixth and higher orders.} \quad (4)$$

By use of the approximation

$$y^2/(R-x)^2=y^2(R+x)^2/R^4+\cdots+6.\ \text{a.h.o.} \quad (5)$$

Equation (4) can further be developed, and yields

$$x^2+y^2+z^2=2\rho x+[1-(\rho/R)]y^2+[(R-\rho)/R^2]xy^2$$
$$-[(R^2-R\rho)/4R^4]y^4+\cdots+5.\ \text{a.h.o.} \quad (6)$$

This latter expression represents a vertex equation for the torus in the form of a power series, excluding members of the fifth and higher orders.

The next step is to represent the lengths of the light paths AP (and PB) as a function of the coordinates x,y,z of the grating point P. In detail, one has

$$[AP]^2=(x-x_a)^2+(y-y_a)^2+(z-z_a)^2$$
$$=r_a^2+z_a^2-2xx_a-2yy_a-2zz_a+x^2+y^2+z^2. \quad (7)$$

Here, r_a is the distance between the origin O and the projection of the point A on the x,y plane. Introducing

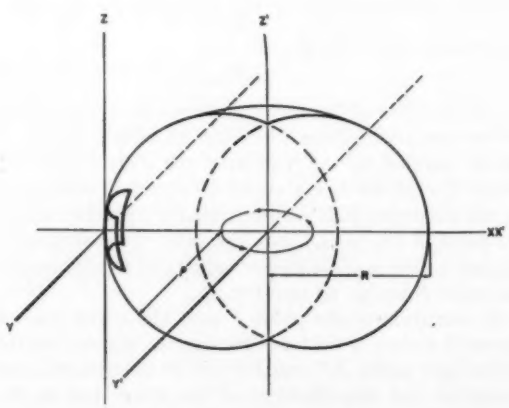

FIG. 1. Generation of a torus by revolving a circle of radius ρ about an axis (z') lying in the plane of the circle at a distance $R-\rho$ from its center.

(6) into (7) yields:

$$[AP]^2=r_a^2+z_a^2-2zz_a+(\rho-x_a)2x$$
$$+[1-(\rho/R)]y^2+[(R-\rho)/R^2]xy^2$$
$$-[(R-\rho)/4R^3]y^4. \quad (8)$$

Drawing

$$2x=\{1/\rho\}\{x^2+z^2+(\rho/R)y^2$$
$$-[(R-\rho)/R^2]xy^2+[(R-\rho)/4R^3]y^4\} \quad (9)$$

out of (6) and introducing it into (8), one finds:

$$[AP]^2=r_a^2+z_a^2-2yy_a-2zz_a$$
$$+[1-(x_a/R)]y^2+[1-(x_a/\rho)][x^2+z^2]$$
$$+(x_a/\rho)\{[(R-\rho)/R^2]xy^2-[(R-\rho)/4R^3]y^4\}. \quad (10)$$

For the following procedure it is convenient to eliminate x and x^2 entirely from (10) by means of (6). Starting with (6) one proceeds as follows:

$$x^2-\{2\rho+[(R-\rho)/R^2]y^2\}\cdot x$$
$$+\{z^2+(\rho/R)y^2+[(R-\rho)/4R^3]y^4\}=0. \quad (11)$$

(11) is a quadratic equation in x which can be solved by the formula for its roots:

$$x=\rho+[(R-\rho)/2R^2]y^2\pm\tfrac{1}{2}\{(2\rho+[(R-\rho)/2R^2]y^2)^2$$
$$-4(z^2+(\rho/R)y^2+[(R-\rho)/4R^3]y^4)\}^{\frac{1}{2}}. \quad (12)$$

By expanding (12), with the negative radical, in a power series, one finds:

$$x=(M/N)+(M^2/N^3)+\cdots;$$
$$M=z^2+(\rho/R)y^2+[(R-\rho)/4R^3]y^4;$$
$$N=2\rho+[(R-\rho)/R^2]y^2. \quad (13)$$

Only the first member of this series must be taken into account, since y and z are already of the fourth order in the second member which becomes negligible if multiplied by y^2 in (10). Eq. (13) can be expanded further and yields the final approximations for x and x^2, to be used for their elimination from (10):

$$x=(1/2R)y^2+(1/2\rho)z^2; \quad (14a)$$

$$x^2=(1/4R^2)y^4+(1/4\rho^2)z^4+(1/2R\rho)y^2z^2. \quad (14b)$$

Introducing (14) into (10) and simplifying, the result will be:

$$[AP]^2=r_a^2+z_a^2-2yy_a-2zz_a+[1-(x_a/R)]y^2$$
$$+[1-(x_a/\rho)]z^2+1/4R^2[1-(x_a/R)]y^4$$
$$+(1/4\rho^2)[1-(x_a/\rho)]z^4+(1/2R\rho)[1-(x_a/R)]y^2z^2. \quad (15)$$

In dealing with the theory of gratings, usually the angles of incidence and diffraction or, speaking geometrically, cylindrical coordinates (r_a, α) with the origin in the center of the grating are introduced. By means of the transformation formula

$$x_a=r_a\cos\alpha; \quad y_a=r_a\cdot\sin\alpha \quad (16)$$

(15) can be transformed:

$$[AP]^2=r_a^2-2yr_a\sin\alpha+z_a^2-2zz_a$$
$$+[1-(r_a/R)\cos\alpha]y^2+[1-(r_a/\rho)\cos\alpha]z^2$$
$$+1/4R^2[1-(r_a/R)\cos\alpha]y^4+(1/4\rho^2)[1-(r_a/\rho)\cos\alpha]z^4$$
$$+(1/2R\rho)[1-(r_a/R)\cos\alpha]y^2z^2. \quad (17)$$

Before extracting the square root (17), it is advisable to apply a further rearrangement:

$$[AP]^2$$
$$=r_a^2-2yr_a\sin\alpha+y^2\sin^2\alpha+y^2\cos^2\alpha$$
$$-y^2(r_a/R)\cos\alpha+[1-(r_a/\rho)\cos\alpha]z^2$$
$$+z_a^2-2zz_a+(1/4R^2)[1-(r_a/R)\cos\alpha]y^4$$
$$+(1/4\rho^2)[1-(r_a/\rho)\cos\alpha]z^4+(1/2R\rho)$$
$$\times[1-(r_a/R)\cos\alpha]y^2z^2$$
$$=(r_a-y\cdot\sin\alpha)^2+[\cos^2\alpha-(r_a/R)\cos\alpha]y^2$$
$$+[1-(r_a/\rho)\cos\alpha]z^2+z_a^2-2zz_a+(1/4R^2)$$
$$\times[1-(r_a/R)\cos\alpha]y^4+(1/4\rho^2)[1-(r_a/\rho)\cos\alpha]z^4$$
$$+(1/2R\rho)[1-(r_a/R)\cos\alpha]y^2z^2. \quad (18)$$

The square root (18) can be extracted by expansion in a power series including members up to the fourth order:

$$AP=r_a-y\cdot\sin\alpha$$
$$+\{1/(r_a-y\cdot\sin\alpha)\}\{\tfrac{1}{2}[\cos^2\alpha-(r_a/R)\cos\alpha]y^2$$
$$+\tfrac{1}{2}[1-(r_a/\rho)\cos\alpha]z^2+\tfrac{1}{2}[z_a^2-2zz_a]$$
$$+(1/8R^2)[1-(r_a/R)\cos\alpha]y^4+(1/8\rho^2)$$
$$\times[1-(r_a/\rho)\cos\alpha]z^4+(1/4R\rho)[1-(r_a/R)\cos\alpha]y^2z^2\}$$
$$-\{1/4(r_a-y\cdot\sin\alpha)^3\}\{\tfrac{1}{2}[\cos^2\alpha-(r_a/R)\cos\alpha]^2y^4$$
$$+\tfrac{1}{2}[1-(r_a/\rho)\cos\alpha]^2z^4+\tfrac{1}{2}[z_a^2-2zz_a]^2$$
$$+[\cos^2\alpha-(r_a/R)\cos\alpha][1-(r_a/\rho)\cos\alpha]y^2z^2$$
$$+[\cos^2\alpha-(r_a/R)\cos\alpha][z_a^2-2zz_a]y^2$$
$$+[1-(r_a/\rho)\cos\alpha][z_a^2-2zz_a]z^2\}. \quad (19)$$

The fractions in the series (19), having the variable y in the denominator, can be eliminated by further series development which after suitable arrangement yields the final equation for the spectrum of the torus grating:

$$AP+PB$$
$$=r_a+r_b-(\sin\alpha+\sin\beta)y \quad (T_1)$$

$$\left.\begin{aligned}
&+\frac{1}{2}\left[\frac{\cos^2\alpha}{r_a}-\frac{\cos\alpha}{R}\right]y^2+\frac{1}{2}\left[\frac{\cos^2\beta}{r_b}-\frac{\cos\beta}{R}\right]y^2\\
&+\frac{1}{2}\frac{\sin\alpha}{r_a}\left[\frac{\cos^2\alpha}{r_a}-\frac{\cos\alpha}{R}\right]y^3\\
&\qquad+\frac{1}{2}\frac{\sin\beta}{r_b}\left[\frac{\cos^2\beta}{r_b}-\frac{\cos\beta}{R}\right]y^3\\
&+\frac{1}{2}\frac{\sin^2\alpha}{r_a^2}\left[\frac{\cos^2\alpha}{r_a}-\frac{\cos\alpha}{R}\right]y^4\\
&\qquad+\frac{1}{2}\frac{\sin^2\beta}{r_b^2}\left[\frac{\cos^2\beta}{r_b}-\frac{\cos\beta}{R}\right]y^4
\end{aligned}\right\} \quad (T_2)$$

$$\left.\begin{aligned}
&+\frac{1}{2}\left[\frac{1}{r_a}-\frac{\cos\alpha}{\rho}\right]z^2+\frac{1}{2}\left[\frac{1}{r_b}-\frac{\cos\beta}{\rho}\right]z^2\\
&\qquad+\frac{1}{2r_a}[z_a^2-2zz_a]+\frac{1}{2r_b}[z_b^2-2zz_b]\\
&-\frac{1}{8r_a}\left[\left(\frac{1}{r_a}-\frac{\cos\alpha}{\rho}\right)z^2+\frac{1}{r_a}(z_a^2-2zz_a)\right]^2\\
&\qquad-\frac{1}{8r_b}\left[\left(\frac{1}{r_b}-\frac{\cos\beta}{\rho}\right)z^2+\frac{1}{r_b}(z_b^2-2zz_b)\right]^2
\end{aligned}\right\} \quad (T_3)$$

$$\left.\begin{aligned}
&+\frac{1}{2}\frac{\sin\alpha}{r_a}\left[\frac{1}{r_a}-\frac{\cos\alpha}{\rho}\right]yz^2+\frac{1}{2}\frac{\sin\beta}{r_b}\left[\frac{1}{r_b}-\frac{\cos\beta}{\rho}\right]yz^2\\
&\qquad+\frac{1}{2}\frac{\sin\alpha}{r_a^2}[z_a^2-2zz_a]y\\
&+\frac{1}{2}\frac{\sin\beta}{r_b^2}[z_b^2-2zz_b]y+\frac{1}{2}\frac{\sin^2\alpha}{r_a^2}\left[\frac{1}{r_a}-\frac{\cos\alpha}{\rho}\right]y^2z^2\\
&\qquad+\frac{1}{2}\frac{\sin^2\beta}{r_b^2}\left[\frac{1}{r_b}-\frac{\cos\beta}{\rho}\right]y^2z^2\\
&+\frac{1}{2}\frac{\sin^2\alpha}{r_a^3}[z_a^2-2zz_a]y^2+\frac{1}{2}\frac{\sin^2\beta}{r_b^3}[z_b^2-2zz_b]y^2
\end{aligned}\right\} \quad (T_4)$$

$$\left.\begin{aligned}
&+\frac{1}{8R^2}\left[\frac{1}{r_a}-\frac{\cos\alpha}{R}\right]y^4+\frac{1}{8R^2}\left[\frac{1}{r_b}-\frac{\cos\beta}{R}\right]y^4\\
&\qquad+\frac{1}{8\rho^2}\left[\frac{1}{r_a}-\frac{\cos\alpha}{\rho}\right]z^4+\frac{1}{8\rho^2}\left[\frac{1}{r_b}-\frac{\cos\beta}{\rho}\right]z^4\\
&+\frac{1}{4R\rho}\left[\frac{1}{r_a}-\frac{\cos\alpha}{R}\right]y^2z^2+\frac{1}{4R\rho}\left[\frac{1}{r_b}-\frac{\cos\beta}{R}\right]y^2z^2
\end{aligned}\right\} \quad (T_5)$$

$$\left.\begin{aligned}
&-\frac{1}{8r_a}\left[\frac{\cos^2\alpha}{r_a}-\frac{\cos\alpha}{R}\right]^2y^4-\frac{1}{8r_b}\left[\frac{\cos^2\beta}{r_b}-\frac{\cos\beta}{R}\right]^2y^4\\
&\qquad-\frac{1}{4r_a}\left[\frac{\cos^2\alpha}{r_a}-\frac{\cos\alpha}{R}\right]\left[\frac{1}{r_a}-\frac{\cos\alpha}{\rho}\right]y^2z^2\\
&-\frac{1}{4r_b}\left[\frac{\cos^2\beta}{r_b}-\frac{\cos\beta}{R}\right]\left[\frac{1}{r_b}-\frac{\cos\beta}{\rho}\right]y^2z^2\\
&\qquad-\frac{1}{4r_a^2}\left[\frac{\cos^2\alpha}{r_a}-\frac{\cos\alpha}{R}\right][z_a^2-2zz_a]y^2\\
&\qquad-\frac{1}{4r_b^2}\left[\frac{\cos^2\beta}{r_b}-\frac{\cos\beta}{R}\right][z_b^2-2zz_b]y^2.
\end{aligned}\right\} \quad (T_6) \quad (20)$$

For the total value of $AP+PB$ in (20) the corre-

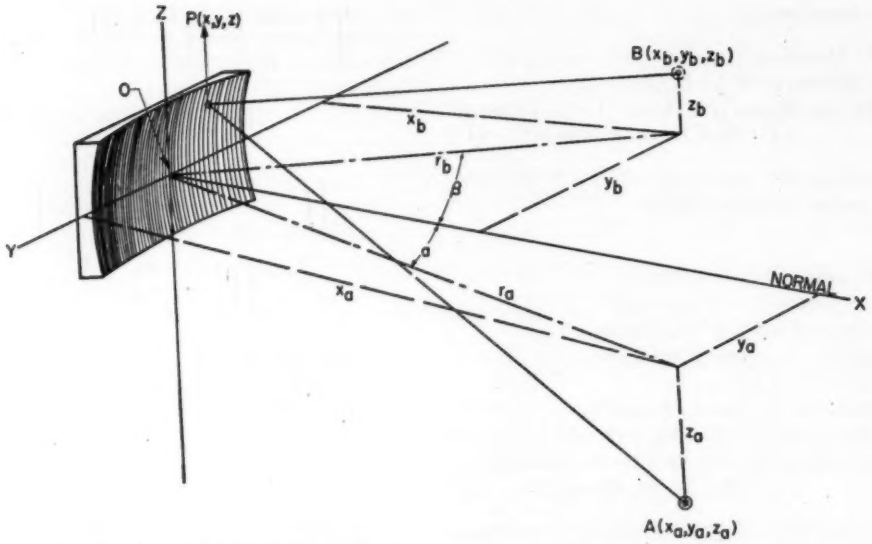

FIG. 2. Denotations of co-ordinates. For details refer to the pertinent paragraphs of the text.

sponding procedure (7) to (19) has been applied also for the light path PB.

As Beutler[5] had demonstrated in detail for a similar equation pertaining to the spherical grating, the consecutive members T_n in (20) have, individually, a physical significance as to the image formation and its imperfections. The individual members control the various conditions for the foci and for the image deficiencies in the following order: T_1: General grating equation; T_2: Primary focus condition (Rowland circle); T_3: Astigmatism; T_4: Coma, inclination and curvature of spectral lines; T_5: Toric aberration; T_6: High order focus condition (Rowland circle).

Excluding cases of very large angles of incidence α, and of diffraction β, the numerical values of the consecutive members T_n are of an order of decreasing magnitude. It might be worth while to compare the series (20) to the corresponding expressions (*10B*) and (*11B*) in Beutler's paper.[5] A comparison of the respective grating equations (sphere and torus) shows that the first two groups of members are identical, whereas certain differences prevail in all other members, accounting for the differences between the two gratings as far as image formation and its imperfections are concerned. The differences between the equations of the two gratings vanish, if $\rho=R$.

III. SCHEME OF DISCUSSION FOR THE EQUATION OF THE TORUS GRATING SPECTRUM

According to the procedure given by Beutler in his paper,[5] Fermat's principle has proved to be a most suitable tool in discussing the theory of image formation by auto-imaging gratings. In view of this fact it is advisable to apply this method in the following investigations. In brief, the necessary formulas are given here, using Beutler's notations in a generalized manner. The conditions for a strict focus requires that the partial derivatives of the consecutive members of (20) with respect to the variables y and z vanish. Since the partial derivatives have the geometrical significance of angles, the displacement of the diffracted rays from the true focus B can be calculated, if the partial derivatives do not vanish. This displacement is given by:

$$\Delta_n=r_b(\partial Tn/\partial v)(1/\cos\varphi) \qquad (21)$$

whence v is the respective variable and φ is the angle between the reflected ray and the normal to the focal plane at B. An examination of the equation for the torus grating shows that only a few members of the series can be made equal to zero. Those retaining finite values are responsible for the various image imperfections as previously outlined. It is, therefore, necessary to calculate the degree of these imperfections under various circumstances. All numerical calculations will be based on a torus grating of the following dimensions:

$$R=914.38\text{ cm};\ \rho=782.83\text{ cm};\ D=0.000127\text{ cm}. \qquad (22)$$

Width of the grating $B=15$ cm; Length of the grooves $L=7.5$ cm. For the sake of brevity we may omit a detailed discussion of the members T_1 and T_2, since such a discussion would be a mere repetition of Beutler's respective chapters. We shall only point out that as a result, the general grating equation:

$$\sin\alpha+\sin\beta=n\cdot\lambda/D \qquad (23)$$

(n=order of spectrum; λ=wave-length), and the condition for the Rowland circle

$$r_a=R\cdot\cos\alpha;\quad r_b=R\cdot\cos\beta, \qquad (24)$$

and its implications hold valid for the torus grating as

well. It may further be noted that condition (24) makes it possible to keep the individual members of T_2 and T_6 equal to zero, as long as slit and image lie on the Rowland circle. The existence of the Rowland circle in the scheme of image formation by the torus grating had to be expected, since there is no difference between the outer equatorial cross section of a torus or radii ρ, R, and that of a sphere of radius R.

IV. T_3: ASTIGMATISM

1. Conditions for the Formation of Stigmatic Images by the Torus Grating

Astigmatism and the conditions for its elimination can be derived by differentiating the member T_3 with respect to z. In the first step we consider only members of T_3 which contain z and z^2, i.e., we restrict the discussion to the primary astigmatism:

$$\partial T_3/\partial z=[(1/r_a)-(\cos\alpha/\rho)+(1/r_b)-(\cos\beta/\rho)]z - (z_a/r_a)-(z_b/r_b)=0. \quad (25)$$

From the law of reflection it can be deduced that the relation $z_a/r_a=-z_b/r_b$ holds for the case now under consideration. Hence, (25) can be satisfied, if

$$[(1/r_a)-(\cos\alpha/\rho)+(1/r_b)-(\cos\beta/\rho)]z=0. \quad (26)$$

The corresponding expression pertaining to the spherical grating is:

$$[(1/r_a)-(\cos\alpha/R)+(1/r_b)-(\cos\beta/R)]z\neq 0. \quad (27)$$

(27) differs from (26) only by having the radius R of the sphere within the parenthesis. This fact makes it impossible to fulfill condition (27); for the parameter R had been applied in relation to the angles α and β by the condition for the Rowland circle (24). Only, if

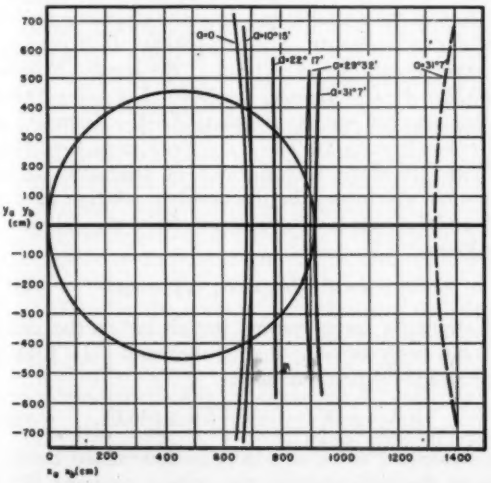

FIG. 3. Primary focal curve (Rowland circle) and a number of secondary focal curves pertaining to indicated values of the angle of incidence α. - - - A single secondary focal curve pertaining to a spherical grating of corresponding dimensions.

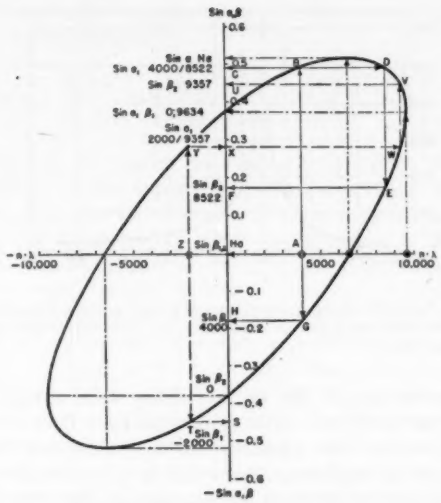

FIG. 4. Relation between stigmatic wave-lengths $n\cdot\lambda$ in angstrom-units and the sinuses of the angles of incidence and diffraction. For details see text.

$\alpha=\beta=0$, (24) and (27) can be satisfied simultaneously; yet, the locus of slit and image, characterized by $\alpha=\beta=0$, is unsuitable, since slit and its neutral image coincide in this case.

In contrast to the spherical grating, condition (26), valid for the torus grating, can be satisfied, since there is still a free choice for the value of the parameter ρ, it being independent from R. This means that the torus grating can produce stigmatic spectral images. Hence, satisfying Eq. (26), we have:

$$(1/r_a)-(\cos\alpha/\rho)+(1/r_b)-(\cos\beta/\rho)=0. \quad (28)$$

Introducing the values (24) for r_a and r_b yields:

$$\rho/R=\cos\alpha\cdot\cos\beta. \quad (29)$$

Equation (29) which connects the ratio of the radii ρ and R with the angles of incidence and diffraction, controls the position of two stigmatic points on the Rowland circle. The positions are given by the pairs of angles α, β, and $\alpha,-\beta$, which fulfill (29). The pairs of angles $-\alpha,-\beta$, and $-\alpha,\beta$, which also satisfy (29), have the same geometrical and optical significance as the two former pairs. The two stigmatic points, characterized by the two angles of diffraction β and $-\beta$, have positions which are symmetrical with respect to the grating normal. The two stigmatic points degenerate into a single one in the case $\beta=0$.

2. The Secondary Focal Curves

The geometrical scheme of stigmatic image formation can more easily be visualized by considering the relative positions of the primary and the secondary focal curves of the astigmatic pencils for different values of α. The Rowland circle, as the primary focal curve, is the locus of the vertical focal lines of the

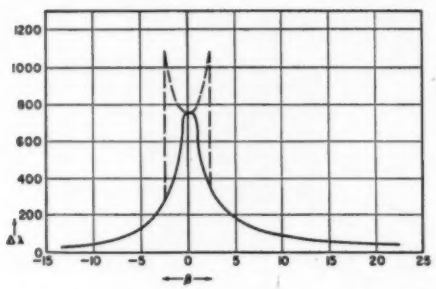

FIG. 5. Width of the quasi-stigmatic range in the torus grating spectrum, expressed in angstrom-units, as a function of the angle of diffraction β.

astigmatic pencils. By the secondary focal curves we understand the loci of the horizontal focal lines of the same pencils. The equations for the secondary focal curves of both gratings, expressed in polar coordinates (r_{bh}, β), can be obtained by introducing (24) into (27) and (26), and solving for r_b:

$$r_{bh}(S) = R/(\cos\beta - \sin\alpha \cdot \tan\alpha) \quad \text{(sphere)} \tag{30}$$

$$r_{bh}(T) = \rho\cos\alpha/\{\cos^2\alpha - [(\rho/R) - \cos\alpha\cdot\cos\beta]\} \quad \text{(torus)}, \tag{31}$$

in which r_{bh} represents the distance of the horizontal focal lines from the center of the gratings. Equations (30) and (31) represent a family of parabolas with their vertices on the grating normal. For the spherical grating the parabolas lie outside the Rowland circle; for the torus grating, however, the parabolas lie partly inside the Rowland circle. Figure 3 shows five secondary focal curves pertaining to the torus grating for different values of α; the broken tracing represents one such curve pertaining to the spherical grating. Obviously, a stigmatic focus is obtained at any point which the Rowland circle and any of the secondary focal curves have in common. There is only one such point in the scheme of focal curves pertaining to the spherical grating: the point characterized by $\alpha=\beta=0$. These conditions clearly illustrate the fact that no stigmatic images can be produced by the spherical grating. For the torus grating, however, points exist which the Rowland circle and the secondary focal curves have in common. According to (31), we have one parabolic focal curve for each angle α, intersecting the Rowland circle, in general, at two points: the stigmatic points. As Fig. 3 demonstrates, there is a certain possible range for the position of the stigmatic points. As can be derived from (29), we can obtain stigmatic images between the limits $0 \leqslant \alpha \leqslant \text{arc}\cos[\rho/R]$, with values of β determined by (29).

3. The Range of Stigmatic Image Formation in the Wave-Length Scale

Speaking in terms of spectroscopy, the wave-lengths brought to a stigmatic focus and not the angles of incidence and diffraction are the most interesting quantities. Moreover, as demonstrated in the preceding section, the stigmatic points can obviously be adjusted to any proper pair of wave-lengths within a wide range of the spectrum, if suitable values for the angles α and β are chosen. In other words, there must be a function which determines the angles α and β, yielding stigmatic images for any wave-length desired. This function can be found by treating (23) and (29) as two simultaneous equations with the unknowns α and β:

$$\sin\alpha + \sin\beta = n\cdot\lambda/D; \quad \cos\alpha\cdot\cos\beta = \rho/R. \tag{32}$$

The signs in the first equation of (32) are determined by the respective signs and values of α, β and λ. The solutions of (32), with all useful possibilities of the signs, are:

$$\sin\alpha = \left\{ \pm\frac{n\cdot\lambda}{2D} \pm \left(1 + \left(\frac{n\cdot\lambda}{2D}\right)^2 - \left[\left(\frac{n\cdot\lambda}{D}\right)^2 + \left(\frac{\rho}{R}\right)^2\right]^{\frac{1}{2}}\right)^{\frac{1}{2}}\right\}, \tag{33a}$$

$$\sin\beta = \pm\left\{ \pm\frac{n\cdot\lambda}{2D} \mp \left(1 + \left(\frac{n\cdot\lambda}{2D}\right)^2 - \left[\left(\frac{n\cdot d}{D}\right)^2 + \left(\frac{\rho}{R}\right)^2\right]^{\frac{1}{2}}\right)^{\frac{1}{2}}\right\}. \tag{33b}$$

Equation (33) is a function of the fourth degree whose useful part, represented as a graph, consists of an oblate closed curve. The range of solutions pertaining to this part of the curve is represented by the minus sign under the root. The graph of the function (33) based on a torus grating (22) is given in Fig. 4. Two sets of tracings in the graph demonstrate two examples how to find the angles α and β for the stigmatic formation of a wave-length. For $\lambda = +4000$A (full tracing) we have: Points $A-B-C(\sin\alpha_1)$; $B-D-E-F(\sin\beta_2, \lambda+8522)$; $A-G-H(\sin\beta_1, \lambda+4000)$. For $\lambda = -2000$A (broken tracing) we have: Points $Z-Y-X(\sin\alpha_1)$; $X-W-V-U(\sin\beta_2, \lambda+9357)$; $Z-T-S(\sin\beta_1, \lambda-2000)$.

There are three special cases of stigmatic image formation which may be discussed in relation to Eq. (33) and its graph. These result from the following conditions:

$$\text{a) } \alpha=0; \quad \text{b) } \beta=0; \quad \text{c) } \alpha=\beta. \tag{34}$$

The stigmatic wave-lengths, pertaining to the cases (34), can easily be computed by means of (32). Taking (34a) and (34b) first, one has:

$$n\cdot\lambda = \pm D[1-(\rho/R)^2]^{\frac{1}{2}} = \pm 6563\text{A}. \tag{35}$$

The numerical value of 6563A is determined by the ratio of the radii and by the grating constant (22); indeed, the values for ρ, R, and D were particularly chosen so that the hydrogen line H_α was imaged stigmatically on the grating normal.

Introducing condition (34c) into Eqs. (32) yields:

$$n\cdot\lambda=\pm 2D[1-(\rho/R)]^{\frac{1}{2}}=\pm 9634\text{A}. \qquad (36)$$

It can be demonstrated, that the wave-length $n\cdot\lambda$, as given by (36)—i.e., for $\alpha=\beta$—is the largest, for which a stigmatic focus can be obtained with a torus grating of a given ρ, R and D. To this effect, Eq. (33) must be solved for $n\cdot\lambda/D$:

$$\frac{n\cdot\lambda}{D}=\sin\alpha\pm\left[\frac{\rho^2}{R^2(\sin^2\alpha-1)}+1\right]^{\frac{1}{2}}. \qquad (37)$$

Differentiating (37) with respect to $\sin\alpha$ yields:

$$d\left(\frac{n\cdot\lambda}{D}\right)\Big/ d(\sin\alpha)=1\mp\rho^2\sin\alpha\Big/$$

$$R^2(\sin^2\alpha-1)^2\left[\frac{\rho^2}{R^2(\sin^2\alpha-1)}+1\right]^{\frac{1}{2}}=0. \qquad (38)$$

Equation (38) must be solved for $\sin\alpha$; this can be done by setting $\sin^2\alpha-1=w$, and transforming (38):

$$[w^2-(\rho/R)^2][w^2+(\rho/R)^2w+(\rho/R)^2]=0. \qquad (39)$$

Equation (39) has the following real solutions:

$$\sin\alpha=\pm[1-(\rho/R)]^{\frac{1}{2}}. \qquad (40)$$

Introducing (40) into (37), one obtains (36):

$$n\cdot\lambda_{\max}=\pm D\{\sin\alpha+[1-(\rho/R)]^{\frac{1}{2}}\}$$
$$=\pm 2D[1-(\rho/R)]^{\frac{1}{2}}. \qquad (36)$$

The special cases, characterized by (34), and their numerical values (35) and (36) are represented in the graph (Fig. 4) by dash-dot tracings.

4. Astigmatism in the Proximity of the Stigmatic Points

In the immediate proximity of the stigmatic points astigmatism within the spectrum will be very small or even negligible, since the size of astigmatism is given by the distance between the two focal curves. The specifications of these conditions will make it possible to define the extension of a "quasi-stigmatic" range at both sides of the stigmatic points. As mentioned before, astigmatism can be derived from the lengths of the light path between the Rowland circle and the respective secondary focal curve. The distances between both curves can easily be obtained by means of (24) and (31); for these equations determine the distance between the center of the grating and the two foci. Hence:

$$s=\rho\cos\alpha/\{\cos^2\alpha-[(\rho/R)-\cos\alpha\cdot\cos\beta]\}-R\cos\beta. \qquad (41)$$

If L is the length of the grooves, one has $A/L=s/r_{bA}$. Then, after suitable arrangement, (41) becomes:

$$A=[L/\rho\cdot\cos\alpha][\cos\alpha+\cos\beta][\rho-R\cos\alpha\cdot\cos\beta]. \qquad (42)$$

Equation (42) shows that, on account of (29), astigmatism vanishes for the stigmatic points.

The practical significance of (42) becomes evident, if it is solved for $\cos\beta$:

$$\cos\beta=\frac{\rho-R\cos^2\alpha}{2R\cos\alpha}+\left[\frac{(\rho-R\cos^2\alpha)^2}{4R^2\cos^2\alpha}+\frac{\rho}{R}\left(1\pm\frac{A}{L}\right)\right]^{\frac{1}{2}}. \qquad (43)$$

Equation (43) gives the angle of diffraction β as a function of the astigmatism. This expression can be utilized to determine the limits of an angular range of the spectrum within which astigmatism is smaller than a certain, pre-assigned value. If this value is taken equal to an astigmatism which can be considered as negligible or tolerable under certain circumstances, Eq. (43) determines the angular extension of a quasi-stigmatic range in the spectrum of the torus grating.

Figure 5 gives a result of (43) which has been evaluated for an astigmatism equal to the diffraction width of the respective spectral images in the z direction. The widths of the quasi-stigmatic ranges is given in angstroms. The evaluation is based on a torus grating of the dimensions (22). The figure demonstrates that a pronounced maximum of the width exists for $\beta=0$. The extension of the quasi-stigmatic ranges is approximately equal at both sides of the stigmatic points with exception of those in which the stigmatic points lie in the proximity of the grating normal. There, the ranges pertaining to the two close stigmatic points begin to fuse and form a single, yet greater range. The broken line on the top of the curve illustrates this phenomenon. The pattern of the curve in Fig. 5 can also be read from Fig. 3. It can also be demonstrated analytically, that the range must have a maximum for $\beta=0$. To this effect, (42) must be differentiated with respect to β:

$$dA/d\beta=(L/\rho)\{[(R\cos^2\alpha-\rho)/\cos\alpha]+2R\cos\beta\}\cdot\sin\beta. \qquad (44)$$

Equation (44) becomes zero for $\beta=0$.

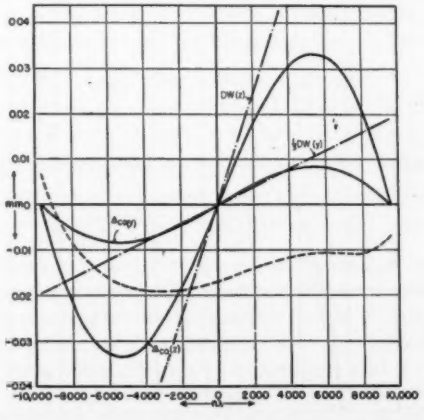

FIG. 6. Coma present in equatorial points of stigmatic wavelengths in the y and the z direction, $\Delta_{Co(y)}$ and $\Delta_{Co(z)}$, respectively. - - - Coma present in equatorial points of a spectrum produced by a spherical grating of corresponding dimensions. —·—·— Diffraction widths (full amount for z, one-third for y) at the same points.

The values of the wave-lengths which are imaged stigmatically in the region of the grating normal are fixed, since they are determined by the ratio of the radii and by the grating constant, according to (35). This fact must be kept in mind when choosing the value for ρ/R of a torus grating; the values for ρ, R and D must be such that stigmatic images of the wave-length range mostly used are formed around the grating normal.

5. Secondary Astigmatism

By secondary astigmatism we understand that which is controlled by those members which, in T_3, contain the variables z, z_a, and z_b in a power higher than the second. These members are expressed in a different way:

$$T_3(SA)=-\frac{1}{8}\left[\frac{1}{r_a}\left(\frac{1}{r_a}-\frac{\cos\alpha}{\rho}\right)^2+\frac{1}{r_b}\left(\frac{1}{r_b}-\frac{\cos\beta}{\rho}\right)^2\right]z^4$$
$$-\frac{1}{4}\left[\frac{1}{r_a^2}\left(\frac{1}{r_a}-\frac{\cos\alpha}{\rho}\right)(z_a^2-2zz_a)\right.$$
$$\left.+\frac{1}{r_b^2}\left(\frac{1}{r_b}-\frac{\cos\beta}{\rho}\right)(z_b^2-2zz_b)\right]z^2$$
$$-\frac{1}{8}\left[\frac{1}{r_a^3}(z_a^2-2zz_a)^2+\frac{1}{r_b^3}(z_b^2-2zz_b)^2\right]. \quad (45)$$

With respect to (26) which must be maintained as the condition for elimination of primary astigmatism, the partial derivative of (45) with respect to z does not, generally, vanish. This means that, in accordance with (21), we will have finite values of the partial derivative of (45) accounting for the existence of secondary astigmatism. This becomes important as the only existent astigmatism in stigmatic spectral lines. As an evaluation shows, the first and the second bracket of (45) can be neglected in view of their insignificance. Secondary astigmatism resulting from these parts of (45) is more than 1000 times smaller than the mean diffraction width of the stigmatic images in the z direction. The third bracket of (45), however, can under certain circumstances become large enough to gain importance. Hence, differentiating and substituting r_a and r_b in accordance with (24), one has:

$$\frac{\partial T_3(SA)}{\partial z}=-\frac{1}{2R^3\cos^3\alpha}[2z_a^2z-z_a^3]$$
$$-\frac{1}{2R^3\cos^3\beta}[2z_b^2z-z_b^3]. \quad (46)$$

z_a can be eliminated by application of the relation: $z_a/\cos\alpha=-z_b/\cos\beta$:

$$\frac{\partial T_3(SA)}{\partial z}=-\frac{1}{2R^3\cos^3\alpha}\left[2\frac{\cos^2\alpha}{\cos^2\beta}z_b^2z+\frac{\cos^3\alpha}{\cos^3\beta}z_b^3\right]$$
$$-\frac{1}{2R^3\cos^3\beta}[2z_b^2z-z_b^3]. \quad (47)$$

Applying Eq. (21), (47) yields, after proper simplification, the amount of secondary astigmatism as a function of z and z_b:

$$\Delta(SA)=-\frac{1}{R^2\cos\varphi}\cdot\frac{\cos\alpha+\cos\beta}{\cos\alpha\cdot\cos^3\beta}z_b^2z. \quad (48)$$

An evaluation of (48) yields 0.01 mm for the value of the secondary astigmatism, if the end points of a spectral line, 200 mm long, are taken. This value of 0.01 mm is smaller than the diffraction width of the spectral images in the z direction. Thus, secondary astigmatism can hardly be a limiting factor even in spectrohelioscopy, where extremely long slits and accordingly long spectral lines are used.

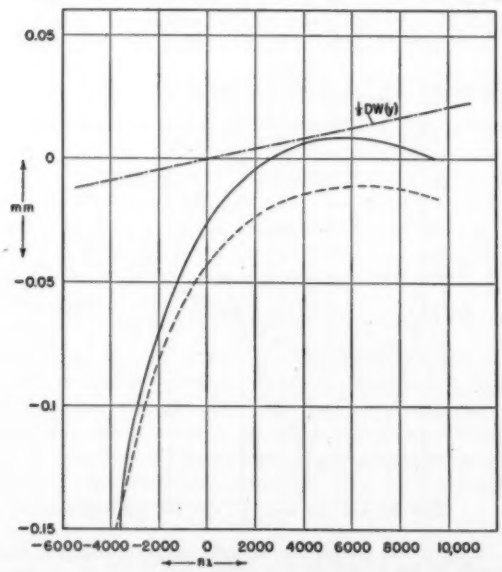

FIG. 7. Coma present in the equatorial cross section of the spectrum for a value of $\alpha=\text{arc}\cos[\rho/R]$ as a function of the wave-length $n\cdot\lambda$. – – – Corresponding values for the spherical grating. —·—·— One-third of the diffraction width in the y direction.

6. Concluding Remarks Regarding Astigmatism of the Torus Grating

In the preceding sections of this chapter, astigmatism and the limits of the quasi-stigmatic ranges have been discussed in relation to the diffraction width of the spectral images in the z direction. The results obtained in these sections, therefore, are valid within the theoretical limits of image formation. In many cases much greater deviations from the stigmatic image, which is attainable theoretically, can be tolerated. Accordingly,

the extension of the quasi-stigmatic ranges will be considerably larger than those given in Fig. 5. Moreover, the values in Fig. 5 are based on a grating having 20,000 grooves per inch; with a grating having a larger grating constant, the widths of the quasi-stigmatic ranges will further be increased considerably. Under certain circumstances, these ranges may easily cover sections as large as the entire visible part of the spectrum.

The chief advantage of the torus grating, besides the elimination of astigmatism for distinguished ranges, lies in the fact that its spectrum exhibits a considerably higher intensity than that produced by a spherical grating, if small-sized light sources are to be investigated. The ratio of the intensities in the spectra of both gratings can be expressed as follows:

$$\frac{I(T)}{I(S)}=\frac{c(\cos\beta/\cos\alpha)+A(S)}{c(\cos\beta/\cos\alpha)+A(T)}, \tag{49}$$

whence c represents the cross section of the light source's image on the slit, $A(S)$ and $A(T)$ are the values of the astigmatism produced by the respective gratings. Equation (49) demonstrates that, for values of C ranging between 10 mm and 0.5 mm, the torus grating produces spectra which are 3 to 50 times brighter than those formed by a spherical grating of otherwise equal dimensions.

Disregarding the higher resolving power which can be obtained by a plane grating, one may say that the torus grating is practically as efficient as a plane grating. In addition to this, the torus grating is distinguished by having two advantages over the former: (1) It does not require collimator- and camera-objectives, and (2) it imposes no limitations on the length of the spectrum to be recorded simultaneously.

V. T_4: COMA AND CURVATURE OF SPECTRAL LINES

Image imperfections, originating in a two-dimensional extension of the optically active part of the grating, are controlled by T_4 in (20) which contains cross products of y and z. Such imperfections are coma and curvature of spectral lines. The individual members of T_4 can be made equal to zero for equatorial points of stigmatic spectral lines only, while simultaneously $\alpha=\beta$. T_4, therefore, must be evaluated for the values of coma, and curvature which are to be anticipated.

1. Coma

The amount of coma, present in the equatorial points of stigmatic spectral lines, can be found by application of (21) to T_4. In constrast to the spherical grating, those members in T_4 which contain z_a and z_b play no part in the formation of coma in the case now under consideration. For stigmatic image formation makes $z_b=0$, if $z_a=0$; however, in the spectrum of the spherical grating, light, contributing to equatorial image points, originates to a large extent from slit points outside the equatorial plane since astigmatism prevails. The members in T_4 which contain z_a and z_b are equal to zero in our case.

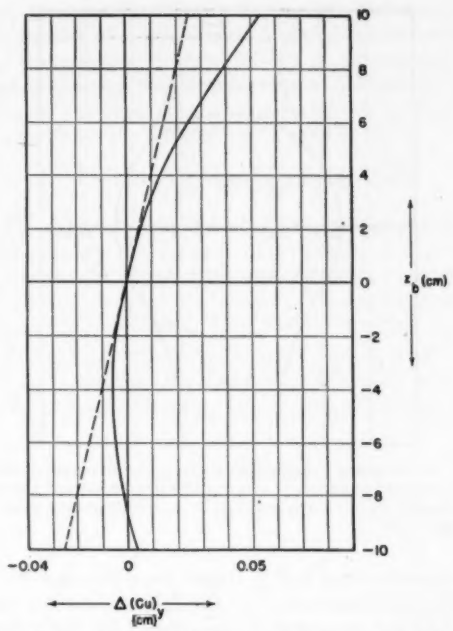

FIG. 8. Inclination (– – –) and curvature (———) of the stigmatic spectral line $n\cdot\lambda=6563$A at the grating normal.

Since astigmatism is equal to zero, the amount of coma must be evaluated for both the y and the z direction. This is done by differentiating the members of T_4 concerned, with respect to both variables y and z, consecutively. With respect to the considerations outlined above, we introduce (24) and, proceeding in accordance with (21), we obtain the amount of coma present in the equatorial points of stigmatic spectral lines in both the y and the z directions:

$$\Delta(\mathrm{CoS}l)_y=(1/2R\rho)[(\sin\alpha/\cos^2\alpha)(\rho-R\cos^2\alpha)+(\sin\beta/\cos^2\beta)(\rho-R\cos^2\beta)]z^2+(1/R^2\rho)[(\sin^2\alpha/\cos^3\alpha)\times(\rho-R\cos^2\alpha)+(\sin^2\beta/\cos^3\beta)(\rho-R\cos^2\beta)]yz^2 \tag{50}$$

$$\Delta(\mathrm{CoS}l)_z=(1/R\rho)[(\sin\alpha/\cos^2\alpha)(\rho-R\cos^2\alpha)+(\sin\beta/\cos^2\beta)(\rho-R\cos^2\beta)]yz+(1/R^2\rho)[(\sin^2\alpha/\cos^3\alpha)\times(\rho-R\cos^2\alpha)+(\sin^2\beta/\cos^3\beta)(\rho-R\cos^2\beta)]y^2z. \tag{51}$$

Equations (50) and (51) have been evaluated numerically for a torus grating of the dimensions (22); the results are represented graphically in Fig. 6. Abscissas are wave-lengths in angstroms. To each wave-length pertains a certain pair of the angles α and β, which have been calculated by means of (33). The broken line gives the corresponding values of coma in the y direction, produced by a spherical grating of similar dimensions. The corresponding values of coma in the z direction, as produced by a spherical grating, are uninteresting, since coma (z) is overlapped by astigmatism.

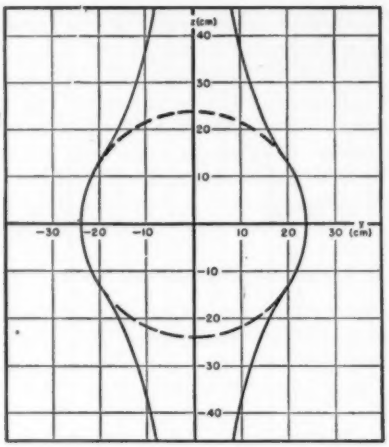

FIG. 9. Outline of a diaphragm necessary to eliminate excessive aberration for the stigmatic spectral line $n\cdot\lambda=6563$A at the grating normal (——— torus grating; - - - corresponding spherical grating).

The dash-dot lines in Fig. 6 give the diffraction widths for the two directions, i.e., the full amount for the z direction and one-third of the amount for the y direction. As can be concluded from Fig. 6, the resolving power of the torus grating is generally not impaired by coma. In some cases, such an impairment can exist; it can be avoided by reducing the width of the ruling (y) or/and of the length of the grooves (z) according to (50) and (51).

Owing to the conditions of stigmatic image formation, the loci of slit and image were different for each wave-length represented in Fig. 6. Yet, in many a case, gratings are used with a fixed setting of the slit (α = constant), while larger sections of the spectrum are

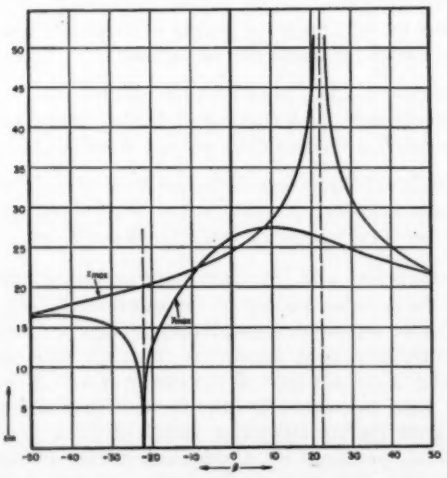

FIG. 10. Maximum permissible half-widths, y_{max} and z_{max}, of the grating's aperture for the angle of incidence $\alpha=\text{arc cos}[\rho/R]^{\frac{1}{2}}$, as a function of the angle of diffraction β.

to be examined simultaneously. Hence, an expression for coma in the equatorial cross section of the spectrum with a constant α must be found. For this case, the expressions in T_4 which contain z_a and z_b play a part in the formation of coma, since with finite values of astigmatism a certain section of the slit contributes to the image point in the equatorial plane. Therefore, the entire expression T_4 is involved, disregarding members containing y^2 as insignificant in comparison to those containing y. Introducing the condition for the Rowland circle (24) and transforming, we obtain:

$$T_4=(1/2R^2\rho)[(\sin\alpha/\cos^2\alpha)(\rho-R\cos^2\alpha)+(\sin\beta/\cos^2\beta)\times(\rho-R\cos^2\beta)]yz^2+(1/R^2)[(\sin\alpha/\cos^2\alpha)\cdot z_a+(\sin\beta/\cos^2\beta)z_b]yz+(1/2R^2)[(\sin\alpha/\cos^2\alpha)\cdot z_a^2+(\sin\beta/\cos^2\beta)z_b^2]y. \quad (52)$$

In order to determine the length of the slit z_a, as measured from the center, which contributes to the image formation at the point z_b, on account of astigmatism, we refer to Eq. (25). Setting $z_b=0$, and introducing the condition (24) one has:

$$z_a=(\cos\alpha+\cos\beta)(\rho-R\cos\alpha\cdot\cos\beta)z/\rho\cos\beta. \quad (53)$$

In (52), setting $z_b=0$, and substituting z_a by the value (53), we arrive at:

$$\Delta(\text{Co})_y=(1/2R\rho)[(\sin\alpha/\cos^2\alpha)(\rho-R\cdot\cos^2\alpha)+(\sin\beta/\cos^2\beta)\times(\rho-R\cos^2\beta)-(2\sin\alpha/\cos^2\alpha\cos\beta)(\cos\alpha+\cos\beta)\times(\rho-R\cos\alpha\cdot\cos\beta)+(\sin\alpha/\rho\cos^2\alpha\cdot\cos^2\beta)\times(\cos\alpha+\cos\beta)^2(\rho-R\cos\alpha\cdot\cos\beta)^2]z^2. \quad (54)$$

according to procedure (21). Figure 7 gives the result of an evaluation of (54) which was carried out for the torus grating (22) with $\alpha=31°7'$ and accordingly the stigmatic image on the grating normal with λ6563. The broken line represents the corresponding values pertaining to the spherical grating under similar conditions; these values have been calculated by means of Beutler's formula (*61B*).[5] As can be concluded from Fig. 7, the resolving power of the torus grating is not impaired for values $n\cdot\lambda>1000$A. In cases where such an impairment might occur, it can be overcome by restricting the length of the grooves z, as Eq. (54) demonstrates.

A calculation of coma in the z direction is not required for the latter case, since astigmatism exceeds coma outside the quasi-stigmatic ranges.

As mentioned above, coma can be controlled by restricting the length of the grating grooves. In his paper,[5] Beutler refers to cases in which coma can preferably be decreased by restricting the illuminated segment of the slit. Restriction of the slit's length has the effect that less points of the slit contribute to the formation of equatorial image points and to their imperfections. Yet it can be shown for the torus grating that its astigmatism is, generally, too small to necessitate application of this second method to check coma.

2. Curvature and Inclination of Spectral Lines

A sheet of light, emerging from a slit point and being limited by a groove, is part of the surface of an oblique circular cone. If astigmatism is small as in our case, the effect of this curvature on the spectral lines is negligible. Yet a finite length of the slit will also cause certain deformations of the spectral lines which may now be discussed. Deformations due to this effect arise whenever z_b appears in any power in T_4, for, if z_b is a variable, i.e., moving up and down the spectral line, the partial derivatives $\partial T_4(Cu)/\partial y$ and $\partial T_4(Cu)/\partial z$ will be functions of z_b. These functions describe the nature of displacement which the focus displays outside the equatorial plane. An inclination of the spectral lines will result, if an odd power of z_b is present; a parabolic curvature will prevail, if an even power of z_b is present. Inclination and curvature will be described, if $T_4(Cu)$ is differentiated with respect to y, whereas an expansion (or contraction) of the spectral lines will be described, whenever the partial derivative with respect to z is taken. Proceeding in accordance with the foregoing, we draw from T_4:

$$T_4(z_b)=\tfrac{1}{2}(\sin\alpha/r_a^2)[z_a^2-2zz_a]y + \tfrac{1}{2}(\sin\beta/r_b^2)[z_b^2-2zz_b]y. \quad (55)$$

In (55), the insignificant members in T_4 containing y^2 have been omitted. In the following we are allowed to neglect astigmatism owing to its smallness; this means, mathematically, that the relation $z_a/\cos\alpha=-z_b/\cos\beta$ is a sufficient approximation. We now introduce this relation into (55), proceed in accordance with (24) and (21), differentiating with respect to y, and we obtain, after proper simplification, the formulas for inclination and curvature as a function of z_b:

$$\Delta(Cu)_y = \frac{z}{R\cos\beta\cdot\cos\varphi}[\tan\alpha-\tan\beta]z_b \quad \text{(inclination)}$$

$$+\frac{1}{2R\cos^2\beta\cos\varphi}[\sin\alpha+\sin\beta]z_b^2 \quad \text{(curvature)}. \quad (56)$$

Developing in the same manner with respect to z yields the amount of expansion or contraction of the spectral lines as a function of z_b:

$$\Delta(Cu)_z=\frac{y}{R\cos\beta\cdot\cos\varphi}[\tan\alpha-\tan\beta]z_b$$

(expansion, contraction). (57)

The displacements as given by (56) and (57) are components of a resultant which determines the locus of the spectral lines on the Rowland cylinder. The combined effect of the deformations bends the spectral lines to parabolas whose vertices are shifted away from the equatorial plane. Figure 8 shows the curvature of the spectral line $n\cdot\lambda 6563$ ($\beta=0$) as an example. The broken line represents the effect of inclination alone, whereas the expansion cannot be shown, because it is too small for the scale on the z_b axis.

VI. T_5: ABERRATION

The member T_5 in the equation of the torus grating (20) controls the amount of aberration found in the spectrum. An examination shows that T_5 vanishes only in the case $\alpha=\beta=0$. As is known, the existence of aberration imposes certain limits on the grating aperture, in both the y and z directions, if intensity losses caused by rays, reaching the focus with improper phase, are to be avoided. Moreover, aberration causes, generally,

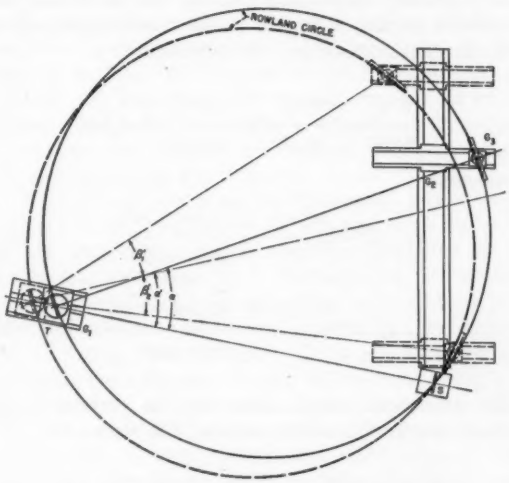

FIG. 11. A mount for a torus grating. For details see the last chapter of this paper.

a broadening of the spectral lines, the amount of which may damage the resolving power of the grating.

1. Aberration and Limitations of the Grating Aperture

Transforming T_5, after the condition for the Rowland circle (24) has been introduced, yields:

$$T_5=\left[\frac{\sin^2\alpha}{\cos\alpha}+\frac{\sin^2\beta}{\cos\beta}\right]\left[\frac{y^4}{8R^3}+\frac{y^2z^2}{4R^2\rho}\right] + \frac{(\cos\alpha+\cos\beta)(\rho-R\cos\alpha\cdot\cos\beta)}{8R\rho^3\cos\alpha\cos\beta}z^4. \quad (58)$$

The limitations which must be imposed on the values y and z can be determined by the condition that the

values of (58) must not exceed one-quarter wave-length:

$$\left[\frac{\sin^2\alpha}{\cos\alpha}+\frac{\sin^2\beta}{\cos\beta}\right]\left[\frac{y^4}{8R^3}+\frac{y^2z^2}{4R^2\rho}\right]$$

$$+\frac{(\cos\alpha+\cos\beta)(\rho-R\cos\alpha\cdot\cos\beta)}{8R\rho^3\cos\alpha\cdot\cos\beta}z^4\leqq\frac{\lambda}{4}$$

or referring to (23):

$$=D/4n(\sin\alpha+\sin\beta). \tag{59}$$

For the following, it may be remembered that y and z are coordinates of a system with its origin at the center of the grating ruling; hence, in this system, we can consider (59) as a function which represents the outlines of a grating diaphragm defining the maximum permissible grating aperture. Under these circumstances, we develop after proper rearrangement:

$$\frac{n\cdot H}{2R^3D}y^4+\frac{n\cdot H}{R^2\rho D}y^2z^2+\frac{n\cdot K}{2R\rho^3D}z^4-1=0, \tag{60}$$

whence

$$H=\cot\frac{\alpha+\beta}{2}\cdot\frac{(1-\cos\alpha\cdot\cos\beta)}{\cos\alpha\cdot\cos\beta}; \tag{61}$$

$$K=\cot\frac{\alpha+\beta}{2}\cdot\frac{(\rho-R\cos\alpha\cdot\cos\beta)}{\cos\alpha\cdot\cos\beta}. \tag{62}$$

The aforementioned function for the outlines of the diaphragm is obtained by solving (60) for z:

$$z=\pm\left\{\frac{R\rho^3D}{n\cdot K}\left[\left(\frac{n^2H^2}{R^4\rho^2D^2}y^4-2\frac{nK}{R\rho^3D}\left\{\frac{nH}{2R^3D}y^4-1\right\}\right)^{\frac{1}{2}}-\frac{n\cdot H}{R^2\rho D}y^2\right]\right\}^{\frac{1}{2}}. \tag{63}$$

We shall obtain the corresponding formulas pertaining to the spherical grating if we substitute ρ by R in T_5. Then we see that $T_5(S)$ becomes an expanded binomial which can be written as follows:

$$T_5(S)=\frac{1}{8R^2}\left[\frac{1}{r_a}-\frac{\cos\alpha}{R}+\frac{1}{r_b}-\frac{\cos\beta}{R}\right]r^4;\ r^4=(y^2+z^2)^2. \tag{64S}$$

r, obviously, is the radius of a circle with its center on the midpoint of the grating ruling. Because of the symmetry of (64S), the diaphragms for the spherical grating are circles.

In contrast to the spherical grating, the diaphragms of the torus grating are oblate closed curves which are, in general, more extended in the z direction than in the y direction. In a few number of cases, the outlines of the diaphragms are more extended in the y direction. If the axial diameters of the diaphragms are equal, and those cases occur only under special circumstances, the outlines are not circles. The stigmatic points are distinguished by special properties of the appertaining diaphragms, inasmuch as no limitations for their extension in the z direction—for $y=0$, exist. This can easily be demonstrated. Since the stigmatic points are determined by the validity of (29), the expression (62) will assume the value zero for the stigmatic points. Hence, the equation for the diaphragms pertaining to the stigmatic points will be found by solving (60) for z, with $K=0$:

$$z=\pm\left[\frac{R^2\rho D}{n}\cdot\tan\frac{\alpha+\beta}{2}\cdot\frac{\cos\alpha\cdot\cos\beta}{1-\cos\alpha\cdot\cos\beta}\cdot\frac{1}{y^2}-\frac{\rho}{2R}y^2\right]^{\frac{1}{2}}. \tag{65}$$

Equation (65) reveals that z_{max} will be infinite for $y=0$. Figure 9 shows the outlines of a diaphragm which represents the optimum aperture of the grating for the stigmatic point at the grating normal ($\beta=0$, $\alpha=\arccos(\rho/R)$, $\lambda=6563$A). The broken circle in Fig. 9 pertains to the spherical grating under the same conditions. The maximum extension y_{max} in both diaphragms is equal; this was to be expected, since the difference between the two gratings vanish for $z=0$.

The numerical evaluation of Eq. (63) for any general case is very laborious. Therefore, we restrict the discussion by examining the axial diameters of the various diaphragms as functions of α and β. The axial half-diameters of the diaphragms, y_{max} and z_{max}, can be determined by means of (60), if z and y are set equal to zero, consecutively; hence:

$$y_{max}=\{|[2R^3D/n][\tan(\alpha+\beta)/2][\cos\alpha\cdot\cos\beta]/[1-\cos\alpha\cdot\cos\beta]|\}^{\frac{1}{4}}. \tag{66}$$

This expression holds for both the spherical and the torus grating; setting $y=0$ in (60) yields:

$$z_{max}=\{|[2R\rho^3D/n][\tan(\alpha+\beta)/2][\cos\alpha\cdot\cos\beta]/[\rho-R\cos\alpha\cdot\cos\beta]|\}^{\frac{1}{4}}. \tag{67}$$

The Eqs. (66) and (67) have been evaluated with β as the independent variable, while α was set equal to $\arccos[\rho/R]^{\frac{1}{2}}$; consequently, as (36) shows, the stigmatic points coincide with the slit and the neutral image in this case. The results of this evaluation are given in Fig. 10, where y_{max} simultaneously represents the radius of the corresponding circular diaphragms of the spherical grating. As can be seen, y_{max} becomes equal to zero for the neutral image on account of (59) with $\lambda=0$. In the case chosen here, z_{max} does not vanish for the neutral image, since it coincides with one of the stigmatic points. We then have: $\alpha=-\beta$, and $\rho-R\cdot\cos\alpha\cos\beta=0$. Hence, an undeterminate form results

from (67) the limes of which fits the course of the z_{max}-curve at the critical point. For a calculation of the complete outlines of the diaphragms for any particular case of α, β, n, and λ we have to refer to Eq. (63).

The numerical values for the dimensions of the grating diaphragms in Fig. 9 indicate that for the usual extensions of the rulings, diaphragms must be applied only for large angles of incidence and diffraction, small radii, and spectra of high order.

2. Aberration and Broadening of Spectral Lines

T_5, which vanishes for $\alpha=\beta=0$ only, gives rise to an imperfection of the image, known as the broadening of spectral lines by aberration. The formula hereto can easily be derived in the same manner as those describing coma. To this effect, we submit T_5 to the procedure (21), differentiating with respect to y. An evaluation of the formula:

$$\Delta(Br)_y=(1/2R^2)[(\sin^2\alpha/\cos\alpha)+(\sin^2\beta/\cos\beta)]y^3 +(1/2R\rho)[(\sin^2\alpha/\cos\alpha)+(\sin^2\beta/\cos\beta)]yz^2 \quad (68)$$

obtained in this manner, demonstrates that the broadening effect on account of aberration is of the order 10^{-3} mm for that range of α and β, where stigmatic images can be obtained. This means that broadening of spectral lines by aberration is, in general, insignificant for the torus grating. Only if the torus grating is used at large angles of incidence and diffraction, maintenance of the gratings's resolving power must be observed by restricting y and z according to (68).

As can be shown, image imperfections, originating in aberration in the z direction, are irrelevant for a torus grating under usual circumstances of its use.

VII. THE MOUNTING OF THE TORUS GRATING

The torus grating suits each mounting which is generally in use for the spherical grating, because all mountings are based on the existence of the Rowland circle common to both gratings. Yet the torus grating demands a more liberal choice of the angles of incidence and diffraction, if the stigmatic image formation is to be utilized in full. For instance, the whole range of stigmatic images the torus grating (22) possesses is accessible only if the mounting permits a setting of α and β at least within the following limits:

$$+22°17' \leqslant \alpha \leqslant +31°7'$$
$$-22°17' \leqslant \beta \leqslant +22°17'. \quad (69)$$

None of the mountings known which are suitable for the spherical grating allows a free choice for the values of α and β simultaneously. Although each wave-length $n\cdot\lambda$ in the spectrum can be imaged with an infinite number of combinations of the angles α and β, the various grating mountings are characterized by certain limitations regarding the choice of the angles:

Rowland	$\beta=0$
Runge-Paschen[6]	$\alpha=$constant
Abney[7]	$\beta=0$
Eagle[8]	$\alpha=\beta$

(70)

The width of the plateholder is the only element which permits a variation of the angle β in the mountings of Rowland, Abney, and Eagle, while, simultaneously, there is a free choice for the angle α. Yet, the plateholders cannot sufficiently be extended to cover the entire range of values which the angle β must assume in order to reach all stigmatic points. With the range of angles given by (69), the position of the slit is restricted to one side of the grating normal ($\alpha>0$), as is the case in all mountings of the spherical grating, except in the Eagle mounting. For all cases of stigmatic image formation in accordance with (69), we have $\alpha>\beta$. Figures 3 and 4 demonstrate that these conditions render those stigmatic points accessible which are closer to the grating normal. Yet this is no disadvantage; for, in general, the image imperfections are smaller for small values of β, and, in particular, the stigmatic ranges have their maximum extension in the proximity of the grating normal, as Fig. 5 shows.

A mounting suitable for the torus grating is given in Fig. 11. It is characterized by a considerable mobility of the plateholder, which affords accessibility of all angles β as determined by (69). S is the slit, T the torus grating; G_1, G_2, and G_3 are guiding ways making possible the necessary adjustments of the plateholder and of the grating. The full and the broken lines in Fig. 11 demonstrate different settings of the mounting. The condition that the slit be in a fixed position is mandatory because of the bulky equipment which, ordinarily, is involved in many laboratorial light sources. The exact adjustment of one of the stigmatic points to a specific spectral line desired, necessitates an accurate measuring and setting of the respective angle of incidence α. Fortunately, the grating, with its ruling in connection with the well-known wave-lengths of light, is an ideal instrument to measure angles. Hence, the adjustment of specific angles α can be carried out to a sufficient accuracy without special means.

The author is not in the position to form an opinion on the technical question, whether a toric surface can be ground appropriately as to accuracy and size, to serve as a blank for a torus grating. In view of the advantages, the torus grating, obviously, has in comparison to the spherical grating, it seems to be worth while to consider the possibilities of grinding such surfaces.

---

[6] Runge and Paschen, Abh. d. K. Akad. d. Wiss. z-Berlin, Anhang 1 (1902).
[7] W. W. Abney, Trans. Roy. Soc. London **A177**, 457 (1886).
[8] A. Eagle, Astrophys. J. **31**, 120 (1910).

Color Correction with Colored Couplers*

W. T. Hanson, Jr.
Kodak Research Laboratories, Eastman Kodak Company, Rochester, New York
(Received November 16, 1949)

The optical characteristics of colored dye-forming couplers of a type suitable for use in color films, such as Kodacolor or Ansco Color, are described. Destruction of the color of the coupler by the image dye-forming reactions of color development leads to a negative image composed of the color-developed dye and a positive image composed of unused coupler. It is shown that the effect on color reproduction of the overlapping absorptions of the image dyes available for use in color negative films can be eliminated by the use of colored couplers which have the proper spectral-absorption characteristics. The role of the six masks which are found to be required by a number of the theoretical treatments of the problem of exact color reproduction can be filled by colored couplers having the proper spectral-absorption characteristics. The effect of colored couplers on film speed is also discussed.

DURING the many years three-color subtractive reproduction has been in use, many cases have arisen in which the results obtained by straightforward means were not satisfactory and methods for improving these results have been sought. The technique of masking which was invented by Albert[1] in 1899 has become one of the important means of effecting improved color reproduction. A great deal of work has been done in developing practical techniques of masking to give better results; and the possible application of masking to the establishment of conditions for exact color reproduction has been investigated. In fact, masking has become an integral part of most of the theories of exact three-color reproduction.

A more recent method of improving color reproduction is the use of "colored couplers." These materials have been described by Hanson and Vittum,[2] and by Vittum, Sawdey, Herdle, and Scholl.[3] The usefulness of such couplers is limited to films, such as Kodacolor or Ansco Color, which contain couplers that react with oxidized developer to form dyes. If the coupler which is originally present in a given layer of such a film is colored, having absorption in the desired region of the spectrum, and if during the coupling or dye-forming reaction the color of the coupler which is converted to dye is destroyed, the final color-developed image will be composed of a negative (or positive, if reversal processing is used) composed of the coupled dye image and a positive (or negative) composed of the residual unused coupler.

The application of this type of coupler to color photographic films requires a knowledge of the optical characteristics of the colored-coupler images and the control of these characteristics so that they conform with the known practical requirements for producing color photographs. It is helpful to study the characteristics of such materials from the point of view of the established theories for exact color reproduction. Such a study may define the behavior required of colored couplers which will make them fulfill the purpose of the six masks which are derived by a number of the studies of three-color reproduction.

Optical Characteristics of Images Derived from Colored Couplers

Since, for the colored coupler to perform its function, it must remain in the film and thus contribute an over-all color or density to the film, films containing colored couplers are not satisfactory for viewing. For this reason, the following treatment will be confined to negative films. Actually, the same principles are involved in dealing with reversal or direct positive images. The most complete description of the optical behavior of images derived from colored couplers is given by spectrophotometric curves. For use in photographic work, it is also necessary to describe such images in terms of their density in three regions of the spectrum—specifically, by means of their density as measured with the sensitivity distributions of the three emulsions of the printing film or paper. For the sake of simplicity, we shall use here three monochromatic lines, 440, 560, and 680 mμ for specifying the densities in the blue, green, and red regions of the spectrum.

Let us assume that we have a colored coupler, which at a given concentration has the spectral-density curve shown in Fig. 1, curve a. In addition, let us assume that when *all* of this coupler has reacted with oxidized developer to form a dye, the spectral-density curve of this dye is that shown as curve b. If the dyes (coupler and coupled dye) follow Beer's law, an intermediate condition, under which part of the coupler has reacted with oxidized developer to form dye, will be represented by the additional curve in Fig. 1. All the curves cross at a point known as the isosbestic point.[4,5] This point occurs

* Communication No. 1299 from the Kodak Research Laboratories.

[1] E. Albert, German Patent 101,379 (1899); German Patent 116,538 (1900).

[2] W. T. Hanson, Jr. and P. W. Vittum, J. Phot. Soc. Am. 13, 94 (1947).

[3] Vittum, Sawdey, Herdle, and Scholl, J. Am. Chem. Soc. (to be published).

[4] W. R. Brode, *Chemical Spectroscopy* (John Wiley and Sons, Inc., New York, 1943), second edition.

[5] Thiel, Dassler, and Wulfken, Fortschr. Chem., Physik u. physik. Chemie 18, 1–120 (1924).

only if the dye formed and any other absorbing materials which are formed or destroyed are strictly proportional to the amount of coupler which is consumed. Observations of the presence or absence of this crossing point are quite useful in studying the reactions which take place in a system of this sort.

If we assume that the various amounts of dye shown in Fig. 1 occur in different areas of a photographic image, then the densities in the three regions of the spectrum (440, 560, and 680 mμ) may be plotted against the logarithms of the exposures which lead to those densities to give the well-known H and D curve of the photographic process. This, however, requires a knowledge of the relationship between the values of log$E$ and the amount of dye formed. Since we are here concerned primarily with the *relative* characteristics of the H and D curves derived from the densities in the three regions of the spectrum, we shall assume that the D-log$E$ relationship for green-light densities is linear, with a slope of unity. If the insignificant densities in the red region are neglected, the H and D curves of the green-light and blue-light densities of this coupler-dye system are shown in Fig. 2. The blue-light density curve has a slope of −0.38. Both curves have definite limits because we are dealing with the case in which all of the coupler has been converted to dye and are assuming a linear characteristic throughout.

For a given distribution of receptor sensitivity, the slope of this blue-light density curve is a function of the shapes of the spectral-density curves of the colored coupler and of the dye formed from it, and of the extinction coefficients of both. Consequently, the slope can be varied by changing any of these factors.

For example, suppose it is desired that the slope of the blue-density curve be made zero by decreasing the extinction coefficient of the colored coupler. The value of D_{440} of the colored coupler shown in Fig. 1 is 0.93 and D_{440} of the magenta dye formed from this coupler is 0.31. It is required to reduce the density of the colored coupler to this lower value, 0.31. The extinction

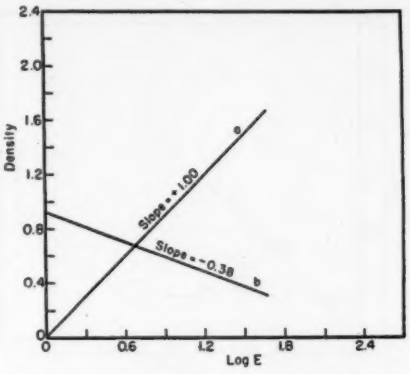

FIG. 2. Assumed H and D curves for dye image shown in Fig. 1: (a) $D_{560}-\log E$, assumed to be linear; (b) $D_{440}-\log E$.

coefficient must be reduced by a factor of 3. Such a colored coupler and dye formed from it (the same dye as shown in Fig. 1) are shown in Fig. 3, curves a and b. The green- and blue-density curves of this pair are shown in Fig. 4.

If it is impossible to change the extinction coefficient of the colored coupler, the same result can be obtained by using a mixture of colored and uncolored couplers, the latter giving the same dye as the colored coupler. To achieve the results shown in Figs. 3 and 4, it would be required to mix two parts of uncolored coupler with one part of the colored coupler shown in Fig. 1. It is also necessary that the two couplers have equal reaction characteristics so that they react to form dye in exactly the same proportions at all density levels. If improper reaction rates occur, one of the couplers will play a greater part in forming the lower densities, and the other, in forming the higher densities. There will be no isosbestic point and the density measured with blue light will not be linearly related to the density measured with green light. Figure 5 shows a typical series of images obtained from a coupler mixture in which the

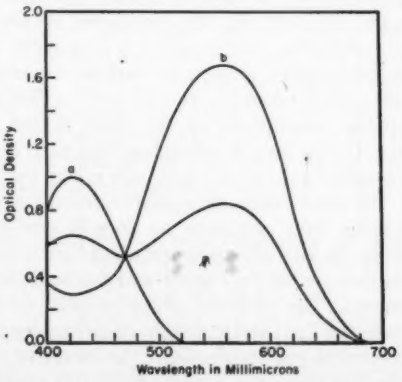

FIG. 1. Spectral-density curves for (a) coupler, (b) magenta dye formed from this coupler. Additional curve shows presence of one-half the coupler and one-half the dye.

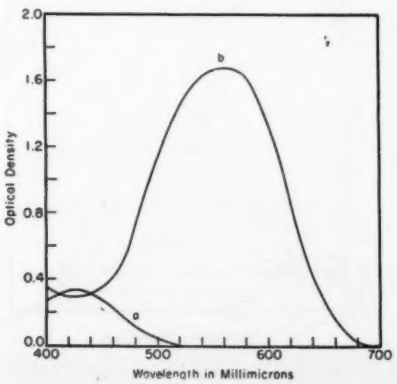

FIG. 3. Spectral-density curves for (a) coupler with lower extinction coefficient than that shown in Fig. 1; (b) magenta dye formed from this coupler.

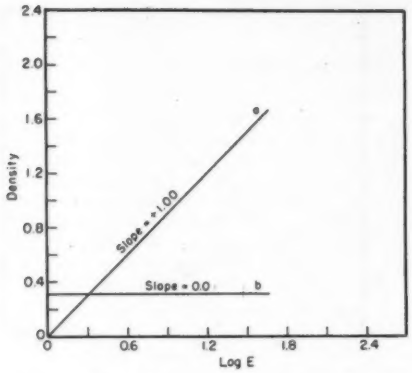

FIG. 4. Assumed H and D curves for dye image shown in Fig. 3: (a) $D_{680}-\log E$, assumed to be linear; (b) $D_{440}-\log E$.

colored coupler, curve a, reacts predominantly in the lower density regions and the uncolored coupler in the higher density regions. The green- and blue-density curves of this series of image components are shown in Fig. 6.

Another useful method of varying the slope of the blue-density curve is the shifting of the position of the absorption band of the colored coupler without a change of extinction coefficient. Figure 7, curve a, shows the spectral-density curve of a colored coupler similar to that shown in Fig. 1, except that the absorption maximum is shifted to 380 mμ. This curve has a density of 0.31 at 440 mμ. Curve b is the same magenta dye shown in Fig. 1. The green- and blue-density curves derived from an image using this colored coupler are similar to those shown in Fig. 4.

Colored couplers can also be made which react with oxidized developer to form cyan dyes. In such cases there is less flexibility in obtaining the proper relationships between the slopes of the three D-log$E$ curves. All cyan dyes have appreciable density in the blue and green regions of the spectrum and the slopes of the green- and blue-density curves must be made to have a given relationship to that of the red-density curve. The colored coupler must have both the proper spectral-absorption characteristics and the proper extinction coefficient. As an example, Fig. 8, curve a, shows the spectral-absorption curve of a typical coupler which forms the cyan dye shown in curve b. This example has been selected so that there are two isosbestic points, at 440 and 560 mμ. The blue- and green-density–log$E$ curves have a slope of zero, as shown in Fig. 9. In this case, the $D_{680}-\log E$ characteristics have been assumed to be linear, with a slope of unity.

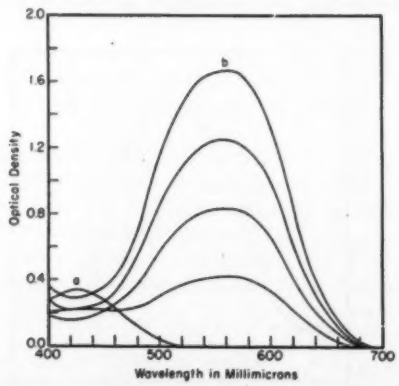

FIG. 5. Spectral-density curves for (a) coupler, and (b) magenta dye formed from a mixture of this coupler with an uncolored coupler. Additional curves show intermediate degrees of dye-forming reaction in which the colored coupler reacts predominantly in the lower density regions.

Compensating for the Dye Absorptions in Negative Films

Experience has shown that, in general, color transparencies made on Monopack-type films, as well as transparencies and prints made from direct camera separation-negatives, give satisfactory quality without the use of masks. However, in making duplicates, where

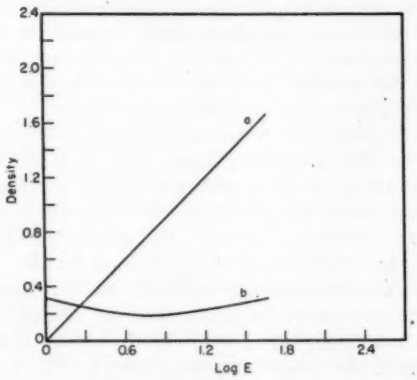

FIG. 6. Assumed H and D curves for dye image shown in Fig. 5: (a) $D_{680}-\log E$ assumed to be linear; (b) $D_{440}-\log E$.

the characteristics of the dyes both in the color original and in the duplicate must be considered, results are not always satisfactory and masking is frequently used. In a negative-positive system of making transparencies or prints, colored couplers can be used to eliminate the overlapping absorptions of the dyes in the original negative. In this case, it is required that each dye image in the negative control one and only one of the printing lights. The cyan image, for example, should control the red printing light and have no density gradient with respect to the blue and green printing lights. An image such as that shown in Figs. 8 and 9 would fulfill this requirement. The magenta image should control the green printing light and should have no density gradient with respect to red or blue light. An image of the type shown in Fig. 3 and Fig. 4 would fulfill this requirement. The yellow image should control the blue printing light and should have no density gradient with respect to

red and green light. Many of the yellow dyes available for use in color photography fulfill this characteristic satisfactorily and can be used directly without a colored coupler.

Color Reproduction Equations Applied to Colored Coupler Characteristics**

The conditions which a subtractive three-color process must fulfill in order to *approach* "exact" color reproduction have been discussed by Yule,[6] MacAdam,[7] Marriage,[8] and by Brewer, Hanson, and Horton.[9] All these treatments of the subject have led to, or assumed, the use of six masks in the reproduction process. Colored couplers may fill the role played by these six masks.

The mathematical relationships between the dye densities in the reproduction and the "exposure densities" of the original subject as stated by Brewer, Hanson, and Horton,[9] are:†

$$\begin{aligned} c &= \gamma_{cr}D_r+\gamma_{cg}D_g+\gamma_{cb}D_b+K_c; \\ m &= \gamma_{mr}D_r+\gamma_{mg}D_g+\gamma_{mb}D_b+K_m; \\ y &= \gamma_{yr}D_r+\gamma_{yg}D_g+\gamma_{yb}D_b+K_y; \end{aligned} \qquad (1)$$

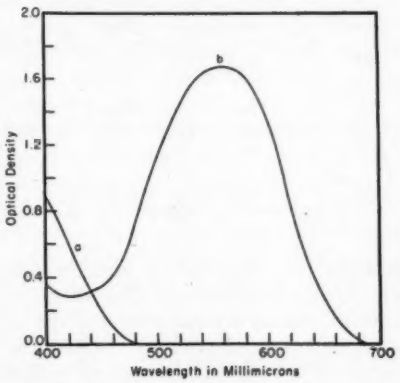

FIG. 7. Spectral-density curves for (a) coupler, and (b) magenta dye formed from this coupler.

where c, m, y are the equivalent neutral densities of the cyan, magenta, and yellow dyes in the reproduction; D_r, D_g, and D_b are the exposure densities of the original subject; and γ_{cr}, etc., are the gammas of the corresponding dye images with respect to the red, green, or blue exposure indicated. The exposure densities are the densities of the subject as measured with the sensitivity distributions of the three film receptors. They are equal

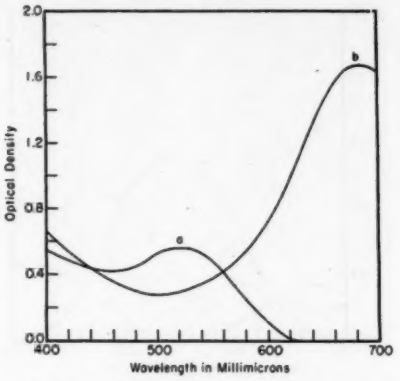

FIG. 8. Spectral-density curves for (a) coupler, and (b) cyan dye formed from this coupler.

to the logarithms of the exposures subtracted from those for white.‡ K_c, K_m, and K_y are constants.

These equations describe the desired structure of the final positive images. If this type of reproduction is arrived at by means of separation negatives (of unit contrast) and masks, the values of γ_{cr}, γ_{mg}, and γ_{yb} are the gammas to which the three positive images must be developed, and the other terms represent the results of the use of masks. The actual gammas of the masks are the coefficients shown in the equations divided by the gammas of the positive images. The mask made from the green negative and used with the red negative in making the cyan image would have a gamma of γ_{cg}/γ_{cr}, etc.

In a three-color process where no masks are used, the reproduction can be expressed by the following simple

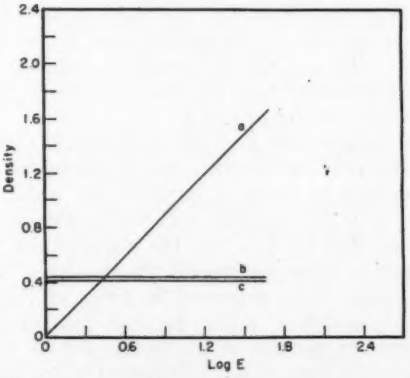

FIG. 9. Assumed H and D curves for dye image shown in Fig. 8: (a) $D_{650}-\log E$ assumed to be linear; (b) $D_{440}-\log E$; (c) $D_{540}-\log E$.

** Calculations similar to those described in this section were made by A. Marriage in 1944 (private communication). The author is happy to acknowledge his priority.

[6] J. A. C. Yule, J. Opt. Soc. Am. **28**, 419 (1938).
[7] D. L. MacAdam, J. Opt. Soc. Am. **28**, 466 (1938).
[8] A. Marriage, Phot. J. **88B**, 75 (1948).
[9] Brewer, Hanson, and Horton, J. Opt. Soc. Am. **39**, 924 (1949).

† These equations do not necessarily describe the actual characteristics of any existing color process. The only means now known for properly controlling the values of the densities of each image component as a function of all three exposure densities is by the use of masks or colored couplers.

‡ Usually image density is related directly to $\log E$ and the gamma of a positive image is, of course, negative. However, in equations relating image density to "exposure density," the arithmetic value of the "gamma" of a positive image is positive since the value of the exposure density is related to $\log E$ by the function constant, $-\log E$.

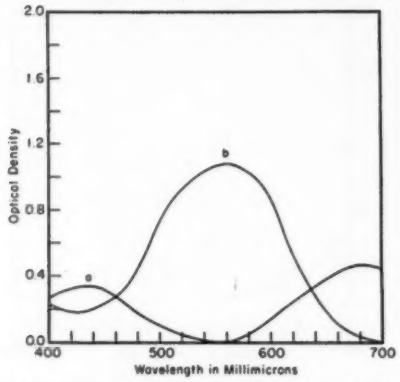

FIG. 10. Spectral-density curves for (a) coupler, and (b) magenta dye formed from this coupler. This pair fulfills the requirements described by Eqs. (6).

equations (assuming linear characteristics):

$$\begin{aligned} c &= \gamma_c D_r + K_c, \\ m &= \gamma_m D_g + K_m, \\ y &= \gamma_y D_b + K_y. \end{aligned} \tag{2}$$

These equations represent the relationships between the c, m, and y equivalent neutral densities of the final positive images and the exposure densities of the original subject photographed. Similar equations can be used to represent the characteristics of the negative and positive stages of a negative-positive system. The positive would be defined by the equations:

$$\begin{aligned} c &= \gamma_c{}^p D_r{}^n + K_c{}^p, \\ m &= \gamma_m{}^p D_g{}^n + K_m{}^p, \\ y &= \gamma_y{}^p D_b{}^n + K_y{}^p, \end{aligned} \tag{2a}$$

where $\gamma_c{}^p$ is the gamma of the cyan image in terms of equivalent neutral density; $\gamma_m{}^p$ and $\gamma_y{}^p$ are the corresponding gammas of the magenta and yellow images; and $D_r{}^n$, $D_g{}^n$, $D_b{}^n$ are the exposure densities of the negative measured with the three sensitivity distributions of the positive process.§

Now, suppose that Eqs. (2a) represent the characteristics of a printing material, such as Kodacolor paper. It is desired to design a negative film which, when printed onto this material, will lead to the characteristics described by Eqs. (1). The negative film will be composed of three dye images, the density of each of these images being expressed in terms of "exposure density," as defined in the previous paragraph. The corresponding gammas of the images will be $\gamma_{cr}{}^n$, the gamma of the cyan image with respect to red exposure density; $\gamma_{cg}{}^n$, the gamma of the cyan image with respect to green exposure density; etc. The density in the negative resulting from a given area in the original subject

§ Since, in the negative, "white" will have higher density than other objects and will thus lead to lower print exposures, the values of the exposure densities, $D_r{}^n$, $D_g{}^n$, and $D_b{}^n$, for objects other than white will be negative. "Exposure density" as used here is similar to "density relative to white," used by Yule (see reference 6).

TABLE I. Numerical values of component image gammas.*

$\gamma_{cr} = 1.846$	$\gamma_{cg} = -0.894$	$\gamma_{cb} = 0.048$
$\gamma_{mr} = -0.651$	$\gamma_{mg} = 2.154$	$\gamma_{mb} = -0.503$
$\gamma_{yr} = -0.516$	$\gamma_{yg} = -0.287$	$\gamma_{yb} = 1.803$

* Derived by Brewer, Hanson, and Horton (see reference 9).

will be the sums of the densities contributed by all three dye images. For subject exposure densities of D_r, D_g, and D_b, the resulting negative exposure densities are

$$\begin{aligned} D_r{}^n &= D_r\gamma_{cr}{}^n + D_g\gamma_{mr}{}^n + D_b\gamma_{yr}{}^n. \\ D_g{}^n &= D_r\gamma_{cg}{}^n + D_g\gamma_{mg}{}^n + D_b\gamma_{yg}{}^n. \\ D_b{}^n &= D_r\gamma_{cb}{}^n + D_g\gamma_{mb}{}^n + D_b\gamma_{yb}{}^n. \end{aligned} \tag{3}$$

The result obtained by printing such a negative onto the positive described by Eqs. (2a) is obtained by substituting these values of $D_r{}^n$, etc., in Eqs. (2a). We obtain

$$\begin{aligned} c &= \gamma_c{}^p(D_r\gamma_{cr}{}^n + D_g\gamma_{mr}{}^n + D_b\gamma_{yr}{}^n) + K_c{}^p. \\ m &= \gamma_m{}^p(D_r\gamma_{cg}{}^n + D_b\gamma_{mg}{}^n + D_g\gamma_{yg}{}^n) + K_m{}^p. \\ y &= \gamma_y{}^p(D_r\gamma_{cb}{}^n + D_g\gamma_{mb}{}^n + D_b\gamma_{yb}{}^n) + K_y{}^p. \end{aligned} \tag{4}$$

These equations are similar in form to those of Eqs. (1). They are identical with Eqs. (1), if

$$\gamma_{cr}{}^n = \frac{\gamma_{cr}}{\gamma_c{}^p}, \quad \gamma_{cg}{}^n = \frac{\gamma_{mr}}{\gamma_m{}^p}, \quad \gamma_{cb}{}^n = \frac{\gamma_{yr}}{\gamma_y{}^p}, \quad K_c{}^p = K_c.$$

$$\gamma_{mr}{}^n = \frac{\gamma_{cg}}{\gamma_c{}^p}, \quad \gamma_{mg}{}^n = \frac{\gamma_{mg}}{\gamma_m{}^p}, \quad \gamma_{mb}{}^n = \frac{\gamma_{yg}}{\gamma_y{}^p}, \quad K_m{}^p = K_m. \tag{5}$$

$$\gamma_{yr}{}^n = \frac{\gamma_{cb}}{\gamma_c{}^p} \quad \gamma_{yg}{}^n = \frac{\gamma_{mb}}{\gamma_m{}^p}, \quad \gamma_{yb}{}^n = \frac{\gamma_{yb}}{\gamma_y{}^p}, \quad K_y{}^p = K_y.$$

These equations, then, can be used for determining the desired characteristics of the three negative images. If the spectral-density characteristics of the developed dye images are known, the characteristics of the colored couplers from which they are derived can be determined.

Color reproduction theory, or the solution of particular problems in color reproduction, leads to values of γ_{cr}, etc. If we assume a print process with given values

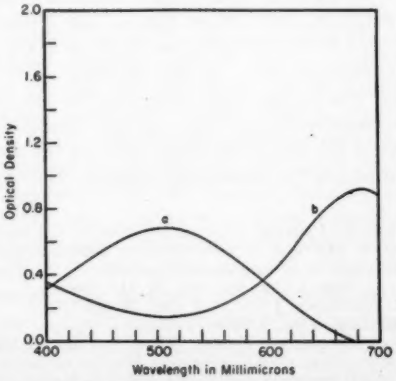

FIG. 11. Spectral-density curves for (a) coupler, and (b) cyan dye formed from this coupler. This pair fulfills the requirements described by Eqs. (6).

of $\gamma^{p}{}_{c,m,y}$, then the desired γ's of the negative images can be calculated.

As an example, let us take Solution II of Brewer, Hanson, and Horton.[9] This represented the best approximate reproduction of a variety of colors. Let us assume that the negative film has the sensitivity distribution of their Fig. 1 and that the print process uses the dyes of their Fig. 2 and has a γ of 2. Their values of γ_{cr}, γ_{cg}, etc., are shown in Table I. Substituting these and the value 2 for $\gamma^{p}{}_{c,m,y}$ in Eqs. (5), we obtain

$$\begin{aligned} &\gamma_{cr}{}^{n} = 0.923, \quad \gamma_{cg}{}^{n} = -0.326, \quad \gamma_{cb}{}^{n} = -0.258, \\ &\gamma_{mr}{}^{n} = -0.447, \quad \gamma_{mg}{}^{n} = 1.077, \quad \gamma_{mb}{}^{n} = -0.143, \quad (6) \\ &\gamma_{yr}{}^{n} = 0.024, \quad \gamma_{yg}{}^{n} = -0.251, \quad \gamma_{yb}{}^{n} = 0.901. \end{aligned}$$

The first row of these equations defines the characteristic of the combined colored-coupler and cyan-dye image, the next row defines the colored-coupler and the magenta-dye image, and the last row defines the colored-coupler and the yellow-dye image. (The sums of the γ's with respect to green, to blue, and to red are all 0.5, the requirement for printing onto a process with a gamma of 2.0.)

These values define the gamma, or density differential, between the dye images and the colored couplers from which they are formed, in three regions of the spectrum. If the spectral-density curves of the image dyes are known, then the three densities of the couplers themselves are defined. For example, suppose the magenta dye is that shown in Fig. 1, curve b. It is repeated in Fig. 10, curve b, in an amount with D_{560}1.077. The values of D_{440} and D_{680} are 0.200 and 0.020, respectively. The colored coupler which forms this amount of dye must have $D_{440}=0.200+0.143=0.343$; $D_{680}=0.020+0.447=0.467$; and $D_{560}=0$. One of the many spectral-density curves which would fulfill this requirement is shown in curve a, Fig. 10.

Similarly, suppose the cyan image dye is that shown in Fig. 8, curve b. It is repeated in Fig. 11, curve b, in an amount with $D_{680}=0.923$. The values of D_{440} and D_{560} are 0.240 and 0.226, respectively. The colored coupler which forms this amount of dye must have $D_{440}=0.240+0.258=0.498$; $D_{560}=0.226+0.326=0.552$; and $D_{680}=0$. One of the many spectral-density curves which would fulfill this requirement is shown in curve a, Fig. 11.

In dealing with the problem of compensating for the dye absorption in negative films, it was stated that many yellow dyes available for use in color photography had no green and red absorption and required no colored coupler. However, the requirements for fulfilling the conditions described by Eqs. (6) are somewhat different. The yellow image dye must contribute the two positive terms, $\gamma_{yr}{}^{n}+\gamma_{yb}{}^{n}$. The yellow dye shown in curve b, Fig. 12, would fulfill the requirements. In the amount shown which has $D_{440}=0.901$ and $D_{680}=0.024$, it has $D_{560}=0.100$. The colored coupler from which it is formed must have $D_{560}=0.100+0.251=0.351$; and D_{440} and $D_{680}=0$. One of the many spectral-density curves which would fulfill this requirement is shown in Fig. 12, curve a.

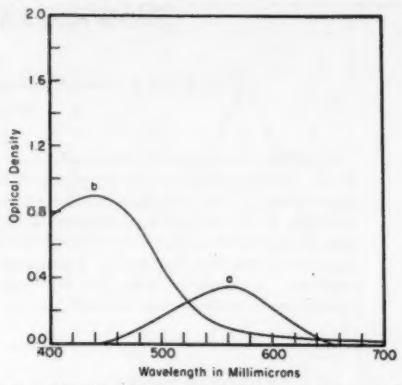

FIG. 12. Spectral-density curves for (a) coupler, and (b) yellow dye formed from this coupler. This pair fulfills the requirements described by Eqs. (6).

Influence of Colored Couplers on Film Speed

The colored couplers which are present in a film absorb some of the light which strikes the film during exposure and thus may cause a loss in effective film speed. Such effects will, of course, be determined by the absorption characteristics of the colored couplers which, in turn, are determined by considerations of the types discussed in the earlier section. For example, the colored couplers required for compensating for the absorptions in a negative film were described in Figs. 3, 4, 8, and 9. The coupler which forms the magenta dye has blue absorption but no green or red absorption. Since, in normal multilayer films, the green-sensitive layer containing the magenta-forming coupler is underneath the blue-sensitive layer, the blue absorption of this colored coupler will have no effect on the film speed. The colored coupler for forming the cyan dye has blue and green absorption. However, the red-sensitive layer containing this coupler is usually underneath the green-sensitive layer, so that the coupler absorption does not influence the green-sensitivity of the film. Thus, when colored couplers are used for compensating for the dye absorptions in a negative film, their absorptions do not influence film speed.

The absorption characteristics of the colored couplers required to fill the role of the six masks derived in the studies of color-reproduction theory do not lead to such fortunate results. For example, the colored coupler required for forming the magenta-dye image described in the previous section had a D_{680} of 0.467. Since this is in the green-sensitive layer which would normally be over the red-sensitive layer in a multilayer film, it would absorb a significant part of the red light before it reached the red-sensitive layer and lead to a decrease in the effective red speed of the film. Similarly, the colored coupler for forming the yellow-dye image would decrease the effective speed of the green-sensitive layer. This influence of the absorption of the colored couplers on the effective film speed may be the limiting factor in extending their usefulness.

Slit-Width Effects in Spectrophotometry

W. H. EBERHARDT
School of Chemistry, Georgia Institute of Technology, Atlanta, Georgia
(Received October 25, 1949)

A technique is suggested which allows an estimate to be made of the errors introduced into spectrophotometric measurements by the use of slits of finite width. The technique depends upon approximate analytic expressions for the slit function, the variation of the instrument sensitivity with wave-length, and the variation of the absorption coefficient with wave-length. A slit function is suggested for use with spectrophotometers with entrance and exit slits of equal width but with optics of varying dispersion. Expressions are derived for two convenient approximations for the absorption coefficient in the neighborhood of a maximum: a parabolic form, and two intersecting straight lines of opposite slope. Application of these expressions is made to experimental data on solutions of benzene, oxyhemoglobin, and neodymium chloride.

INTRODUCTION

ALTHOUGH it has long been realized that the use of slits of finite width in spectrophotometry will give rise to errors in the measurement of spectral contours and absorption coefficients, a rigorous quantitative treatment of these errors has been made only recently by Hardy and Young.[1] These authors write the measured transmittance of an absorbing material as an integral equation in the monochromatic spectral transmittance of the material, $t(\lambda)$, and determine $t(\lambda)$ by inversion of the integral equation by means of Fourier transforms. Their results are valid generally providing the absorption is sufficiently smooth so that derivatives higher than the second of the observed transmittance with respect to the wave-length setting of the monochromator will be sufficiently small.

In this report an alternate technique for estimating slit-width effects is suggested in which measured values for the transmittance are used as a first approximation for $t(\lambda)$ and corrections are estimated to give higher approximations. Although this technique is not as quantitatively precise as that suggested by Hardy and Young,[1] it appears simpler in application and readily provides analytic expressions for the dependence of the measured transmittance on slit-width and concentration of an absorbing species in solution.

DERIVATION OF THE EXPRESSIONS

It is assumed for the treatment that the absorption is smoothly continuous and that the Beer-Lambert law holds for monochromatic radiation. Thus, for a single wave-length, λ, the optical density

$$D(\lambda) = -\log E(\lambda)/E_0(\lambda) = -\log t_s(\lambda) = \epsilon(\lambda)cl/2.303, \quad (1)$$

where $E(\lambda)$ is the radiant energy of wave-length λ transmitted by a cell containing a solution with concentration of dissolved solute, c, and path length, l, and $E_0(\lambda)$ is the energy transmitted by an identical cell containing the solvent alone. The quantity $t_s(\lambda)$ is referred to as the spectral transmittancy of the solution or simply the transmittancy. The absorption coefficient, $\epsilon(\lambda)$, is assumed to be independent of the concentration of dissolved solute.

In a spectrophotometer, radiation from a continuous source, $H(\lambda)$, is passed through a monochromator characterized by a spectral transmittance, $M(\lambda)$, commonly referred to as the "slit function" for the monochromator, through a cell containing either the pure solvent or a solution of an absorbing species characterized by Eq. (1), and onto a receiver characterized by the spectral response, $S(\lambda)$.* The response of the instrument when the cell contains solvent alone may be written as

$$R_0 = \int_0^\infty H(\lambda)S(\lambda)M(\lambda)t_0(\lambda)d\lambda, \quad (2)$$

and the response when the solvent is replaced by a solution as

$$R = \int_0^\infty H(\lambda)S(\lambda)M(\lambda)t(\lambda)d\lambda, \quad (3)$$

where $t_0(\lambda)$ is the transmittance of the cell containing solvent and $t(\lambda)$ is that of the cell containing the solution. The ratio R/R_0 is the measured transmittancy, T_s; the ratio $t(\lambda)/t_0(\lambda) = t_s(\lambda)$ is the monochromatic transmittancy of the solution as defined by Eq. (1). In common usage, the wave-length scale of the monochromator is calibrated by means of radiation from a discontinuous source, generally a mercury arc, using the narrowest possible slits. Measurements are made by setting the monochromator to an arbitrary wave-length, λ_0, adjusting the widths of the entrance and exit slits to obtain adequate response from the instrument, and measuring R_0 and R and hence $T_s(\lambda_0)$. The relationship between this measurement of $T_s(\lambda_0)$ and

TABLE I. Slit functions for Beckman Model DU quartz spectrophotometer as determined by monochromatic radiation from Hg λ546.0 mμ.

Slit-width	λ_1 calc.	λ_1 obs.	λ_2 calc.	λ_2 obs.	$\Delta\lambda$	α	β
0.12 mm	542.9 mμ	543.0 mμ	549.1 mμ	549.0 mμ	3.0 mμ	1.00	1.00
0.52	533.0	533.6	559.9	559.6	13.0	0.96	1.04
1.02	521	522	574	573	25.5	0.94	1.06
1.52	510	511	590	588	38	0.92	1.10
2.02	500	503	607	603	50	0.86	1.14

[1] A. C. Hardy and F. M. Young, J. Opt. Soc. Am. 39, 265 (1949).

* For convenience, the notation of reference 1 will be employed in this report as far as practicable.

$t_s(\lambda_0)$ may be found only if the nature of $H(\lambda)$, $S(\lambda)$, $M(\lambda)$, $t_0(\lambda)$, and $t(\lambda)$ is known at least approximately. In the following calculation reasonable approximations are introduced for these quantities so that the dependence of $T_s(\lambda_0)$ on observable variables may be exhibited analytically.

The choice of a suitable slit function, $M(\lambda)$, for any particular application depends largely on the optics of the monochromator.[2] In the most favorable case where the entrance and exit slits of the monochromator are the same width† and the dispersion may be considered constant over the narrow range covered by the slit, the slit function has the character represented by the expressions: $M(\lambda)=1+[(\lambda-\lambda_0)/(\Delta\lambda)]$ for $\lambda_0-\Delta\lambda\leq\lambda\leq\lambda_0$, $M(\lambda)=1-[(\lambda-\lambda_0)/(\Delta\lambda)]$ for $\lambda_0\leq\lambda\leq\lambda_0+\Delta\lambda$, and $M(\lambda)=0$ everywhere outside of the range $\lambda_1=\lambda_0-\Delta\lambda\leq\lambda\leq\lambda_0+\Delta\lambda=\lambda_2$. In these expressions λ_0 is the wave-length for which the monochromator is adjusted and $\Delta\lambda$ is the "half-band width" or "nominal slit-width." This function is represented by the dashed curve in Fig. 1. For relatively wide slits in prism instruments the condition of constancy of dispersion is not satisfied and a modification of this simple slit function is required. This modification may be deduced as follows: the image of the entrance slit of the monochromator for a wave-length λ in the plane of the exit slit will be the same shape as that for the wave-length λ_0 but displaced from the latter by a distance s which may be expressed in terms of the wave-length λ to a first approximation by means of the formula‡ $s/k=1/\lambda_0^2-1/\lambda^2$. For rectangular slits the fraction of the light of wave-length λ transmitted by the exit slit will be $M(s)=1+(s/\Delta s)$ for $-\Delta s\leq s\leq 0$, and $M(s)=1-(s/\Delta s)$ for $0\leq s\leq\Delta s$, where Δs is the mechanical slit-width and it is assumed that the instrument is in sharp focus and that the entrance slit is uniformly illuminated. Together with the above displacement expression, this function allows a calculation of the slit function, $M(\lambda)$. Although an analytic expression for $M(\lambda)$ is quite complex, it has been found that such a slit function may be represented with good accuracy by an expression similar to that given for constant dispersion except that the lower wave-length limit $\lambda_1=\lambda_0-\alpha\Delta\lambda$ and the upper limit $\lambda_2=\lambda_0+\beta\Delta\lambda$, where $\Delta\lambda$ is the half-band width calculated from the dispersion of the instrument at λ_0 and α and β are constants the values of which are determined as solutions of the equation $M(\lambda)=0$. An example of such a slit function is provided by the solid lines in Fig. 1. The experimental points in Fig. 1 represent the fraction of light from the mercury line at λ546.0 mμ actually transmitted by the monochromator with a mechanical slit-width of 0.52 mm for various settings of the monochromator. Table I presents data based on this mercury line for various slit-widths and indicates values of α and β measured as outlined and computed as

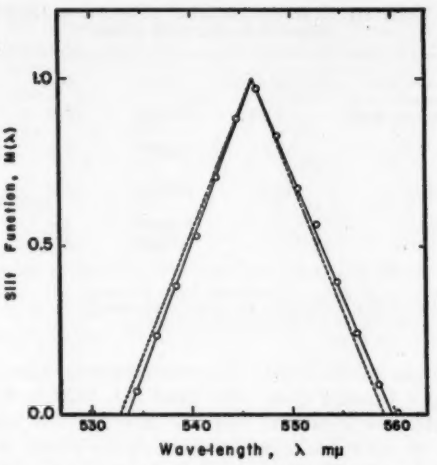

FIG. 1. Slit function for Beckman Model DU quartz spectrophotometer. Dashed curve: simple slit function calculated for constant dispersion. Solid curve: slit function corrected for varying dispersion.

TABLE II. Dependence on slit-width of the extinction coefficient of benzene in isooctane solution for the mean wave-length λ2540A.

Half-band width*	ϵcalc.	ϵobs.
2.8A	214	212±2
3.6	211	212
4.4	207	204
5.2	204	202
6.4	199	199
8.0	192	190
12.0	174	170
16	156	154
20	137	136

* The values for the slit-width are one-half those tabulated by Hogness (see reference 2) because of the difference in definition of slit-width.

[2] Hogness, Zscheile, and Sidwell, J. Phys. Chem. 41, 379 (1937).

† This condition is very nearly realized in the Beckman Model DU quartz spectrophotometer and similar instruments for which this treatment has been particularly adapted.

‡ This expression was deduced for the Beckman Model DU quartz spectrophotometer from the dispersion data supplied by the manufacturer. The constant k has the value 3.15×10^6 with the wave-length expressed in millimicrons and the distance s in millimeters and was chosen to get the best fit for the data over the wave-length range from 200 to 800 mμ.

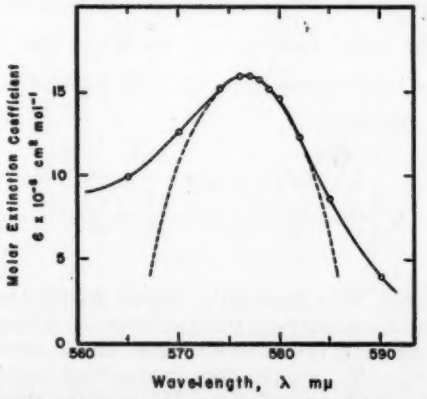

FIG. 2. Extinction coefficient of oxyhemoglobin. Dashed curve: parabolic form assumed for calculations.

TABLE III. Extinction coefficient of benzene at λ2540A corrected for slit-width effects.

Laboratory	Half-band width	Conc.	$\epsilon_{obs.}$	$\epsilon_{calc.}$
Hogness *et al.*	2.8A	0.0016*F*	212	225
B.L.[a]	16.7	0.0054	171	253
N.R.L.[b]	10.5	0.00286	203	249
S.D.[c]	5	0.00321	228	249
		0.00205	224	245

[a] Serial No. 1, Beacon Laboratories, Texas Company.
[b] Serial No. 11, U. S. Naval Research Laboratories.
[c] Serial No. 40, Shell Development Company.

TABLE IV. Dependence on slit-width of optical density of oxyhemoglobin solution measured at λ576.5 mμ. Concentration of $HbO_2 = 3.50 \times 10^{-5}$ mole/cm³.

Slit-width, mμ	$D_{calc.}$	$D_{obs.}$
0.9	0.561	0.561
2.4	0.557	0.553
3.7	0.550	0.547
6.7	0.529	0.525
12.8	0.455	0.465
18.9	0.357	0.400

solutions of $M(\lambda)=0$. The measurements were made using a Corning glass color filter No. 5120 to remove interference from the mercury line at λ580 mμ. In making the calculations, a constant correction of 0.02 mm was added to all mechanical slit-widths as suggested by the manufacturer to account for aberrations of the optical system. The tabulated values of α and β are based on the observed slit functions.

For continuous light sources it is practicable to assume that the product $H(\lambda)S(\lambda)t_0(\lambda)=r_0(\lambda)$ varies only slowly with wave-length over the range of the slit and hence may be expressed to good accuracy by the linear approximation

$$r_0(\lambda)=r_0(\lambda_0)[1+\mu(\lambda-\lambda_0)]. \tag{4}$$

The quantity $r_0(\lambda)$ may be estimated by measuring with a fixed slit-width the response of the instrument relative to that at λ_0 for various values of the wave-length setting and dividing this response by the linear dispersion in the plane of the exit slit corresponding to the wave-length λ. It should be noted that with a simple slit function such as that described above and in a wave-length region where r_0 varies linearly with wave-length, the response of the instrument will increase nearly as the *square* of the mechanical slit-width and consequently correction of the measured relative response of the instrument must be made through the linear dispersion as indicated and cannot be made by simply modifying the mechanical slit inversely as the dispersion.

A general calculation of the behavior of an absorbing solute under arbitrary conditions is rather difficult because of the complex character of $\epsilon(\lambda)$ and although accurate calculations may presumably be made by graphical integration of the expressions suggested above, it is much more convenient to utilize an analytical result based on some simplified form of $\epsilon(\lambda)$. Two such forms have been found particularly useful. In the first, $\epsilon(\lambda)$ is expanded as a power series about λ_0 and if the series converges sufficiently rapidly, terms of order higher than the second may be neglected and a relatively simple expansion for the transmittancy may be obtained in terms of the slit-width. Thus, if $\epsilon(\lambda)=\epsilon_0(\lambda_0)+\gamma(\lambda-\lambda_0)+\delta(\lambda-\lambda_0)^2$, the transmittancy becomes

$$T_s=\exp(-\epsilon_0 cl)\left\{1+\frac{\frac{\gamma clz}{3}(\alpha^2-\beta^2)+\frac{\gamma^2c^2l^2z^2}{12}(\alpha^3+\beta^3)\left(1-\frac{2\mu}{\gamma cl}-\frac{2\delta}{\gamma^2cl}\right)+\frac{\gamma^3c^3l^3z^3}{60}(\alpha^4-\beta^4)\left(1-\frac{3\mu}{\gamma cl}-\frac{6\delta}{\gamma^2cl}-\frac{24\mu\delta}{\gamma^3c^2l^2}\right)}{(\alpha+\beta)-(\mu z/3)(\alpha^2-\beta^2)}\right\}, \tag{5}$$

where the symbol z stands for the half-band width, $\Delta\lambda$.

The second form for $\epsilon(\lambda)$ which has been found convenient is that $\epsilon(\lambda)=\epsilon_0(\lambda_0)+\gamma_1(\lambda-\lambda_0)$ for $\lambda\leq\lambda_0$ and $\epsilon(\lambda)=\epsilon_0(\lambda_0)-\gamma_2(\lambda-\lambda_0)$ for $\lambda\geq\lambda_0$. In terms of this expression, the transmittancy becomes

$$T_s=\exp(-\epsilon_0 cl)\times\left\{1+\frac{\frac{clz}{3}(\alpha^2\gamma_1-\beta^2\gamma_2)+\frac{c^2l^2z^2}{12}[(\alpha^3\gamma_1^2+\beta^3\gamma_2^2)-2\mu(\alpha^3\gamma_1+\beta^3\gamma_2)]+\frac{c^3l^3z^3}{60}[(\alpha^4\gamma_1^3-\beta^4\gamma_2^3)-3\mu(\alpha^4\gamma_1^2-\beta^4\gamma_2^2)]}{(\alpha+\beta)-(\mu z/3)(\alpha^2-\beta^2)}\right\}. \tag{6}$$

Although these expressions appear formidable, their practical application is straightforward once the numerical constants have been evaluated, and if the slits are not too wide, the expressions are simplified considerably since α and β approach unity. This condition is generally met, but in an application using very wide slits the correction resulting from the deviation of α and β from unity may well represent a large fraction of the total correction since terms involving this correction are linear in the slit-width and concentration. Likewise, very frequently terms involving the quantity μ will be small relative to terms involving γ or δ and may be

neglected. Such terms give large contributions almost only when measurements are made in a region with nearly linear dependence of ϵ on λ. In circumstances where α and β may be set equal to unity and terms in μ may be neglected, the above expressions may be reduced to the following:

$$T_s=\exp(-\epsilon_0 cl)\left\{1+\frac{\gamma^2c^2l^2z^2}{12}\left(1-\frac{2\delta}{\gamma^2cl}\right)\right\} \quad (5a)$$

and

$$T_s=\exp(-\epsilon_0 cl)\left\{1+\frac{clz}{6}(\gamma_1-\gamma_2)+\frac{c^2l^2z^2}{24}(\gamma_1^2+\gamma_2^2)+\frac{c^3l^3z^3}{120}(\gamma_1^3-\gamma_2^3)\right\}, \quad (6a)$$

corresponding to the two different forms assumed for $\epsilon(\lambda)$.

It is to be expected that an absorbing material which follows either of the above expressions accurately will be rare indeed, but one or the other of these expressions is generally capable of approximating fairly closely many actual cases and the correction which may be computed from them gives a fair estimate of the errors attending a series of measurements.

APPLICATIONS

Benzene

An application of these considerations to benzene is of particular interest since the spectrum of benzene in liquid solution in isooctane has been investigated carefully by Hogness *et al.* under conditions of varying slit-width.[2] Because of the relatively narrow slits employed, the constants α and β may be assumed equal to unity. No data is provided from which to estimate the dependence of r_0 on wave-length and hence terms involving the constant μ must be ignored. Because of the sharpness of the absorption, however, it is probable that terms involving the slow variation of r_0 with wave-length will be very small relative to those determined by the absorption itself. The absorption coefficient has been estimated by successive approximations and may be represented approximately over a small wave-length range by the expression $\epsilon(\lambda)=519+37.1\times(\lambda-\lambda_0)$ for $\lambda\leq 2540$A and $\epsilon(\lambda)=519-17.3(\lambda-\lambda_0)$ for $\lambda\geq 2540$A. With these constants the transmittancy for a mean setting at λ2540A may be expressed as

$$T_s=\exp(-519cl)\{1+9.1clz+74c^2l^2z^2+470c^3l^3z^3\}, \quad (7)$$

where z is the half-band width in angstrom units, c is the concentration in formula weights per liter and l is the path length in cm. Using this expression, values of the extinction coefficient§ have been computed for the slit-widths used by Hogness *et al.* and are presented in Table II.

Assuming the same correction formula, the data presented in the Catalogue of Ultraviolet Spectrograms of the A.P.I. Research Project No. 44 at the National Bureau of Standards may be corrected for slit-width

TABLE V. Variation of optical density with concentration of oxyhemoglobin solutions measured at λ567.5 mμ with fixed slit-width Δs=0.22 mm or 6.7 mμ.

Conc. HbO_2 mole/cm³ $\times 10^5$	$D_{calc.}$	$D_{obs.}$	$D^0_{obs.}$
1.57	0.236	0.240	0.250
2.58	0.387	0.388	0.410
3.89	0.586	0.588	0.620
5.36	0.806	0.800	0.852
7.05	1.067	1.063	1.126

TABLE VI. Dependence on slit-width of optical density of neodymium chloride solution. Concentration $NdCl_3$=0.042*F*.

Wave-length	Slit-width	$D_{obs.}$	$D^0_{calc.}$
574.2 mμ	0.03 mm	0.263	0.270
	0.04	0.262	0.271
	0.05	0.259	0.270
794.0 mμ	0.03	0.360	0.412
	0.04	0.343	0.413
	0.05	0.328	0.416

TABLE VII. Variation of optical density with concentration of $NdCl_3$ measured at λ794.0 mμ with fixed slit-width, Δs=0.036 mm or 2.25 mμ.

Conc.	$D_{obs.}$	$D_{calc.}$	$D^0_{calc.}$
0.01*F*	0.089	0.086	0.100
0.02	0.176	0.172	0.199
0.03	0.261	0.253	0.298
0.04	0.344	0.337	0.398
0.05	0.426	0.421	0.497
0.06	0.503	0.503	0.597
0.07	0.573	0.585	0.696

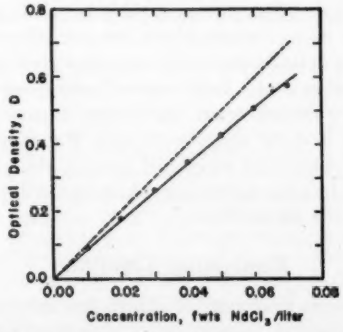

FIG. 3. Variation of optical density with concentration of $NdCl_3$ measured at λ794 mμ with fixed slit-width. Dashed curve: calculated for zero slit-width. Solid curve: calculated for slit-width used in measurements, 2.25 mμ.

§ The term "absorption coefficient" is used in this work when ϵ is computed relative to natural logarithms. The term "extinction coefficient" is used when the computations are based on common logarithms.

effects. Sufficient data obtained by three laboratories is presented which allows the above calculations to be made. Table III summarizes the data and the computed values of ϵ along with the previous results of Hogness *et al.*[2] The agreement is satisfactory in view of the incomplete data and the severe simplification of the function $\epsilon(\lambda)$. The low value of Hogness *et al.* may probably be ascribed to problems of purity and analysis.

Oxyhemoglobin

The absorption spectrum of hemoglobin is well known[3] and provides an interesting example of the application of the quadratic form for the absorption coefficient. Measurements have been made on hemolyzed whole blood in the vicinity of $\lambda 576.5$ mμ. Figure 2 represents the extinction coefficient determined from these measurements based on Horecker's value of 16.0×10^6 mole cm^{-1} for the extinction coefficient at the maximum. The absorption curve is fitted reasonably well in the neighborhood of the maximum by a simple parabolic expression of the form

$$\epsilon(\lambda)=36.9\times10^6-2.88\times10^5(\lambda-576.5)^2.$$

This expression leads to an estimate of the transmittancy of a sample of arbitrary concentration c measured with a half-band width z centered around the maximum by the expression

$$T_s=\exp(-\epsilon_0 cl)\{1+4.80\times10^4 clz^2\}. \quad (8)$$

Since the measurements pertain to a maximum in the spectrum, no linear term in z appears in the expression and the variation of the light source represented by the constant μ appears only in the third-order term which is very small for moderate slit-widths. Table IV presents data obtained on this system with a fixed concentration of oxyhemoglobin and varying slit-widths, and Table V presents data obtained with a fixed slit-width at various concentrations. The concentrations in the first column of Table V were computed from the measurements with a slit-width of 0.035 mm which are presented in Table V in the column D^0_{obs}. Both tables include estimates of the density based upon the above expression. The agreement is quite satisfactory over the range of slit-widths for which the simplified form of the absorption curve may be expected to provide a reasonable approximation to the correct form.

Neodymium Chloride

The extreme sharpness of absorption spectra of rare-earth compounds necessitates a consideration of slit-width effects at even the narrowest slits practically usable. The absorption is sufficiently sharp so that to a fair approximation it may be represented by the second form suggested. For neodymium chloride solutions the absorption coefficients were evaluated by a method of successive approximations applied to measurements of a solution of concentration $0.061F$ in $NdCl_3$.[4] Around $\lambda 574.2$ mμ ϵ may be represented approximately by the expressions $\epsilon(\lambda)=16.0+1.35(\lambda-\lambda_0)$ for $\lambda\leq\lambda_0$ and $\epsilon(\lambda)=16.0-1.08(\lambda-\lambda_0)$ for $\lambda\geq\lambda_0$. Around $\lambda 794.0$ mμ the expressions become $\epsilon(\lambda)=23.0+7.5(\lambda-\lambda_0)$, for $\lambda\leq\lambda_0$ and $\epsilon(\lambda)=23.0-0.8(\lambda-\lambda_0)$, for $\lambda\geq\lambda_0$, with the concentration expressed in formula weights per liter and the wave-length in millimicrons. Using these formulas for $\epsilon(\lambda)$ it is possible to evaluate the effect of slit-width by the following expressions valid for mean wave-length settings at the maximum absorption:

$$T_{s,574}=\exp(-16.0cl)\{1+0.41clz+0.13c^2l^2z^2+0.03c^3l^3z^3\} \quad (9)$$

and

$$T_{s,794}=\exp(-23.0cl)\{1+1.4clz+2.4c^2l^2z^2+0.36c^3l^3z^3\}. \quad (10)$$

These expressions have been applied to measurements with a fixed concentration of solute and varying slit-widths. The results are summarized in Table VI. Corrections were computed from the above expressions and added to observed values of the optical densities to obtain a corrected density which should apply to zero slit-width, $D^0_{cal'd}$.

In addition, the expression valid for $\lambda 794$ mμ has been applied to measurements at a constant slit-width with varying concentrations. In all measurements the constant 0.02 mm has been added to the mechanical slit-width as discussed. The results are summarized in Table VII, and in Fig. 3.

The results in this application are of particular interest since the major correction term is the first (linear) term which gives approximately a linear dependence of optical density on concentration as indicated in Fig. 3 but with a slope and hence absorption coefficient which is sensitive to slit-width. Thus, contrary to general belief, the simple linear dependence of optical density on concentration cannot be assumed sufficient to justify ignoring slit-width corrections in calculations of absorption coefficients when either the slopes on opposite sides of the absorption maximum are greatly different or where large slit-widths necessitate a consideration of the deviation of α and β from unity. It is also interesting to observe that measurements made at a wave-length just slightly greater than that of the maximum would exhibit practically no deviation from ideality for small slits such as utilized in these measurements.

ACKNOWLEDGMENT

The author would like to express his appreciation to Dr. W. T. Ziegler for permission to use unpublished data on neodymium chloride and also to the Research Corporation for a grant-in-aid of this work.

[3] B. L. Horecker, J. Biol. Chem. **148**, 173 (1943).

[4] W. T. Ziegler, Georgia Institute of Technology, Atlanta, Georgia (private communication).

Letters to the Editor

Comment on "Spark Spectra of Elements 43 and 61"

C. C. KIESS
National Bureau of Standards, Washington, D. C.

December 27, 1949

IN a paper published in 1922[1] on the *long* wave-length region of the arc spectra of neodymium and samarium, I stated, "When the tabulated wave-lengths . . . were intercompared it was found that many lines, for the most part faint, were common to the spectra of both. It has not been possible to identify them with the spectra of known elements, and, therefore, they have been brought together in a separate table. While it would be a hasty conclusion to regard these lines as characteristic of a new element, yet the idea seems plausible in view of the fact that the present accepted scheme of the periodic table of elements requires a new element of atomic number 61 coming between neodymium and samarium." Further along I stated, "Later research may reveal them either as lines properly belonging to each spectrum and approximately of the same wave-length or as lines belonging to the spectra of other known elements."

In 1923 Yntema used the grating spectrograph of the Sloane Laboratory, at Yale University, to investigate the same rare-earth materials used in the 1922 investigations, and also some oxides of intermediate fractions. He stated, "Corroboration of the work of Kiess was found in the examination of a small region of the ultraviolet spectrum. Five lines . . . were found, common to pure neodymium and samarium and to the intermediate fractions."[2]

In his recent paper in this Journal[3] Timma's references to this work may leave the reader with some erroneous conclusions that should not be drawn. To keep the record straight, I wish to call attention to the following facts: (1) my investigation did not contain any ultraviolet measurements; (2) it merely called attention to the possibility that the unknown lines in the spectra of Nd and Sm might belong to element 61 without claiming unqualifiedly that they did so; (3) it made no claim that "element 61 would be concentrated in the neodymium and samarium fractions;" (4) Yntema did not repeat my work nor did I join Hopkins in thinking that the ultraviolet lines were "due to element 61."

[1] C. C. Kiess, Sci. Pap., Bur. Stand. 18, 201 (1922).
[2] L. F. Yntema, J. Am. Chem. Soc. 46, 37 (1924).
[3] D. L. Timma, J. Opt. Soc. Am. 39, 898 (1949).

Bronze Glass Molds Replacing Cast Iron Glass Molds

VLADIMIR A. GRODSKY
United States Naval Gun Factory, Washington, D. C.

November 25, 1949

SINCE World War I the U. S. Naval Gun Factory built up a large optical shop where a considerable part of the optical instruments and apparatus required by the Navy and other armed forces, are produced.

All high grade glass parts for these instruments are melted and pressed in the glass division of the National Bureau of Standards. The procedure of forming glass is as follows: Lumps of glass are heated in gas furnaces and after acquiring a pasty consistency are placed into molds set in presses. In order to keep the molds at a more uniform temperature, they are heated by a gas jet. This combination of high temperatures and pressure results in a very severe strain on the metal of the mold.

Cast iron is the material most widely used for glass molds. To increase the heat resistance and strength of the cast iron, it may be alloyed with chromium or nickel and minor quantities of cobalt, molybdenum, vanadium and other elements.

When a charge of hot glass is placed in the iron mold, the surface layers quickly acquire a temperature much higher than the rest of the mold. However, on account of the low heat conductivity of iron, the propagation of heat through the mold is slow, so that different parts of the mold body have very different temperatures. This creates distortion, warping, and cracking. The face of the mold becomes soon covered with a network of fine cracks, which increase in size and depth. Graphite flakes exposed to the heat slowly burn out in the presence of air, leaving tiny cavities, and the scale of oxide formed on the iron surface cracks and peels off. Gradually the iron mold loses its smooth surface and the pressed glass becomes rough and opaque, a condition which makes inspection difficult. All this shows that cast iron can not be considered an ideal material for glass molds.

Several years ago the author greatly improved a bronze covered by Federal Specification for Aluminum Bronze QQ-B-671a. This bronze is an alloy of copper aluminum, iron, manganese, and nickel, and has many outstanding properties and can be easily cast, forged, machined, polished and welded. It has good corrosion resistance and a heat conductivity considerably higher than that of iron; also when heated, it is covered with a self-healing protective oxide coating. This bronze was suggested as a material for glass molds and with the encouragement of J. E. Crown and A. J. Devlin, master mechanincs of the foundry and optical shop, respectively, glass molds were made from it and tested at the National Bureau of Standards in 1944. The results proved so conclusive that five tons of this bronze were ordered and many cast iron glass molds replaced by bronze molds. The latter have been in use for five years with excellent results and little need for replacements. Glass pressed in highly polished bronze molds has a good luster and can be readily inspected without additional treatment. As for cost, bronze is more expensive than plain cast iron, but the cost of alloyed cast iron is also high and, besides, its casting and machining are more difficult. Moreover, bronze has always a much higher scrap value than alloyed iron.

Accurate Thickness Measurements with a Fabry-Perot Interferometer

L. G. SCHULZ
Institute for the Study of Metals, University of Chicago, Chicago, Illinois

January 23, 1950

WHEN an extra deposit, D, of a dielectric is added to one of the mirrors of a Fabry-Perot interferometer, as shown in Fig. 1A, there will be a shift in the circular fringes, as indicated in Fig. 1B. Since the interval between rings is not linear the uncorrected fringe shift S/R cannot be used as a measure of the thickness of D. Rather than apply a correction it is more convenient to use a measuring unit which changes at the same rate as the ring separation. Such a unit is effectively provided by the double set of fringes given by the sodium D-lines. Their separation will be used as an "internal standard" in the following manner: When the mirror separation is a multiple of $\lambda_1\lambda_2/2(\lambda_1-\lambda_2)$ the two sets of rings coincide (as in Fig. 1B). If the separation is decreased there will be a certain position at which the appearance is that of Fig. 1C. Likewise an increase in separation will lead to Fig. 1D. The thickness, T, in angstroms of the deposit in Fig. 1A is given by

$$T=\left[\frac{M_{C-D}}{2}\right]\left[\frac{2(\lambda_1-\lambda_2)}{\lambda_1\lambda_2}\right]\left[\frac{\lambda_1+\lambda_2}{4}\right][10^7]=5070M_{C-D}. \quad (1)$$

The mirror motion, M_{C-D}, from position C to D is expressed in mm.

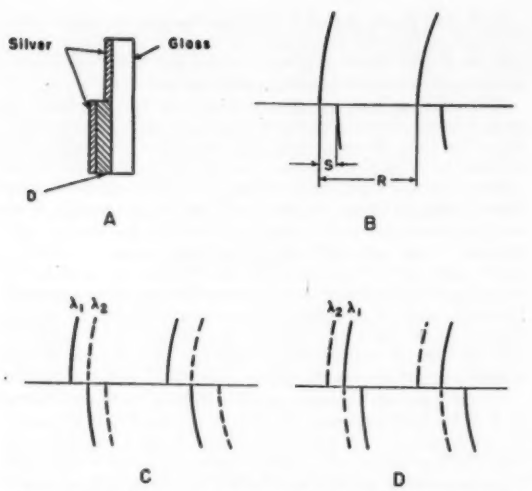

FIG. 1. Drawing A shows one of the mirrors of a Fabry-Perot interferometer. The deposit, D, is a dielectric with a thickness of approximately one-tenth the wave-length of the sodium D-lines. Drawing B shows the double set of fringes in coincidence; C and D show them separated in a manner such that some of the fringes are continuous across the boundary of the deposit D.

In addition to avoiding corrections for the non-linearity of ring separation the method has several other advantages: (1) The thickness can be obtained directly from the screw motion M_{C-D} using Eq. (1). (2) The positions C and D of Fig. 1 can be set with great exactness; an accuracy equivalent to ± 15A in T is easily obtainable.

A more complete evaluation of the method, together with results from applications to the study of metallic films, will be given later.

Wave-Lengths of the Potassium Lines 3446A and 3447A

ALFRED ROMER, ROBERT D. TURNER, AND IRENE COMFORT STEHLI
Department of Physics, The St. Lawrence University, Canton, New York
November 23, 1949

THE best measurements of the wave-lengths of the potassium lines in the visible and near ultraviolet appear to be those made by Datta in 1921.[1] His values were adopted for the MIT tables, and a search of the literature since the time of their publication has brought to light no more recent work. We have, however, been led to question them in one particular, for the doublet at 3446A and 3447A, the third member of the principal series.

During a spectrochemical analysis of some rock specimens, our attention was aroused by the apparent coincidence of what should have been λ3446.7A of potassium with λ3446.3A of nickel in the adjacent comparison spectrum of an iron wire. A cross-check in the Kayser-Ritschl tables gave the same potassium line as 3446.37A, and in the face of this discrepancy it seemed worth our while to remeasure it.

Our measurements were made in the first order of our 1.5-meter grating spectrograph with a dispersion of 6.95A/mm. We used three spectra on two separate negatives, each of a powdered sample containing a standard mixed with a small quantity of potassium chloride, placed in a shallow crater in the graphite anode of a d.c. arc. In two of the spectra the standard was iron and the potassium lines were measured by interpolation between 3445.15A and 3450.33A. In the third it was titanium and the reference lines were 3443.64A (or in one case 3441.31A) and 3452.47A.

As averages of these measurements, the wave-lengths of the two lines of the potassium doublet were 3446.43 ± 0.02A and 3447.38 ± 0.04A, the estimate of uncertainty being in each case the average deviation. They are in definite disagreement with Datta's values of 3446.722A and 3447.701A, and we are publishing this note to call the problem to the attention of those who may be better equipped to settle it.

[1] S. Datta, Proc. Roy. Soc. **A99**, 69 (1921).

An Integrating Sphere for Reflectance Measurements in the Ultraviolet

NISSON A. FINKELSTEIN
Department of Physics, Massachusetts Institute of Technology, Cambridge, Massachusetts
January 23, 1950

AN integrating sphere coated on its inside surface with magnesium oxide has long been recognized as a highly efficient device for use in visible spectrum spectrophotometry. For a sphere with no holes the light collecting efficiency is simply dependent upon the reflectance of the wall coating material, while in the case of a sphere with ports, account must be taken of light escaping through the ports. Since magnesium oxide has a reflectance of 0.98 in the visible region of the spectrum,[1] efficiencies of 20 percent are easily obtained with a sphere containing beam entrance and sample ports. In the course of studies on the ultraviolet reflectance of living human skin[2] it was necessary to design an ultraviolet integrating sphere for use with the Harrison automatic recording spectrophotometer.[3,4] Because of a low reflectance (0.92) of magnesium oxide[5] on the short wave-length end of the 2400 to 6000A region under study, calculations of expected sphere efficiency were made to ascertain the feasibility of using such a device.

The sphere designed has two beam entrance ports and a port against which the sample to be measured is placed. The inside surface of the sphere coated with magnesium oxide serves as a standard surface and the 1P28 photo-multiplier tube used as a detector is mounted inside the sphere with its envelope coated with magnesium oxide except for the region directly over the sensitive cathode area. Under the assumption of uniform illumination, i, within such a sphere the efficiency of flux collection is given by

$$E=\frac{\text{light flux absorbed by photo-multiplier cathode}}{\text{light flux reflected by the sample}}$$

$$E=\frac{i(1-\rho)c}{Fr},$$

where ρ = reflectivity of cathode surface, F = amount of light flux incident upon the sample, r = reflectivity of the sample, and c = area of photomultiplier cathode surface. Now, a fraction of the light flux reflected from the sample goes back out through the sphere holes while the remainder is absorbed in the photo-multiplier cathode surface, the sphere walls, the photo-multiplier envelope, or the sample. That is,

$$Fr=2ei+i(1-\rho)c+i(A-a-2e)(1-R)+i(1-R)(P-c)+i(1-r)a$$

where e = area of each beam entrance port, a = area of the sample port, R = reflectivity of inner surface of sphere and photo-multiplier envelope coating, A = area of inner surface of sphere, and P = surface area of photo-multiplier envelope.

If we let $\epsilon = e/A$ and $\alpha = a/A$,

$$Fr=iA[2\epsilon+(1-R)(1-\alpha-2\epsilon)+(1-r)\alpha]+i(1-\rho)c+i(1-R)(P-c)$$

$$E=\frac{(1-\rho)c}{A[2\epsilon+(1-R)(1-\alpha-2\epsilon)+(1-r)\alpha]+(1-\rho)c+(1-R)(P-c)}.$$

Because of the low reflectance, R, of magnesium oxide in the ultraviolet, the leading term in the efficiency equation for an ultraviolet sphere of the above type is $A(1-R)(1-\alpha-2\epsilon)$ in the denominator. For this reason it was desirable to keep the sphere surface area, A, as small as possible. On the other hand, if the condition of uniform illumination within the sphere is to be satisfied,[6] the total area of holes in the sphere must be no greater than 1–2 percent of the sphere wall area. A compromise between these two conditions was obtained with a 5-inch diameter sphere in which the combined area of the entrance ports is 1.25 inches, 1.6 percent of the sphere wall area.

Taking 0.92 as the ultraviolet reflectance of magnesium oxide and substituting in the efficiency equation, the sphere efficiency was found to be about 4 percent in the ultraviolet. In the visible spectrum where the reflectance of magnesium oxide is 0.98 the calculated efficiency is 16 percent. It is seen from the equation that the main limitation on obtaining a higher efficiency in the ultraviolet is the low reflectance of the coating material, since the efficiency varies inversely as $(1-R)$.

By comparison of the detected signal intensity for reflectance measurements made using the integrating sphere with that for transmission measurements made without the sphere it was possible to measure experimentally the efficiency of the sphere. The measured values of efficiency for a freshly smoked sphere agreed with the values calculated from the equation to an accuracy of ± 10 percent in both the ultraviolet (2400 to 4000A) and visible (4000 to 6000A) portions of the spectral region studied.

[1] Benford, Lloyd, and Schwarz, J. Opt. Soc. Am. 38, 445 (1948).
[2] Duntley, Edwards, and Finkelstein, J. Opt. Soc. Am. 39, 1056A (1949); N. A. Finkelstein, J. Opt. Soc. Am. 39, 1056A (1949).
[3] G. R. Harrison and E. P. Bentley, J. Opt. Soc. Am. 30, 290 (1940).
[4] N. A. Finkelstein, Rev. Sci. Inst. (to be published).
[5] Benford, Schwarz, and Lloyd, J. Opt. Soc. Am. 38, 964 (1948).
[6] A. C. Hardy and W. Pineo, J. Opt. Soc. Am. 21, 502 (1931).

Some New Infra-Red Phosphors*

DONALD W. LYON AND E. LOUISE POORE†
Pigments Department, E. I. du Pont de Nemours and Company, Newport, Delaware
January 5, 1950

IT has been known for some time that zinc sulfide and the sulfides and selenides of the alkaline earth metals are infra-red phosphors; that is, they can emit energy in the form of visible light when stimulated with infra-red radiation, if they have been previously subjected to suitable excitation. It is only during the last few years, however, that certain oxygen-containing compounds have been prepared which are infra-red-sensitive. These include calcium silicate,[1] lanthanum oxysulfide,[2,3] magnesium sulfate,[4] zinc beryllium stannogermanate,[5] and zinc phosphate.[4]

We have recently prepared a number of new infra-red phosphors in this laboratory. All of these compounds are oxy-salts, and were the only infra-red-sensitive substances found in all the series which were tested. For the sake of completeness, those which were not stimulable by infra-red are also included.

These materials were made by firing combinations of basic oxides, ZnO, CdO, and MgO, or compounds which decomposed on heating to give basic oxides, $CaCO_3$, $Sr(NO_3)_2$, and $Ba(NO_3)_2$, with oxides of a more acidic nature, Al_2O_3, As_2O_3, B_2O_3, Cb_2O_5, GeO_2, MoO_3, SiO_2, SnO_2, Ta_2O_5, TiO_2, V_2O_5, WO_3, and ZrO_2. The oxides, all of which were highly purified, were mixed in such proportions that the oxygen ratio between the basic oxide and the more acidic oxide was unity (see Table II). Each oxide pair was thoroughly mixed with solutions of activators and a flux, and calcined in silica crucibles for 30 minutes in air at 1100°C. The nine activator combinations used with each of the 78 double-oxide charges are listed in Table I.

TABLE I. Activator Concentrations.

Sample No.	%Mn	%Sm	%Ce	%Pb	%Cu
1	1.	0.004			
2	0.1	0.004			
3	0.01	0.004			
4		0.004	0.1		
5		0.004	0.01		
6		0.004	0.001		
7				3.	0.01
8				3.	0.001
9				3.	0.0001

The quantities given in the above table represent the amount in weight percent added before calcination. In the case of lead, the quantity remaining after firing was of the order of 0.5 percent or less. Calcinations were made with 3 percent NaCl. If any infra-red-sensitivity was observed, then similar samples were fluxed with (1) 3 percent LiF and (2) no flux, all other conditions being the same. The excitation period was about ten seconds with (1) 1850A, (2) 2537A, and (3) 3650A ultraviolet radiation. The 1850A source was a Mineralight lamp with the filter removed, while a Gates Dual Raymaster lamp served as the source of the other exciting radiations. Stimulation was effected with infra-red radiation (0.8–1.3μ) from a 100-watt tungsten lamp fitted with a No. 2540 Corning filter.

TABLE II. Infra-red phosphors (1850A excitation).

Charge	1	2	3	4	5	6	7	8	9
$3CaO \cdot Al_2O_3$	LO	LO	NL	NL	NLO	NL	LO	LO	LO
$2CaO \cdot GeO_2$				N				N	
$3CaO \cdot MoO_3$	LO	LO	NLO	LO	NLO	LO	NLO	NLO	NLO
$2CaO \cdot SiO_2$	..	..	N	..	N	..	LO	LO	LO
$2CaO \cdot SnO_2$	O	O	O	O	O	O	NO	NO	NO
$2CaO \cdot TiO_2$	LO	LO	LO	LO	L	L	LO	NLO	NLO
$5CaO \cdot V_2O_5$	L	L	L	O	O	O	NO	NLO	NO
$3SrO \cdot Al_2O_3$	..	..	O	NO	O	O	LO	LO	LO
$2ZnO \cdot GeO_2$	LO	O	O	O	O	O	LO	LO	LO
$2ZnO \cdot TiO_2$	..	..	..	..	..	..	..	..	N

TABLE III. Infra-red phosphors (2537A excitation).

Charge	1	2	3	4	5	6	7	8	9
$3CaO \cdot Al_2O_3$	..	..	N	N	N	N	..	..	..
$2CaO \cdot GeO_2$	..	..	..	..	..	..	..	..	..
$3CaO \cdot MoO_3$	..	O	NLO	LO	NLO	LO	NLO	NLO	NLO
$2CaO \cdot SiO_2$	..	..	N	..	N	O	O	O	O
$2CaO \cdot SnO_2$	O	O	O	O	O	O	O	O	NO
$2CaO \cdot TiO_2$	..	..	..	L	L	L	LO	NLO	NLO
$5CaO \cdot V_2O_5$	..	..	..	..	..	..	O	LO	NO
$3SrO \cdot Al_2O_3$	..	..	..	..	..	..	O	O	LO
$2ZnO \cdot GeO_2$	LO	O	O	O	O	O	LO	LO	LO
$2ZnO \cdot TiO_2$	..	..	..	..	..	..	..	..	N

TABLE IV. Infra-red phosphors (3650A excitation).

Charge	1	2	3	4	5	6	7	8	9
$3SrO \cdot Al_2O_3$	..	..	..	..	..	..	O	O	O
$2ZnO \cdot GeO_2$	LO	O	O	..	..	..	O	..	L
$2ZnO \cdot TiO_2$	..	..	..	..	..	..	..	..	N

The 1850A source furnishes a large amount of 2537A radiation. However, as shown in Tables II and III, many samples which were excited with 1850A ultraviolet were sensitive to infra-red, but were non-stimulable following 2537A excitation.

Tables II–IV summarize the behavior of various double oxides

TABLE V. X-ray diffraction data.

Charge	Found
$3CaO \cdot Al_2O_3$	$5CaO \cdot 3Al_2O_3$
$2CaO \cdot GeO_2$	Unidentified compound
$3CaO \cdot MoO_3$	Unidentified compound
$2CaO \cdot SiO_2$	β-Ca_2SiO_4
$2CaO \cdot SnO_2$	$CaSnO_3$
$2CaO \cdot TiO_2$	$CaTiO_3$
$5CaO \cdot V_2O_5$	Unidentified compound
$3SrO \cdot Al_2O_3$	$Sr_3(AlO_3)_2$
$2ZnO \cdot GeO_2$	Unidentified compound
$2ZnO \cdot TiO_2$	Zn_2TiO_4

under excitation by 1850, 2537, and 3650A radiation followed by infra-red stimulation. The numbers used as column headings refer to the activator combination (see Table I). The symbols N, L, and O indicate 3 percent NaCl, 3 percent LiF, and no flux, respectively. The dots (..) reveal that the material had no impared phosphorescence.

X-ray diffraction data revealed that compound formation occurred in every instance (see Table V). In several cases, the compound was not identified because of lack of data in the literature.

Similar preparations were made of all of these, in which the oxide ratio was unity ($3CaO \cdot Al_2O_3$, etc.), but the products were inferior in infra-red stimulability to those previously described.

Stimulation and emission spectra have not yet been determined for these phosphors. It is hoped that when these data are obtained, they can be reported in a later paper in which a more complete description of the preparation and properties of these phosphors will be given. However, it was observed that calcium aluminate, molybdate, and silicate were much better with respect to infra-red stimulability than the others, but none of these approached zinc sulfide infra-red phosphors in brightness.

We wish to express our appreciation to Miss M. L. Barnard of the du Pont Experimental Station for the x-ray data; and to Mr. Louis Reiss of Squier Signal Laboratory, Fort Monmouth, New Jersey, and Dr. J. H. Schulman of the Naval Research Laboratory for their interest and helpful suggestions.

* This research was done under Contract No. W-36-039 sc-32256 with the U. S. Army Signal Corps.

† Now at Spruance Rayon Laboratory, E. I. du Pont de Nemours and Company, Richmond, Virginia.

[1] Schulman, Ginther, and Evans, J. Opt. Soc. Am. **38**, 817 (1948).
[2] Pitha, Smith, and Ward, J. Am. Chem. Soc. **69**, 1870 (1947).
[3] J. J. Pitha and R. Ward, U. S. Pat. 2,462,547 (February 22, 1949).
[4] N. F. Miller, Final report, "Infra-red stimulation of phosphors," P. B. Report No. 33363.
[5] Shrader, Leverenz, and Wood, J. Opt. Soc. Am. **36**, 353 (1946).

A Variable Frequency Electronic Interrupter for the Direct Current Arc

ROBERT J. DWYER
Lane-Wells Company, San Gabriel, California
January 13, 1950

A NUMBER of interrupted d.c. arcs and intermittent sparks have been devised for use in emission spectroscopy. They have certain advantages over the continuous d.c. arc. For example, the electrodes are kept cooler[1] and the intermittent character of the discharge causes a new spot of the electrode to be sampled on each discharge.[2] By adjusting the conditions of the discharge either arc or spark lines may be made to predominate and combinations of the two may be chosen with their relative intensities selected to suit the particular problem. In this way the background in the region of a particular emission line may frequently be reduced.

The installations required are generally complicated and expensive. They usually attain the intermittent feature by utilizing the alternations of the a.c. line and are thus limited to the frequency of the line. The circuit shown in Fig. 1 is of a system which may be used with any d.c. arc supply source of about 100 to 200 volts in order to obtain an intermittent arc. The condenser C_1 charges through the resistor R_1 until the firing voltage of the thyratron, determined by the setting of the grid potential, is reached. At this potential the thyratron becomes conducting and current passes through it and the input of the Tesla coil. This applies a high voltage at radio frequency across the electrodes and

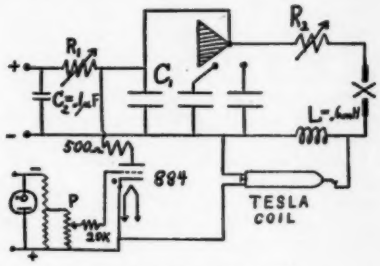

FIG. 1. Intermittent arc circuit.

the gap becomes conducting, thereby discharging the condenser C_1. The cycle repeats, the circuit acting as a relaxation oscillator whose frequency is determined by the time constant of the R_1C_1 combination together with the firing voltage for which the thyratron grid potential is set.

By using electrolytic condensers of several hundred microfarads at C_1 the frequency may be made less than a cycle per second if desired. C_2 is an r-f by-pass condenser for protection of the d.c. power supply. The Tesla coil used is an ordinary vacuum leak tester. The grid potential is taken from a regulated supply so that for a given setting of P the thyratron will always fire at the same potential across C_1, thus assuring uniformity of the arc excitation conditions. The frequency and voltage at which discharge occurs are independent of the gap widths over its operating range.

Both spark and arc lines are obtained. By varying the values of R_1, R_2, C_1 and P, the frequency and the conditions of the arc discharge may be adjusted and the relative intensities of the spark and arc lines controlled. By operating at a low frequency it is possible to keep the arc electrodes quite cool.

[1] H. Hemmindinger, J. Opt. Soc. Am. **32**, 149 (1942).
[2] V. J. Caldecourt and J. L. Saunderson, J. Opt. Soc. Am. **36**, 99 (1946).

Book Reviews

Manual of Spectroscopy. THEODORE A. CUTTING. Pp. 220+vi. Chemical Publishing Company, Brooklyn, New York, 1949. Price $6.50.

This manual has been written as a guide for instrumentation and qualitative analysis for the amateur physical scientist or field geologist. Through the use of replica gratings and a variety of improvised parts, the construction of a "home-made" spectrograph is described. With the assistance of laboratory fabricated sources, the author has indicated procedures for qualitative spectrochemical analysis. About half of the book is devoted to a description of the properties and characteristics of the separate elements, a part of which is historical and not pertinent to the subject of the book. A condensed series of wave-length tables of the elements is included. Some of the more recently characterized elements are omitted, and some elements are included which are not generally considered as detectable with the usual spectrographic equipment.

No attempt has been made to document the procedure described with the usual literature references. The book provides suggestions for apparatus construction which need to be carefully considered and modified to provide better safety from electrical hazard and a stability in instrument form. The illustrations of characteristic spectra are not satisfactory and there is much to be added to provide entirely satisfactory directions for qualitative and semiquantitative ore analysis.

There is a general absence of information as to the author's position. The sources of the materials, equipment and data essential to the suggested analyses are not adequately indicated. This latter deficiency might have been alleviated and the book improved by a more critical review of the manuscript by the publishers.

WALLACE R. BRODE
National Bureau of Standards
Washington, D. C.

Spectroscopic Properties of Uranium Compounds. (Div. III, Vol. 2, of the National Nuclear Energy Series, Manhattan Project Technical Section). G. H. DIEKE AND A. B. F. DUNCAN. Pp. 290+xviii. McGraw-Hill Book Company, Inc., New York, 1949. Price $2.75.

This book is one of a series to be issued by the Project Editorial Advisory Board of the Atomic Energy Commission. It presents a discussion of the work of Dieke at Johns Hopkins University and Duncan at Columbia and their co-workers on the x-ray crystal structure and the fluorescence and absorption spectra of uranium compounds. This work is concerned primarily with uranyl-type compounds, and instructions are given for the synthesis and crystallization of these materials. Some experiments are reported showing the effects of temperature and isotopic composition of the samples upon the spectroscopic properties of the compounds. The bibliography is extensive, supplementing the Gmelin references, and brings the literature survey up to 1944.

An extensive appendix contains 42 wave-length–wave number tables of the fluorescence and absorption lines and bands of uranium compounds with notes on appearance, intensity, observed isotopic shifts, and classification. The classification is not too clearly given at some points and there is an admitted lack of sufficient information to allow a complete analysis of the spectra of uranyl salts. The instructions for sample preparation, the bibliography, and the references throughout the text to phases of the work needing further investigation make this book a valuable reference for anyone interested in further work on the optical properties of uranium compounds.

D. L. TIMMA
Mound Laboratory
Monsanto Chemical Company
Miamisburg, Ohio

Crystals and X-Rays. KATHLEEN LONSDALE. Pp. 199+viii, Figs. 138, Plates XIII, 5¼×8½ in. D. Van Nostrand Company, Inc., New York, 1949. Price $3.75.

The name of Kathleen Lonsdale has been associated with many major developments in the field of x-ray diffraction from crystals. As a member of Sir William Bragg's research group at University College and at the Royal Institution she took part in the early work on the structures of organic crystals, on the application of space-group theory to structure work and on the relationship of structure and physical properties. In recent years her work on lattice vibrations in relation to x-ray scattering has been outstanding. Although an experimentalist at heart, her excursions into theory have been noted for their clarity and precision.

In the 200-page book under review, Dr. Lonsdale has given an account of some of her experience in the field of x-ray analysis, basing her discussion on a series of lectures which she gave in London in 1946 to a non-technical audience. The book starts with a historical introduction and has sections on the physics of x-rays, the physics and geometry of crystals, the determination of the lattice geometry of a crystal and of the atomic and electron distribution which underlies that geometry. In two final chapters the applications of x-rays to problems of crystal texture and crystal dynamics are emphasized and the effects of the results of x-ray analysis on modern chemistry and metallurgy are brought to light.

The many subjects treated are interspersed with a wealth of incidental detail which makes the book interesting reading but it seems to the reviewer that these many details would confuse the beginner for whom the book is written. There are a large number of excellent figures and plates which add very much to the value of the book. The x-ray photographs in the plates (mostly from Dr. Lonsdale's own work) are particularly useful. Unfortunately a number of errors and omissions occur which may well puzzle the reader. From the discussion of the reciprocal lattice techniques, it would be difficult to ascribe their origin to von Laue, Ewald, and Bernal. The method of reference to review articles by the journal, month, and year, without reference to the author's name or the page, seems unfortunate. The caption of Fig. 54 may well baffle the uninitiated since it contains three monoclinic space-groups in addition to the orthorhombic groups which it professes. Figure 76 is also confusing since it is not drawn according to convention and the two parts of the figure are inconsistent.

The book is highly recommended for those with some experience in the field or for beginners with some guidance. It is well reproduced and reasonably priced.

A. L. PATTERSON
Institute for Cancer Research
Philadelphia, Pennsylvania

Principles of a New Energy Mechanics. JAKOB MANDELKER. Pp. 73. Philosophical Library, New York, 1949. Price $3.75.

This little book presents one of those tantalizing discussions which presume to derive the "true" and "ultimate" knowledge

of the laws of physics from a set of postulates which are assumed to be "self-evident" or "general knowledge." The new Energy Mechanics is supposed to replace Einstein's theory of special relativity. Its postulates are: (1) the equivalency of energy and mass, (2) the invariance of $r^2-(ct)^2$, and (3) the existence of an absolute time concept. On this basis the laws for the rectilinear transport of mass-energy are developed by two methods to show that the arguments are self-consistent. The resulting equations are interpreted in terms of suitably defined new concepts such as the matter momentum mc and a new type of kinetic energy. In a second part these new concepts are connected with the dualistic particle-wave nature of energy. The discussion is in mathematical terms but involves only simple algebra, geometry, and calculus.

While the book advances several intriguing ideas it fails to prove the exaggerated claims of its author. A new physical theory is not necessarily true because it is mathematically self-consistent, but first and above all it must be able to explain all the pertinent facts. With the exception of Fizeau's experiment the author ignores all the numerous observations which have confirmed Einstein's theory. Since he does not attempt it, one suspects that he is unable to demonstrate that his theory agrees better than Einstein's with any set of data (e.g., for the Compton effect). It would seem that the author does not expect to have his work judged on the basis of facts but rather by its aesthetic or logical implications. But even in this respect we cannot gain much satisfaction because too many questions are left unanswered. For instance: In the new mechanics the velocity of light is not an invariant, but it can never be exceeded. For a moving observer $c'^2=c^2-v^2$. But we are not told relative to what system v must be measured. If v is relative to the source would this not imply that light from different stars should have different velocities? Is c or c' the limiting velocity for a moving observer? In the second part of the book one cannot understand why mv and not the invariant mc should be related to the de Broglie wavelength and it is mysterious how the author can be elated over his result that the group velocity of these waves is not the particle velocity. Many other objections against logic or interpretation could be raised.

There are several instances in the history of physics where works of similar character have later proved themselves to be of extreme importance. This reviewer can find no justification to classify this book among those potentially revolutionizing contributions.

HANS MUELLER
Massachusetts Institute of Technology
Cambridge, Massachusetts

Introduction to Theoretical and Experimental Optics. JOSEPH VALASEK. Pp. 454+x. John Wiley and Sons, Inc., New York, 1949. Price $6.50.

There is a greater emphasis in this book than in many other textbooks of theoretical and experimental optics, on the applied fields of Emission Spectroscopy and a corresponding lesser emphasis on the field of color description. Following the descriptive text is a series of 24 experiments covering the major topics in the preceding text and a brief description of the photographic process. Some 160 problems are included and a considerable mathematical discussion of theories provides the background for a thorough theoretical course which requires a general knowledge of Physics and Calculus.

The text portion is divided nearly equally between discussions on Geometrical Optics, Physical Optics, and Radiation and Spectra. In addition to its intended use as a text in a set course in Experimental and Theoretical Optics, the text provides an excellent reference for engineers, physicists, and chemists who use optical research methods and desire detailed references in lens principles, refractometry, spectroscopy, x-ray analysis, and photography.

WALLACE R. BRODE
National Bureau of Standards
Washington, D. C.